

A COMPARATIVE STUDY OF STRENGTH ASSESSMENT METHODS
FOR RC COLUMNS

by

FERAIDON FARAHMAND ATAIE

B.S., Kabul University, Kabul, Afghanistan, 2006

A THESIS

submitted in partial fulfillment of the requirements for the degree

MASTER OF SCIENCE

Department of Civil Engineering
College of Engineering

KANSAS STATE UNIVERSITY
Manhattan, Kansas

2010

Approved by:

Major Professor
Asad Esmaeily

Copyright

FERAIDON FARAHMAND ATAIE

2010

Abstract

Realistic strength assessment of reinforced concrete structural elements, especially columns in bridges and tall buildings is a critical need not only at design time, but also when an accurate evaluation of the strength is needed for decisions such as retrofit or replacement of an existing structure.

Assessment of the flexural strength of a column under a specific axial load level is usually done by constructing the axial force-bending moment interaction response curve of the section. This assessment can be done using the code procedure. However, the code does not consider the confinement effect, and is based on the “stress block” assumption for a pre-assumed failure strain for concrete.

It has been shown by various experimental and analytical studies that the performance of a reinforced concrete section is affected by different factors such loading history and material behavior. A realistic performance assessment should consider not only proper models for the monotonic and cyclic response of the material, but also analytical methods and procedures that can capture the effects of loading pattern and provide realistic predictions of the section capacity.

Accuracy of the analytical methods in strength assessment of reinforced concrete sections was explored in a comparative study. These methods were compared and validated against the existing experimental data. The factors considered in these analytical procedures, included the effect of confinement, and the method employed in assessment of the axial-force-bending moment interaction response of a column section. The experimental data were collected from tests conducted on circular and rectangular columns under a constant axial load.

It has been shown that the axial force-bending moment interaction curve, constructed based on the moment-curvature response of a section using a more detailed analytical method such as fiber-model, considering the confining effect of the lateral reinforcement, represents the most realistic and optimal response of a cross section.

" بسم الله الرحمن الرحيم "

بنام خداوند بخشنده و مهربان

In the name of the God, the most gracious and merciful

Table of Contents

List of Figures.....	vii
List of Tables.....	ix
Acknowledgements.....	x
Preface.....	xi
Chapter One- Overview	1
1.1- Introduction:	1
1.2- Concrete columns and their behavior:	3
1.3- Concrete Confinement, strength, and ductility:.....	7
1.4- Research significance:	10
Chapter Two- Literature review	11
2.1- Chapter opening	11
2.2- Mander material model.....	14
2.3- Codes and confinement:.....	19
2.4- Analytical methods for obtaining F-M diagrams:	23
2.4.1- Simplified method for unconfined concrete:	24
2.4.2 – Simplified method for confined concrete:	31
2.4.3- Simplified curvature-based method:	33
2.4.3.1- Moment-curvature (M-C) diagrams for columns:	34
2.4.3.2- Obtaining the F-M diagram from M-C diagrams:	41
2.4.4- Detailed method.....	42
Chapter Three- Exploring Analytical Methods	45
3.1- Chapter opening:	45

3.2- Computation of F-M diagrams for unconfined RC columns:.....	45
3.2.1- Computation of F-M diagram based on the simplified method:.....	46
3.2.2- Obtaining F-M diagram based on simplified-curvature-based method:.....	51
3.2.3- Constructing the F-M diagrams based on detailed methods:.....	56
3.3- Computation of F-M diagrams for confined cross sections:	58
3.3.1- Confined F-M diagrams based on simplified method:	60
3.3.2- Confined F-M diagram based on simplified curvature-based method:	64
3.3.3- Computation of F-M diagram based on detailed method:	66
3.3.4- Obtaining the F-M diagrams based on detailed curvature-based method:	68
3.4- Chapter summary:.....	72
Chapter four- Validation of Analytical Methods Against the Experimental Data	73
4.1- Chapter Opening:.....	73
4.2- Comparison of unconfined simplified and unconfined detailed F-M diagrams:	73
4.3-1. Comparison of unconfined and confined F-M diagrams based on detailed method:.	82
4.4- Comparison of detailed method and detailed-curvature-based method for confined cross sections:.....	88
4.5- Validation of detailed and detailed-curvature-based methods against the experimental results:.	105
Chapter five- Summary and Conclusion	109
References:	112
Appendix – Notations	115

List of Figures

Figure 1.1. Tied and spiral columns	3
Figure 1.2. Capacity of concentric axially loaded concrete column	4
Figure 1.3. F-M diagram for an elastic steel column	6
Figure 1.4. Confinement pressure generated by confinement	8
Figure 1.5. Axial stress-strain curve for concrete subjected to triaxial compression	9
Figure 2. 1. Mander model for confined and unconfined concrete	15
Figure 2. 2. Parameters of confined rectangular cross section	17
Figure 2. 3. Determination of maximum confined concrete strength for rectangular cross sections.....	18
Figure 2. 4. Equivalent stress block for confined concrete	18
Figure 2. 5. Transverse reinforcement details	22
Figure 2. 6. Different stages of strain distribution on the column cross section.....	24
Figure 2. 7. Six important points on F-M diagram for concrete column.....	25
Figure 2. 8. Column cross section and strain distribution for the first point.	25
Figure 2. 9. Stress and strain distribution for the second point.....	26
Figure 2. 10. Stress and strain distribution for the third point.	28
Figure 2. 11.(b). θ and \bar{y}	30
Figure 2. 12. Parameter of the cross section for the confined concrete.....	31
Figure 2. 13. Strain distribution for confined concrete cross section.....	32
Figure 2. 14. Curvature of a cross section.....	35
Figure 2. 15. Simplified M-C diagrams. (a) Displacement-controlled (b) force-controlled.....	36
Figure 2. 16. Parameters of the generalized formula.	38
Figure 2. 17. Axial force-Moment diagram based on M-C diagrams.....	41
Figure 2. 18. The cross section discretization in fiber-element model.....	42
Figure 2. 19. KSU-RC interface ^[37]	44
Figure 3. 1. Columns' cross section.....	45
Figure 3. 2 (a). Simplified-unconfined F-M diagram for square cross section.....	49
Figure 3. 3. Simplified-unconfined F-M for circular concrete column.....	50
Figure 3. 4. M-C diagram Point labeling.....	52
Figure 3. 5- Simplified-unconfined Moment-Curvature diagram for axial load of 455 kips.	55
Figure 3. 6 (a). Detailed-unconfined F-M diagram for square cross section.....	56
Figure 3.7. Detailed-unconfined M-C diagram for axial load of 407.2 kips.....	57
Figure 3. 8. Simplified-Confined F-M diagram for square cross section.....	63
Figure 3. 9(a). Detailed-confined F-M diagram for square cross section.....	67
Figure 3. 10. detailed-confined M-C diagram for axial load 1813 kips.....	68

Figure 3. 11. Detailed-confined M-C diagram for axial load of 1540 kips.	69
Figure 3. 12. Detailed-confined M-C diagram for axial load of 1200 kips.	69
Figure 3. 13. detailed-confined M-C diagram for axial load of 523.8 kips.	70
Figure 3. 14(b). detailed-confined curvature-based F-M diagram for circular section.	72
Figure 4. 1. Unconfined F-M diagrams based on Simplified and Detailed methods	74
Figure 4. 2. Exact strain-stress distribution for unconfined concrete column section.	75
Figure 4. 3. ACI stress block.	76
Figure 4. 4. Line of action of compressive forces.	77
Figure 4. 5. Internal forces for point (1).	78
Figure 4.6. Internal forces for point (2).	79
Figure 4.7. Internal cross section forces for axial force of -328 kips.	80
Figure 4.8. F-M diagrams for 25x25 in. unconfined square cross section.	81
Figure 4.9. Simplified and Detailed F-M diagrams for unconfined circular cross section.	82
Figure 4.10. Confined and Unconfined detailed F-M diagrams for square cross section.	83
Figure 4.11. Confined and unconfined F-M diagram for one inch cover.	84
Figure 4.12. Detailed F-M diagrams for compressive strain of 0.003.	85
Figure 4.13. Stress-strain curve for cover and core concrete for #3@4 in. stirrups.	86
Figure 4.14. F-M diagrams of circular column for compressive strain of 0.003.	87
Figure 4.15. detailed and “detailed curvature-based” F-M diagrams.	88
Figure 4.16. Moment versus compressive strain for different axial loads.	91
Figure 4.17. Confined F-M diagrams.	92
Figure 4.18. Confined F-M diagrams for circular cross section.	93
Figure 4.19. Moment versus compressive strain for circular cross section.	94
Figure 4.20. Confined and unconfined stress-strain curve for square cross section	95
Figure 4.21. Confined and unconfined concrete models for circular cross section	96
Figure 4. 22. Confined F-M diagrams for square cross section with #3@2 in. stirrups.	98
Figure 4. 23. M-S diagrams for confined square section with 2 in. cover.	99
Figure 4. 24. Stress-strain model for square cross section with #3@2 in. stirrups.	99
Figure 4. 25. Confined F-M diagrams for circular cross section with #3@2 in. stirrups.	100
Figure 4.26. M-S diagrams for circular cross section with #3@2 in. stirrups.	101
Figure 4. 27. Confined F-M diagrams for square cross section with zero cover.	102
Figure 4. 28. M-S diagrams for square cross section with zero cover	103
Figure 4. 29. Confined F-M diagrams for circular cross section with zero cover.	104
Figure 4. 30. M-S diagrams for circular cross section with zero cover.	105

List of Tables

Table 3.1 – Coordinates of points for confined-detailed F-M diagram	66
Table 3.2 - Confined-detailed M-C diagram data	71

Acknowledgements

I am grateful to the government of Afghanistan, my home country, for his valuable offerings and funding throughout my study at Kansas State University (KSU). Without the assistance of the government, I would have not been able to continue my studies up to this level.

Special thanks to my immediate academic advisor, Dr. Asad Esmaily, for his support regarding this thesis and throughout my study at KSU. He has been available often to help me with my academic problems and concerns.

This is also the place to express my gratitude to my precious parents and my beloved wife for their priceless support and encouragement.

Preface

Reinforced Concrete (RC) columns play an important role in stability and strength of reinforced concrete structures, such as buildings and bridges. So, refined, realistic performance assessment of these structural members is a critical need. This need is more pronounced when an important structure is designed based on the emerging performance-based design method. Besides the models used for monotonic and cyclic behavior of the material; different analytical methods are used to predict the performance of RC columns. These methods are explored in this report to find the procedure that yields the best realistic prediction of the performance of the RC columns.

The axial force-bending moment interaction response, referred to as F-M in this report, is commonly used as a strength indicator of the RC columns; different analytical methods are employed to construct the axial force-bending moment (F-M) response of a section. The results of these methods are compared to each other and validated against the existing experimental data.

The first chapter is an overview, including an introduction to reinforced concrete columns and their behavior under combined axial load and uniaxial bending moment; as well as the basic concept of concrete confinement. The second chapter includes a literature review of the topic, and provides the details of the material model used in the analytical work for plain and confined concrete. This chapter also covers the computational procedure of F-M diagrams based on the different analytical methods explored in this study.

Next, the third chapter addresses the computations of the confined and unconfined F-M diagrams, based on these analytical methods. The fourth chapter, includes the comparison of the results obtained using the aforesaid analytical methods. The results of the analytical methods are also validated against the existing experimental data in this chapter. Finally, the summary and conclusions of the research is covered in the fifth chapter.

Chapter One- Overview

1.1- Introduction:

Concrete structures are commonly used for various types of structures all over the world, including a wide range of buildings, bridges, dams, etc. Moreover, they are designed and constructed in different climates and seismic zones. In general, overall performance and behavior of concrete structures under applied loads depends on the response of their force resisting systems. Behavior of the force resisting systems, in turn, depends on the response of the individual structural elements, such as reinforced concrete columns. Specifically, deformation capacity or the so-called “ductility” of these force resisting systems is an important parameter that influences the performance of structures under various loading conditions.

In particular, RC columns are important structural elements, and play a significant role in overall ductility and capacity of the reinforced concrete structures. Not surprisingly, accurate performance assessment of a reinforced concrete structure is closely tied to realistic assessment of the strength and performance of its columns. Different indicators are used for prediction of the strength and performance of RC columns. Three commonly used strength and performance indicators to evaluate the concrete columns' behavior are the axial force-bending moment interaction response, moment-curvature response, and the Force-deflection response.

Realistic assessment of the performance and strength of reinforced concrete columns using these indicators is significantly affected by load pattern and history, analytical method used in the assessment analysis, and the material models employed to analyze reinforced concrete (RC) columns.

It has been shown that the load pattern and history significantly affect the performance and capacity of reinforced concrete columns^{[1][2][3]}, which means a reasonably accurate and realistic assessment of the strength and performance of a reinforced concrete

column, using the aforesaid indicators, requires the study to address the effects of the load pattern in the process.

Second, material models implemented in the analytical procedure are of great importance in the accuracy of the results. For instance, models used to determine the monotonic stress-strain relationship of confined concrete play a vital role in the final results^[4].

A third important aspect of a realistically accurate analysis is the procedure employed in the analysis. As an example, the axial force-bending moment interaction response of a section can be evaluated by assuming a specific compressive strain at one side of the section and generating the curve by changing the strain at other locations, such as tensile steel. However, this procedure will not lead to a realistic value, as will be shown in this study. The more accurate and realistic moment capacity of the section for a given axial load is the maximum moment achieved in a moment-curvature analysis under that axial load.

In this study, several commonly used methods and procedures for strength assessment of reinforced concrete columns are explored, and their accuracy has been validated against the existing experimental results. Notably, the effects of load pattern and history as well as the type of the material model used in the analysis are not addressed in this study.

The dominant method used in strength assessment of columns is the axial force-bending moment interaction response, as authorized by the code^[5]. However, this method does not consider the effects of confining material, and the predictions using the method prescribed by the code lead to extremely conservative results.

In general, all of these methods are based on strain compatibility and force equilibrium. However, results using these methods defer widely, and there is a need to find a method that can provide a reasonably accurate and realistic prediction of the capacity and performance of a RC column. This is critical for replacement, retrofit or repair of an existing and apparently deficient column.

Therefore, this study explores various methods and proposes the one that can provide an optimal realistic prediction of the response of reinforced concrete columns subjected to monotonic axial load and uniaxial bending moment.

1.2- Concrete columns and their behavior:

Columns are structural members that support axial load with or without bending moments; however, if the member supports axial load and moment, it is called a beam-column. These structural members can be horizontal, vertical or inclined. In this text, by columns we mean vertical structural members that support axial load with or without moments. In a structure, these vertical members support the loads of floors and roof and eventually transmit these forces to the structure's foundation. Although concrete columns can have several types of cross sections, such as rectangular, circular, T-shape, L-shape, this study considers only the RC columns with circular and square cross sections. Also, based on the type of the lateral reinforcement used in these RC columns, they are divided into two main categories of tied columns and spiral columns.

Tied columns have individual hoops (stirrups); spiral columns are those that their hoops have the form of a spiral. Figure 1.1 shows tied and spiral column.

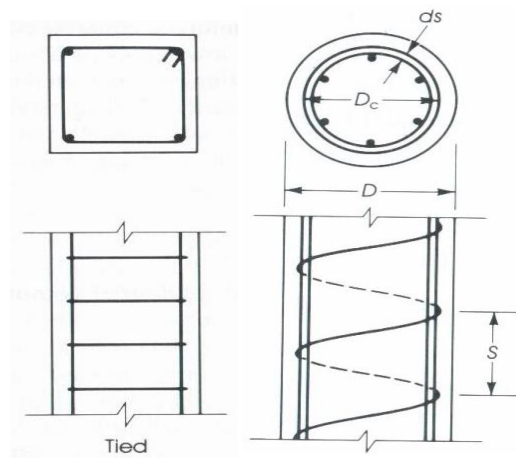


Figure 1.1. Tied and spiral columns ^[6].

All rectangular columns are tied columns while the circular columns can have either tied stirrups or spiral hoops. Tied columns are less ductile than spiral ones and, consequently, tied columns are subjected to brittle failure^[7].

In tied columns, which are mostly used in non-seismic regions, the ties (stirrups) are spaced so apart from each other that the core concrete is not effectively confined; therefore, in the result of lateral strain, the ties are bent, the longitudinal reinforcement buckles, and the concrete crushes in a brittle manner. However, in spiral columns the pitch (indicated as (s) in Figure 1.1) is small, and the spirals provide sufficient lateral pressure on the core concrete to prevent buckling of the longitudinal reinforcement, consequently, preventing the sudden collapse of the core concrete^[7].

As stated, RC columns can be under both axial load and bending moments. If the column is under the axial load only, its behavior can be analyzed simply. The capacity of concentrically loaded concrete columns can be found by summation of the strength of the concrete and the strength of the reinforcement used within its cross section. Figure 1.2 shows this procedure.

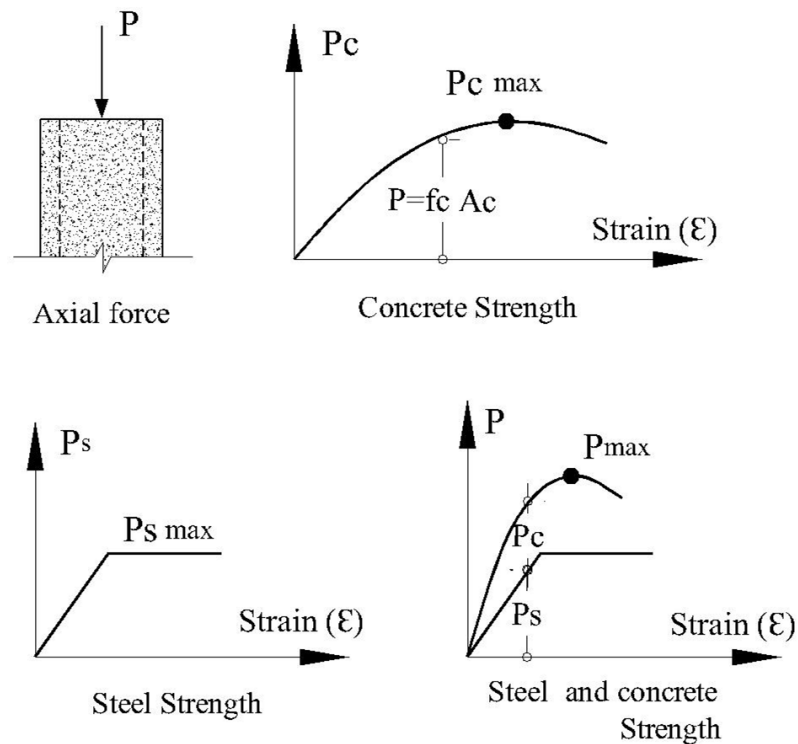


Figure 1.2. Capacity of concentric axially loaded concrete column^[7].

However, evaluating the response of concrete columns under axial load and bending is not that simple. Consider a column made of linear and elastic materials with a maximum allowable compressive stress of f_{\max} . This column will fail if the compressive stress is more than f_{\max} . According to mechanics of material:

$$\frac{P}{A} + \frac{My}{I} = f_{\max} \quad \text{Eq. 1.1}$$

Where P is the applied axial load, M is the applied bending moment, y is the distance between centroid of the section to the most compressed fiber, A is the area of the cross section, and (I) is the moment of inertia of the cross section^[7].

In Eq. 1.1, the maximum axial load P_{\max} that the cross section can carry occurs when the bending moment M is zero; similarly, the moment capacity of the section is at its maximum value if the applied axial load is zero. Thus,

$$P_{\max} = A \cdot f_{\max} \quad \text{Eq. 1.2}$$

$$M_{\max} = \frac{I}{y} \cdot f_{\max} \quad \text{Eq. 1.3}$$

$$\frac{P}{P_{\max}} + \frac{M}{M_{\max}} = 1 \quad \text{Eq. 1.4}$$

Eq.1.4 is called the interaction equation for a linear and elastic column because it shows the relationship between bending moment and axial load at failure^[7]. Figure 1.3 is the plot of Eq.1.4 for a steel cross section that is within its elastic range. In Figure 1.3, any point that is located outside the shaded area is considered as failure of the column. While an accurate interaction diagram can be drawn for a linear and elastic column by plotting Eq.1.4, the F-M diagrams for concrete columns are not so simply feasible because concrete behavior is not elastic within the whole range of compressive axial strains. Nevertheless, different analytical methods can be used to construct the F-M diagrams for RC columns; this will be explained in more detail in this text.

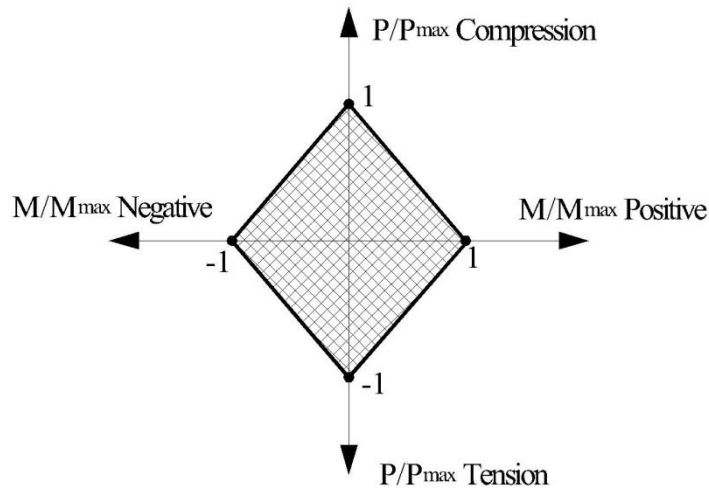


Figure 1.3. F-M diagram for an elastic steel column [7].

Another way to assess the response of a concrete column is to use its Moment-Curvature (M-C) diagram. The relation between moment and curvature of a linear and elastic cross section can be written as:

$$M = EI\phi \quad \text{Eq. 1.5}$$

In this equation, M is the applied bending moment on the cross section, E is the modulus of elasticity of material, (I) is the moment of inertia of the cross section, and ϕ is the curvature. In Eq.1.5 as long as the EI term is linear, the relation between moment and curvature is linear. This statement is true for a steel cross section that is stressed below its yielding point.

This concept and definition can be applied, with little modifications, on concrete cross sections. A simplified M-C diagram for a concrete column consists of three straight lines with different slopes. The first line is from zero point up to the cracking of the concrete; the second line is the portion of the graph from cracking point up to the yielding of the steel reinforcements, and the third line connects the point of yielding to the ultimate point. Each of these moment-curvature (M-C) diagrams is plotted for a given axial load applied on the reinforced concrete (RC) column. There are, also, several analytical methods used to obtain the M-C diagram for RC columns. Additionally, both the M-C and F-M responses are used to predict and evaluate the behavior of RC columns.

1.3- Concrete Confinement, strength, and ductility:

The relationship between stress and strain for an isotropic material that is within its linear and elastic range can be expressed by Hooke's law. The generalized Hooke's law for a cubic element of a linear and elastic isotropic material subjected to normal stresses in three orthogonal directions can be written as [8]:

$$\begin{aligned}\varepsilon_x &= \pm \frac{\sigma_x}{E} \mp \frac{\nu \cdot \sigma_y}{E} \mp \frac{\nu \cdot \sigma_z}{E} \\ \varepsilon_y &= \mp \frac{\nu \cdot \sigma_x}{E} \pm \frac{\sigma_y}{E} \mp \frac{\nu \cdot \sigma_z}{E} \\ \varepsilon_z &= \mp \frac{\nu \cdot \sigma_x}{E} \mp \frac{\nu \cdot \sigma_y}{E} \pm \frac{\sigma_z}{E}\end{aligned}\quad \text{Eq. 1.6}$$

Where ε_x , ε_y , and ε_z are strains, and σ_x , σ_y , σ_z are the normal stresses in x , y and z directions respectively; ν is the Poisson's ratio for the material and E is the modulus of elasticity of the material. As indicated in Eq.1.6, a negative (compressive) stress in a normal direction will cause a normal negative strain in the same direction and some positive strains in the other two orthogonal directions depending on the Poisson's ratio. This phenomenon that will usually lead to a change in volume is called dilatation. Likewise, a RC column subjected to axial stress induced by axial load experiences dilatation. For concrete, lateral strain associated with the axial strain can be expressed as [9]:

$$\varepsilon_t = \eta \cdot \varepsilon_c \quad \text{Eq. 1.7}$$

Where η is the dilatation ratio for concrete, ε_t is the transverse (lateral) strain, and ε_c is the compressive axial strain in concrete. In this formula, the dilatation ratio that relates the transverse strain to axial strain is a function of the modulus of elasticity of the concrete cross section and the compressive axial strain level [9].

This lateral expansion of concrete is prevented, to some extent, by confining the cross section; this confinement can be provided in various ways, such as with Fiber-Reinforced-polymer (FRP) and/or with conventional lateral reinforcement. Preventing the lateral expansion of concrete with a confining material produces a lateral pressure on

the confined portion of the concrete. This lateral pressure is called confining pressure. This process is illustrated in Figure 1.4.

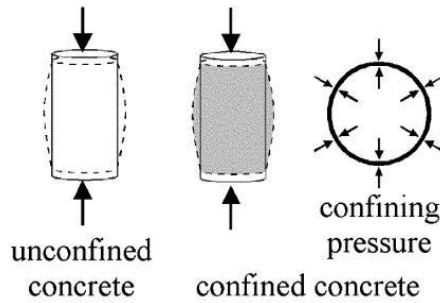


Figure 1.4. Confinement pressure generated by confinement ^[9].

The confining pressure produced on the core concrete by a confining material together with the axial compressive stress can be treated as triaxial loading of the concrete specimen.

As evident from Eq.1.6 the compressive stress for a given compressive strain in one direction, such as x , is more if the strains in the other two orthogonal directions, y and z , are zero, and less if dilation is allowed. However, for a confined core, we have partial dilation that activates the lateral confining pressure, leading to enhancement of the compressive stress in the other direction, here referred to as x .

Richart et al.^[10] were among the first researchers who conducted some tests on small size concrete columns under constant lateral hydrostatic pressure. These tests were done to predict the strength enhancement of concrete under applied axial loads. Richart showed that the axial compressive strength of concrete columns increases as the lateral pressure is increased. He proposed the following equation for the confined concrete stress.

$$\sigma_1 = f'_c + 4.1\sigma_3 \quad \text{Eq. 1.8}$$

Where σ_1 is the axial compressive stress, $\sigma_2 = \sigma_3$ is the lateral stress due to lateral pressure, and f'_c is the axial compressive stress of unconfined concrete under uniaxial loading. Figure 1.5 shows the relation between the axial compressive stress and lateral confining pressure, σ_3 . In this figure, the compressive stress of unconfined concrete is 3000 psi ^[7].

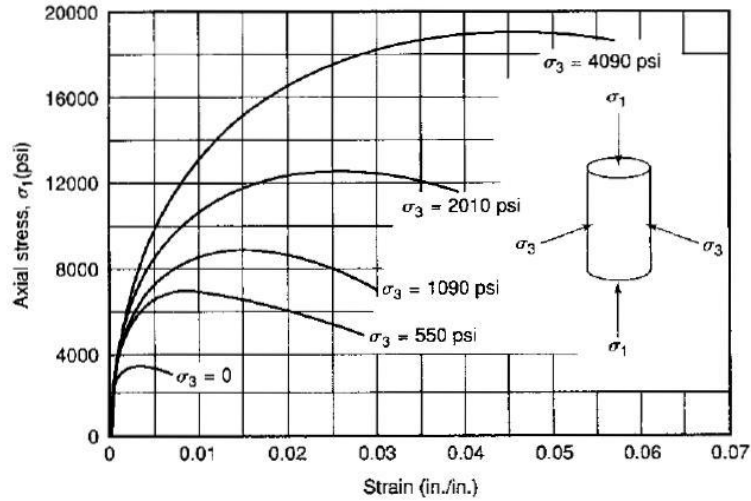


Figure 1.5. Axial stress-strain curve for concrete subjected to triaxial compression [7].

Two important characteristics are evident in Figure 1.5. First, the compressive strength of concrete increases when the lateral pressure is increased. Second, the compressive axial strain capacity of concrete is amplified as a result of confinement pressure. So, the confinement that creates a constant lateral pressure on the concrete specimen can enhance the concrete compressive strength, depending on the level of confinement provided within the cross section. Also, since the compressive axial strain capacity as well as the compressive strain under the maximum achieved axial stress of the core concrete is improved by confinement, the ductility of the core concrete column is also improved.

In real world situations, concrete confinement is, commonly, provided in two different ways. The first is conventional lateral reinforcement, and the second is Fiber-Reinforced-Polymer (FRP) used as a confining material. Also, a combination of these two can be seen for cases where a deficient RC column with conventional lateral reinforcement is retrofitted by FRP material. Several researchers have proposed different stress-strain models (stress-strain curves) for concrete confined by FRP and by lateral reinforcement; this will be discussed further in the next chapter.

Although the strength and ductility of concrete are improved by considering confinement, some of the design codes, such as ACI^[5], have implicitly incorporated the

ductility enhancement of confined concrete but have not considered the strength gained by confinement. More details will be given in the second chapter.

1.4- Research significance:

As it was mentioned earlier, the assessment of a RC column's response and behavior can be affected by different parameters, such as load pattern and history, material models, and analytical methods. Acknowledging the effects of these parameters on the assessment of the performance of reinforced concrete columns, this study is limited to exploring the role of various analytical procedures, and all other factors are kept constant. As an example, in the course of this study, the load pattern is monotonic and the monotonic models used for stress-strain relationship of plain and confined concrete, steel, and their hysteresis rules are fixed. The reinforced concrete columns to be analyzed in this study are considered to be under combined axial force and uniaxial bending moment.

The main objective of this research is to find the analytical procedure that will predict the best realistic performance of a reinforced concrete column, subjected to combined axial load and uniaxial bending moment.

To do so, various analytical methods are used to construct the axial force-bending moment (F-M) diagrams for two concrete columns, one with a square cross section and the other with a circular cross section. The F-M diagrams are obtained for both confined and unconfined cross sections. The analytical methods used in this study are the conventional simplified method, fiber-element method, and curvature-based method. These methods are applied for both confined and unconfined cross sections.

Axial force-bending moment diagrams that are derived using these analytical methods are, then, compared to each other. At the end, the aforementioned analytical methods are validated against the existing experimental data^[11] to find the analytical procedure that has the most realistic prediction.

Chapter Two- Literature review

2.1- Chapter opening:

Materials stress-strain models that represent the relationship between the stress and corresponding strain provide important information about materials behavior under applied loads. Massive studies have been conducted to model the stress-strain relationship of the material forming the reinforced concrete structures and structural members. When analyzing reinforced concrete (RC) elements, there are three material models to be used in the analysis; the stress-strain model for steel reinforcement, the stress-strain curve for unconfined (plain) concrete, and the stress-strain model for confined concrete. Also, there is a need for the cyclic (hysteresis) rules for the cyclic behavior of plain concrete, confined concrete and steel. Following is a brief review of the material models for steel reinforcement and confined concrete.

a- Stress-strain model for steel reinforcement:

Researchers proposed several models for reinforcing steel. For example, Mander et al.^[12], Dhakal and Maekawa^[13], Raynor et al.^[14] are among those who have proposed stress-strain models for steel reinforcement bars. Dhakal and Maekawa^[13], have studied the “reinforcement (bar) stability” and suggested an analytical method to determine the buckling length of the longitudinal reinforcement steel bars of RC structural members; their model takes into account the buckling effect of reinforcement. While these models are developed for monotonic loadings only, Chang and Mander^[15] and Hoehler and Stanton^[16] have proposed cyclic stress-strain curves for steel reinforcement.

b- Stress-strain models for concrete confined by FRP:

Concrete confinement by Fiber-Reinforced-Polymers (FRP) has been a hot topic during the last two decades; hence, various stress-strain models have been proposed. Mirmiran et al.^[17], Samaan et al.^[18] Lam and Teng^[19], Teng and Lam^[20], Teng et al.^[21], Wu and Wang^[22] have all proposed stress-strain models for FRP confined concrete that can be used to monotonic loadings. Shao et al.^[23] have proposed a stress-strain model that can be used for cyclic loadings. However, the most commonly used model for FRP

confinement is the Lam and Teng^[19] model; this model has been adopted by the Concrete Society (2004) in England and also by ACI-440-2R (2008) with some modifications^[24].

c- Stress-strain models for concrete confined by steel reinforcement:

Several different material models exist in the literature for conventional confinement due to steel reinforcement. For instance, Sheikh and Uzumeri^[25], Mander et al.^[26], Legeron and Paultre^[27] are some the investigators who have proposed stress-strain curves for concrete confined by lateral reinforcement under monotonic loadings. Mander et al.^[26], Martinez et al.^[28], and Sakai and Kawashima^[29] are some of the researchers who have come up with stress-strain models for conventional confinement due to the steel reinforcement under cyclic loadings.

Although the idea of confinement due to transverse reinforcement was originated by Richart et al. in 1929^[30], the first primarily stress-strain model was proposed by Kent and Park in 1971^[31]. In this model which was for concrete columns with rectangular cross sections, the strength gained by confinement was ignored; however, the improvement in ductility due to confinement was incorporated in this model.

The model by Sheikh and Uzumeri^[25] which takes into account the enhancement of both strength and ductility due to confinement has three separate equations; one of these equations that is a parabolic equation is used to find the curve up to the maximum (pick) confined stress, and the other is a straight line with zero slope, while the third equation is also a straight line but with a descending slope. In this method, for the first time, the concept of effective core area was used.

The Mander^[26] model is the most commonly used stress-strain model for steel-confined concrete and is used for both circular and rectangular cross sections. Furthermore, only one equation is used for the entire curve; in other words, the model is a unified one. The model accounts for different configurations for longitudinal and transverse reinforcement, and it uses the effective core concrete area. More details about this model are given latter in this chapter.

Although the Mander model is the most commonly used model, Sheikh and Yeh^[32] have shown that this model overestimates the moment capacity of columns with square cross sections. They drew this conclusion from testing and experimental data for 15 square RC

columns with different arrangement of longitudinal and transverse reinforcement. This study also showed that the model that is proposed by Sheikh and Uzumeri^[25] had a better prediction of actual behavior of square columns than did the Mander model^[26]; however, the model by Sheikh and Uzumeri^[25] can be applied to concrete columns with square cross sections only. Thus, each of these models has its own deficiencies and strengths.

The stress-strain relationship for unconfined concrete can be obtained using the aforementioned stress-strain models for confined concrete due to the steel reinforcement; this is done by assuming zero lateral pressure (confining pressure).

In this report, the Mander^[25] model is used for unconfined and confined concrete, and the model developed by Esmaily^[2] is used for steel reinforcement.

Even though the behavior of confined concrete has the attention of many investigators, most building codes over the world have not yet suggested any specific model for reinforcement-confined concrete to be used in design of concrete structures. However, some of these codes have some limitations on the size of concrete column cross sections and on the amount of longitudinal and transverse reinforcement within the cross section. For instance, the American Concrete Institute (ACI)^[5] design code suggests minimum and maximum amount of longitudinal and lateral reinforcement for elements of concrete structures. Also, the amount of transverse reinforcement is different for those columns that will not be subjected to seismic loads compared to the columns in seismic regions; more detail is provided in section 2.3. The Uniform Building Code (UBC)^[33] is another code that considers the improvement of ductility of concrete structures due to concrete confinement. As the ductility of a structure is improved, this code suggests a reduction of the seismic forces induced on the structure; this is also discussed further in section 2.3.

In this chapter, Mander model will be discussed in detail, and the requirements and limitations of both the ACI code and the UBC for ductile behavior of concrete structures will be explained. After that, the discussion continues about different analytical methods for obtaining the axial force-bending moment diagrams for reinforced concrete columns.

2.2- Mander material model :

The Mander model for confined concrete is based on experimental data from “nearly full-size circular, square and rectangular reinforced concrete columns” [26]. Mander has considered both static and dynamic loading, either monotonic or cyclic, in his research. Unlike other confined concrete models, this model is considered to be constructed by employing a single formula; this means that this strain-stress curve is a unified curve [26]. In this section, the formulations that Mander has come up with to derive his proposed stress-strain curve are presented.

The compressive strength of confined concrete is proposed to be obtained by the following formulas:

$$f_c = \frac{f'_{cc} \cdot x \cdot r}{r - 1 + x} \quad \text{Eq. 2. 1}$$

$$x = \frac{\varepsilon_c}{\varepsilon_{cc}} \quad \text{Eq. 2. 2}$$

$$\varepsilon_{cc} = \varepsilon_{co} \left[1 + 5 \left(\frac{f'_{cc}}{f'_{co}} - 1 \right) \right] \quad \text{Eq. 2. 3}$$

$$r = \frac{Ec}{Ec - E_{sec}} \quad \text{Eq. 2. 4}$$

$$Ec = 5000 \sqrt{f'_{co}} \quad \text{Eq. 2. 5}$$

$$E_{sec} = \frac{f'_{cc}}{\varepsilon_{cc}} \quad \text{Eq. 2. 6}$$

In the above equations, f'_{cc} is the maximum compressive strength of confined concrete, ε_c is the compressive strain of plain concrete, f'_{co} is the maximum compressive strength of unconfined (plain) concrete, ε_{cc} is the compressive strain of confined concrete corresponding to the maximum compressive strength of confined concrete, and ε_{co} is the strain corresponding to the maximum compressive strength of plain concrete. In

these equations, the unit for compressive strength is in M.Pa. Figure 2. 1 shows the strain-stress curve for both confined and plain concrete as proposed by Mander.

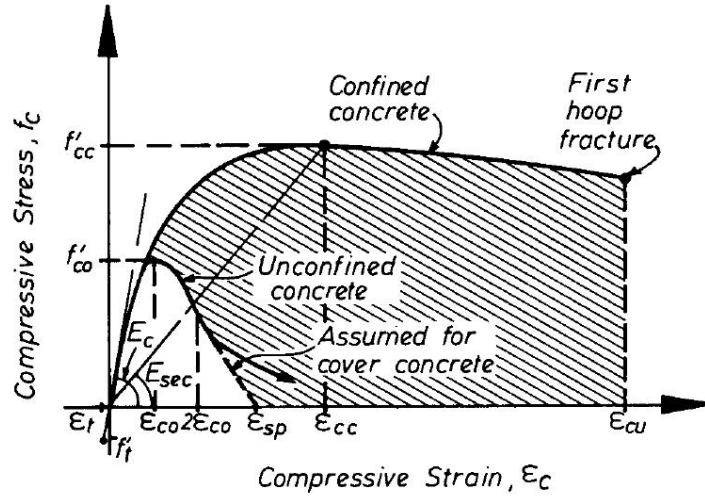


Figure 2. 1. Mander model for confined and unconfined concrete. Adopted from [26]

As stated, the Mander model can be used for both circular and rectangular cross sections; therefore, he proposed specific equations for computing the confinement pressure of circular and rectangular cross sections. The following formulas are used to calculate the lateral confinement pressure of transverse reinforcement for circular cross sections.

$$f'_l = k_e \cdot f_l \quad \text{Eq. 2. 7}$$

In this formula f'_l is the effective lateral confining pressure, k_e is the effectiveness coefficient, and f_l is the lateral pressure provided by transverse reinforcement.

$$k_e = \frac{A_e}{A_{cc}} \quad \text{Eq. 2. 8}$$

$$A_{cc} = A_c (1 - \rho_{cc}) \quad \text{Eq. 2. 9}$$

Where A_e is the effective area of confined core concrete for circular cross sections, A_{cc} is the area of the concrete core enclosed by centerlines of spirals or hoops, and ρ_{cc} is the ratio of the area of transverse reinforcement to the area of the core concrete.

$$A_e = \frac{\pi}{4} \left(d_s - \frac{s'}{2} \right)^2 \quad \text{Eq. 2. 10}$$

$$A_{cc} = \frac{\pi}{4} d_s^2 (1 - \rho_{cc}) \quad \text{Eq. 2. 11}$$

Where, d_s is the diameter of transverse reinforcement bars and s' is the clear vertical distance between the transverse reinforcement, the lateral confining pressure that is produced by the transverse reinforcement can be obtained as:

$$f_l = \frac{2 \cdot f_{yt} \cdot A_{st}}{s \cdot d_s} \quad \text{Eq. 2. 12}$$

Where f_{yt} is the yielding strength of transverse reinforcement, A_{st} is the cross section area of the transverse reinforcement, and (s) is the center to center distance between spirals or hoops. Similarly, Eq.2.12 can be written in terms of the ratio of volume of the lateral reinforcement, spirals or hoops, to volume of the confined core concrete as:

$$f_l = \frac{1}{2} \rho_s \cdot f_{yt} \quad \text{Eq. 2. 13}$$

Where ρ_s is the ratio of volume of lateral reinforcement to the volume of confined concrete core, and is equal to:

$$\rho_s = \frac{4A_{st}}{d_s \cdot s} \quad \text{Eq. 2. 14}$$

With f'_l from Eq.2.7, we can find the maximum compressive strength of confined concrete for circular sections as:

$$f'_{cc} = f'_{co} \left(-1.254 + 2.252 \left(\sqrt{1 + \frac{7.94 f'_l}{f'_{co}}} \right) - 2 \frac{f'_l}{f'_{co}} \right) \quad \text{Eq. 2. 15}$$

$$\varepsilon_{cu} = 0.004 + 1.4 \cdot \rho_s \frac{f_y \cdot \varepsilon_{sm}}{f'_{cc}} \quad \text{Eq. 2. 16}$$

To obtain the maximum compressive strength and the lateral confining pressure for rectangular cross sections, following formulas are employed.

$$\rho_x = \frac{A_{sx}}{s \cdot d_c} \quad \text{Eq. 2. 17}$$

$$\rho_y = \frac{A_{sy}}{s \cdot b_c} \quad \text{Eq. 2. 18}$$

Where $A_{s,x}$ and $A_{s,y}$ are the transverse reinforcement area in x and y directions, respectively. The parameters (b_c) and (d_c) are shown in Figure 2. 2.

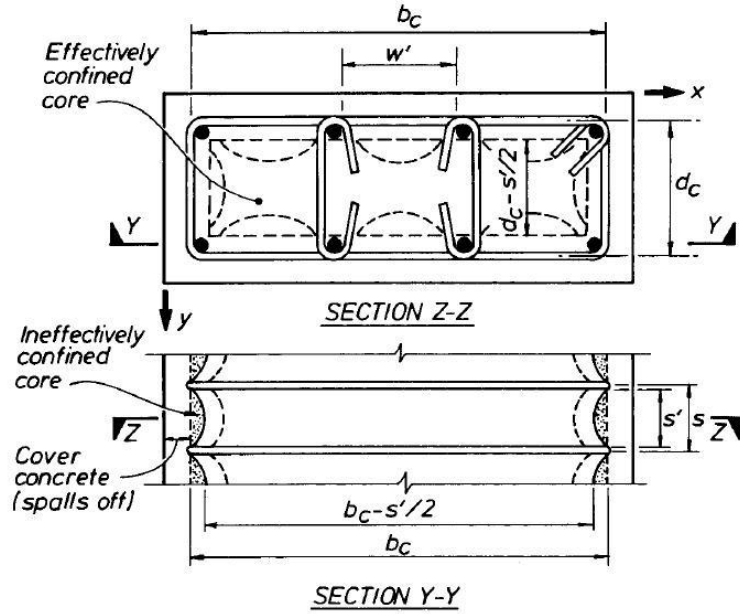


Figure 2. 2. Parameters of confined rectangular cross section. Adopted from [26].

$$f_{lx} = \rho_x \cdot f_{yt} \quad \text{Eq. 2. 19}$$

$$f_{ly} = \rho_y \cdot f_{yt} \quad \text{Eq. 2. 20}$$

$$f'_{lx} = k_e \cdot f_{lx} \quad \text{Eq. 2. 21}$$

$$f'_{ly} = k_e \cdot f_{ly} \quad \text{Eq. 2. 22}$$

Where f'_{lx} and f'_{ly} are the effective lateral confinement pressure in x and y directions, respectively; for rectangular cross sections $\rho_s = \rho_x + \rho_y$ and k_e is obtained using the following equation.

$$k_e = \frac{\left(1 - \sum_{i=1}^n \frac{(w'_i)^2}{6b_c \cdot d_c}\right)}{(1 - \rho_{cc})} \left(1 - \frac{s'}{2b_c}\right) \left(1 - \frac{s'}{2d_c}\right) \quad \text{Eq. 2. 23}$$

Where w'_i is shown in Figure 2. 2.

The typical values of k_e are 0.95 for circular sections and 0.75 for rectangular sections. Obtaining f'_{lx} and f'_{ly} from Eq.2.21 and Eq.2.22, and having f'_{co} (maximum strength of unconfined concrete), we can sue figure 2.3 to compute the maximum compressive strength of confined concrete (f'_{cc}) for rectangular cross sections.

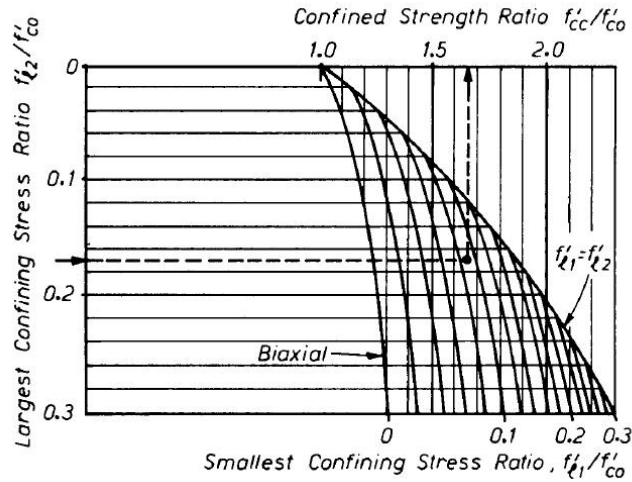


Figure 2. 3. Determination of maximum confined concrete strength for rectangular cross sections. Adopted from [26]

The concept of equivalent stress block for confined concrete is also suggested by Mander et al. Figure 2.4 shows the Mander equivalent stress block and its parameters for confined concrete.

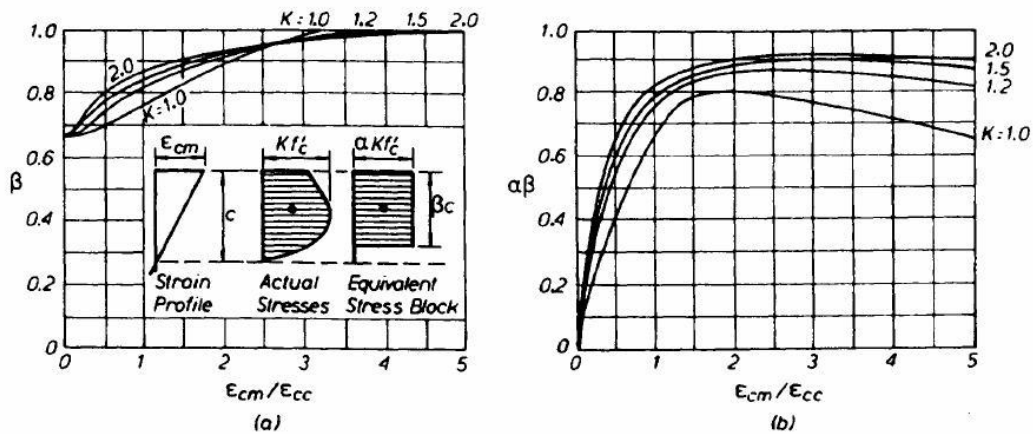


Figure 2. 4. Equivalent stress block for confined concrete. Adopted from [26]

In Figure 2. 4, $K = (f'_{cc} / f'_{co})$, $f'_c = f'_{cc}$, $\varepsilon_{cm} = \varepsilon_{cu}$.

To obtain the stress-strain curve for unconfined concrete based on the Mander model, we set lateral confining pressure f_l equal to zero. Then, employing the previous equations, we can construct the unconfined stress-strain curve.

2.3- Codes and confinement:

Lateral loads, such as earthquake loads, are the devastating loads for concrete structures. One of the methods to avoid absorbing seismic energy is to design the structure with dynamic properties that leads to natural frequencies as different as possible from the frequency content of the earthquake excitation in a specific region. Moreover, a good energy dissipation mechanism in structures plays a vital role in mitigating destructive seismic effect. Although there are many ways to increase the amount of energy dissipation in structures during an earthquake, conventionally the energy dissipation mechanism is provided by ductility (displacement capacity of the structure without failure) of the structure itself. Therefore, increasing the ductility of a structure increases the dissipated energy.

The ductility of concrete structures depends on many factors, such as the compressive strength of concrete used in the structure, the type of the horizontal force resisting system used in the structure, and the amount of steel reinforcement used in the structural elements. If the amount of longitudinal steel reinforcement in a concrete cross section gets higher than a certain limit, the behavior of the concrete becomes brittle and its ductility decreases. On the other hand, the transverse (lateral) reinforcement has a significant effect on the ductility of the structure; the higher the level of transverse reinforcement in a RC cross section, the higher its ductility.

Based on these considerations, ACI-318-08^[5] has divided the “seismic-force-resisting systems” into three broad categories; Ordinary, Intermediate, and Special resisting systems; this classification is, mainly, based on the ductility of the force-resisting

systems. Special-moment-resisting systems are one of the force-resisting systems that support both lateral and gravity loads. In these systems columns and beams are the main elements for resisting loads.

ACI 318-08^[5] recommends some limitations for RC columns in concrete special moment-resisting systems. These reinforced concrete (RC) columns should be specially detailed and designed; the area of longitudinal reinforcement shall not be less than 0.01 A_g or more than 0.08 A_g . Additionally, the following suggestions are made in ACI for transverse (lateral) reinforcement:

Section 21.6.4.3 of ACI 318-08:

The spacing of transverse reinforcement shall not be *more* that the smallest of the following three values:

- a) One fourth of minimum dimension of the cross section.
- b) Six times the diameter of the smallest longitudinal bar within the member.

c) S_0 :

$$4 \leq S_0 = 4 + \left(\frac{14 - h_x}{3} \right) \leq 6 \text{ in} \quad \text{Eq. 2. 24}$$

Where h_x is the longest horizontal distance between the legs of transverse reinforcement.

The spacing mentioned in ACI section 21.6.4.3 should be provided for within the length of l_0 ; this is defined as follows.

Section 21.6.4.1 of ACI 318-08: the value of l_0 should not be considered less than the largest value of the following:

- a) “The depth of the member at the joint face or at the section where flexure yielding is likely to occur”^[5].
- b) One-sixth of the column clear span.
- c) 18 in.

While section 21.6.4.3 ACI addresses the minimum spacing of transverse reinforcement, section 21.6.4.4 of ACI-318-08 puts some limitation on the volumetric ratio of

transverse reinforcement in special moment resisting frames; these limitations are as follows:

a) The volumetric ratio of the circular hoops or spirals shall not be less than the following :

1. Section 21.6.4.4:

$$\rho_s = 0.12 \frac{f'_c}{f_y} \quad \text{Eq. 2. 25 (ACI Eq.21.3)}$$

2. Section 10.9.3:

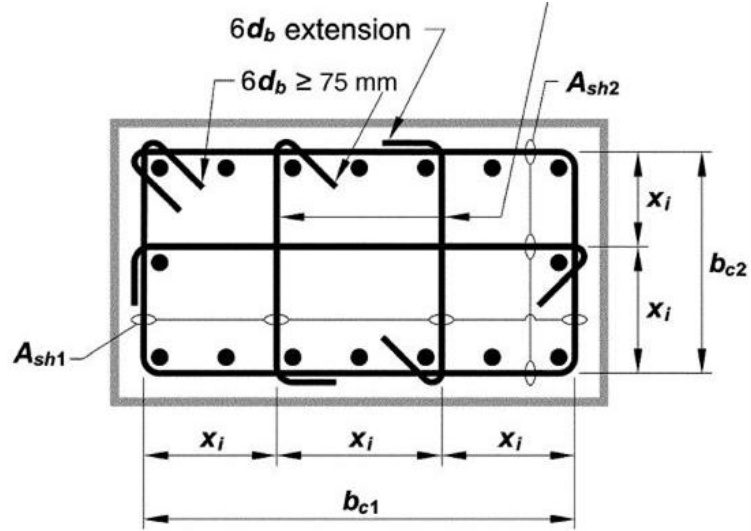
$$\rho_s = 0.45 \left(\frac{A_g}{A_{ch}} - 1 \right) \frac{f'_c}{f_y} \quad \text{Eq. 2. 26 (ACI Eq.10.5)}$$

b) A_{sh} , the transverse reinforcement area in each direction of the section in the square or rectangular cross sections shall be taken the larger of:

$$A_{sh} = 0.3 \frac{S \cdot b_c \cdot f'_c}{f_y} \left(\frac{A_g}{A_{ch}} - 1 \right) \quad \text{Eq. 2. 27 (ACI Eq.21.4)}$$

$$A_{sh} = 0.09 \frac{S \cdot b_c \cdot f'_c}{f_y} \quad \text{Eq. 2. 28 (ACI Eq.21.5)}$$

Where S is the center to center vertical spacing of the ties, A_{ch} is the cross section area measured outside to outside of the transverse reinforcement, $A_{ch} = b_{c1} \cdot b_{c2}$, and other parameters are shown in Figure 2. 5. Furthermore, ACI code has some limitations on the transverse reinforcement beyond the length l_0 . ACI section 7.10 suggests that the maximum and minimum clear spacing between the spirals shall be 3 in. and 1 in. respectively. Moreover, this section indicates that the minimum spacing of the ties shall be taken the smallest of: 16 times diameter of the longitudinal bar, 48 times the diameter of the tie bars, or the smallest dimension of the cross section. According to ACI section 7.10, the minimum spiral diameter should not be less than 3/8 in.



The dimension x_i from centerline to centerline of tie legs is not to exceed 350 mm. The term h_x used in equation 21-2 is taken as the largest value of x_i .

Figure 2. 5. Transverse reinforcement details. Adopted from [5]

UBC-97^[33] is another building code that considers the effects of confinement. UBC-97^[33] also classifies the lateral-force-resisting systems into three categories, Ordinary, Intermediate, and Special. These categories are defined in ACI 318-08 based on their ductility. Given UBC-97, the base shear force produced by ground motion, i.e. an earthquake, is computed by the following equation.

$$V_b = \frac{C_v \cdot I}{R \cdot T} W \quad \text{Eq. 2. 29 (UBC Eq.30.4)}$$

The maximum design base shear force is calculated by Eq.2.30 and the minimum base shear force for seismic zone 4 is computed by Eq.2.31; equation 2.32 gives the minimum design base shear force for seismic zones other than zone 4.

$$V_b = \frac{2.5 \cdot C_a \cdot I}{R} W \quad \text{Eq. 2. 30 (UBC Eq.30.5)}$$

$$V_b = \frac{0.8 \cdot Z \cdot N_a \cdot I}{R} W \quad \text{Eq. 2. 31 (UBC Eq.30.7)}$$

$$V_b = 0.11 \cdot C_a \cdot I \cdot W \quad \text{Eq. 2. 32 (UBC Eq.30.6)}$$

The value of R (Response Modification Factor) depends on the type of lateral-force-resisting systems, and is given in table 16-N of the UBC-97^[33]. Specifically, the value of R is 3.5 for ordinary concrete moment-resisting frame systems and 8.5 for special moment-resisting frame systems. Therefore, in special moment-resisting frame systems, the seismic base shear force is reduced by 50% compared to that of the ordinary moment-resisting frame systems. Thus, the limitations that the ACI^[5] code applies to the special lateral force resisting system along with considerations of CUB-97 improve the ductility of the system and, consequently, decrease the level of seismic force induced on these types of structures.

In recent years, AASHTO^[38] has permitted considering the confining effects directly in analysis of reinforced concrete sections. In section 5.7.2.1 it states that “If the concrete is confined, a maximum usable strain exceeding 0.003 in the confined core may be utilized if verified. Calculation of the factored resistance shall consider that the concrete cover may be lost at strains compatible with those in the confined concrete core.” In C5.7.2.1 the research by Bae and Bayrak^[39] has been cited showing that “for well-confined High Strength Concrete (HSC) columns, the concrete cover may be lost at maximum useable strains at the extreme concrete compression fiber as low as 0.0022. The heavy confinement steel causes a weak plane between the concrete core and cover, causing high shear stresses and the resulting early loss of concrete cover.”

2.4- Analytical methods for obtaining F-M diagrams:

As it was stated earlier, various analytical methods can be used to evaluate the behavior of reinforced concrete columns under applied loads. In this section, the procedure needed to obtain axial load-bending moment (F-M) diagrams, which are used as the capacity indicators of RC columns, is described. The procedure is explained for each analytical method separately.

2.4.1- Simplified method for unconfined concrete:

This method which is recommended by ACI code considers the concept of “equivalent stress block”. Based on this concept, the strain at the most compressed edge of the cross section is assumed to be constant and equal to 0.003; this is said to be the ultimate compressive strain of the unconfined concrete. For obtaining F-M diagrams based on this method, compressive strain at the extreme fiber is taken to be constant while the strain at the tension reinforcement is variable. Figure 2. 6 shows different states of strain distribution of the RC column cross section.

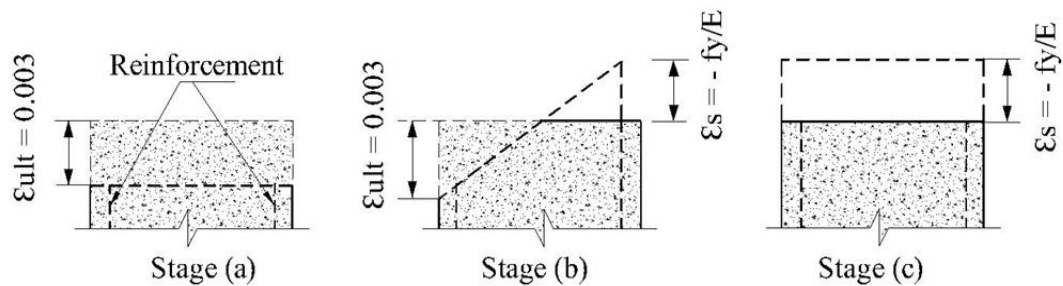


Figure 2. 6. Different stages of strain distribution on the column cross section.

In this figure, stage (a) indicates that the cross section is completely under compression while stage (b) shows that the steel reinforcement has reached its yielding strain and the compressive strain in the concrete remains constant. In stage (c), the cross section is under pure tension. From stage (a) to stage (b) and from stage (b) to stage (c), small incremental values of strain for steel reinforcement are considered, and for every incremental value of this strain, the axial load and bending moment in the cross section are computed. The smaller is the incremental values of strain at the bottom layer of reinforcement, the more accurate is the F-M diagram.

In general, a simple F-M diagram can be drawn by defining six important points while a more accurate diagram can be constructed if the number of points on F-M is increased. These six points are the pure compression point, the point where the strain in the bottom layer of reinforcement is zero, the point at which the strain in the bottom layer of reinforcement is equal to $-\frac{f_y}{E}$, the point where the strain at the bottom layer of

reinforcement is -0.005, the point at which the axial force is zero, and the pure tension point. These points are shown in Figure 2. 7.

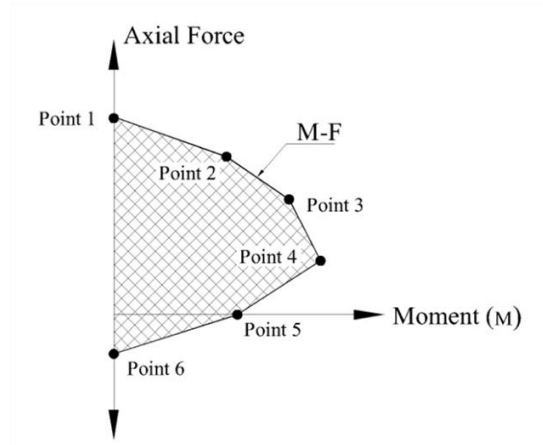


Figure 2. 7. Six important points on F-M diagram for concrete column.

The computation process for obtaining the coordinates of these points is described next.

Coordinates of the first point (Point 1):

At the first point, the cross section is completely under compression and the value of compressive force is defined based on ACI section 10.6.3 as:

$$P_n = [0.85 f'_c (A_g - A_{st}) + A_{st} f_y] \quad \text{Eq. 2. 33 (ACI Eq.10-1)}$$

Where P_n is the nominal axial force, f'_c is the maximum compressive strength of the concrete and f_y is the yielding strength of steel reinforcement. Therefore, the coordinates of this point on the F-M graph is $(M_n, P_n) = (0.00, P_n)$.

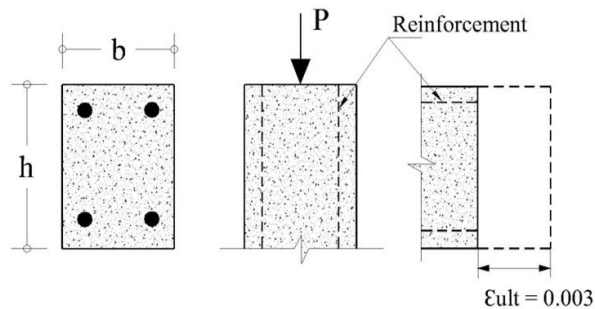


Figure 2. 8. Column cross section and strain distribution for the first point.

Coordinates of the second point (Point 2):

At the second point, the strain at the bottom layer steel reinforcement is zero. This condition is described in figure 2.9. In this stage there is no tension force in the section, but the capacity of the column is decreased because of the existence of the bending moment.

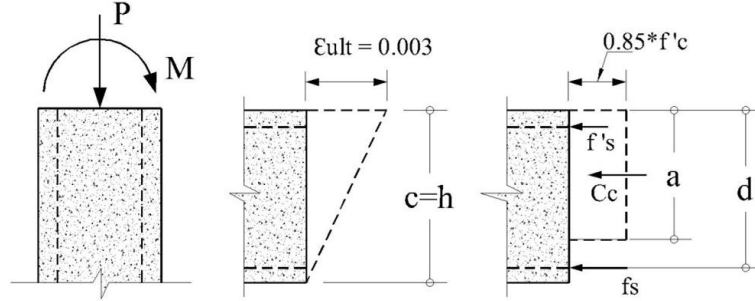


Figure 2. 9. Stress and strain distribution for the second point.

Following is the procedure for computing the coordinates of the second point:

$$C_c = (0.85 \cdot f'_c)(a \cdot b) \quad \text{Eq. 2. 34}$$

$$a = \beta_1 \cdot c \quad \text{Eq. 2. 35}$$

$$F_s = \varepsilon_{st} \cdot E \cdot A_s \leq f_y \cdot A_s \quad \text{Eq. 2. 36}$$

$$F_s' = (\varepsilon'_s \cdot E - 0.85 \cdot f'_c) A'_s \leq f_y \cdot A'_s \quad \text{Eq. 2. 37}$$

$$c = \left(\frac{\varepsilon_{ult}}{\varepsilon_{ult} - \varepsilon_{st}} \right) d = \left(\frac{0.003}{0.003 - \varepsilon_{st}} \right) d \quad \text{Eq. 2. 38}$$

$$\varepsilon_{si} = \left(\frac{c - di}{c} \right) \varepsilon_{ult} = \left(\frac{c - di}{c} \right) 0.003 \quad \text{Eq. 2. 39}$$

$$0.85 \geq \beta_1 = 0.85 - 0.05 \frac{f'_c - 4000 \text{ psi}}{1000 \text{ psi}} \geq 0.65 \quad \text{Eq. 2. 40}$$

In these equations, c and a are the depth of neutral axis and the depth of compressive stress block, respectively. ε_{st} is the tensile strain in the bottom layer of tension reinforcement, ε'_s is the strain in the compression steel reinforcement, ε_{si} is the strain in

the reinforcement corresponding to the depth (d_i), E is the modulus of elasticity of steel, F'_s , and F_s are forces in compressive and tensile reinforcement, respectively; C_c is the compressive force in concrete stress block, and β_1 is the factor that adjusts the depth of the compressive stress block.

Having calculated C_c , F'_s , and F_s , we can compute the coordinates of the second point as follows:

$$P_n = (C_c + F_s + F'_s) \quad \text{Eq. 2. 41}$$

$$M_n = C_c * \left(\frac{h}{2} - \frac{a}{2} \right) + F_s \left(\frac{h}{2} - d \right) + F'_s \left(\frac{h}{2} - d' \right) \quad \text{Eq. 2. 42}$$

These are the nominal coordinates for the second point.

Coordinates of the third point (balanced point):

Obtaining the third point's coordinates requires the same procedure that was used for the second point. But for this point, the strain-stress distribution is different; the strain at bottom tensile reinforcement is equal to the yielding strain of the steel, that is ($\varepsilon_{st} = -f_y/E$). Since the strain in concrete is at the ultimate level and strain in the bottom layer of tensile reinforcement is at the yielding level, this point is characterized as the point of balanced failure.

Note that the depth of neutral axis decreases as the strain in the tensile steel increases. Nominal axial force (P_n) and nominal bending moment (M_n) for this point can be obtained using Eq.2.34 to Eq.2.42 by considering ($\varepsilon_{st} = -f_y/E$).

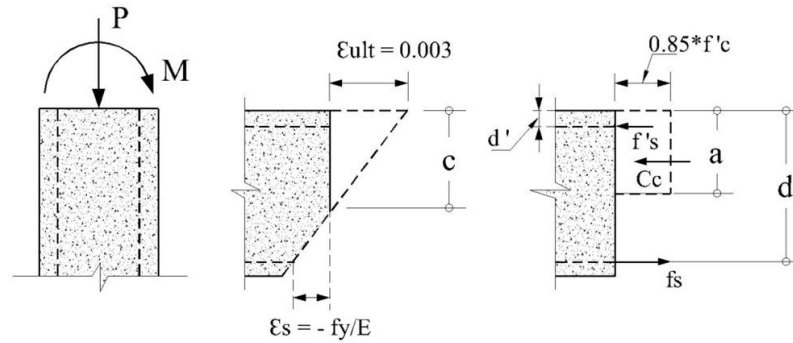


Figure 2. 10. Stress and strain distribution for the third point.

Coordinates of the fourth point (Tension-controlled point):

The coordinates of this point are calculated in the same manner as for third point except that here the value of strain in tensile steel is (-0.005). The fourth point is called the tension-controlled point because the steel fails prior to the crushing of the concrete.

Coordinates of the fifth point:

This is a pure bending point where the axial load is zero. For the preceding points either the depth of neutral axis or the strain in the tensile reinforcement was known. For this point, the depth of neutral axis (c) can be found by putting the Eq.2.41 equal to zero. Next, having (c) the strain in the tensile reinforcement can be obtained by Eq.2.39. Having c and strain in reinforcement layers, the coordinates of the fifth point are then computed in the same way as was the third point.

Coordinates of the sixth point:

For this point, the entire section is in tension and, thus, the tension force is calculated as followings.

$$P_n = -f_y \cdot (A_s + A'_s) \quad \text{Eq. 2. 43}$$

Where A_s and A'_s are the area of the tensile and compression reinforcement, respectively. The bending moment (M_n) is zero for this point.

To obtain a more accurate interaction diagram for a RC column, the number of points on this diagram should be increased. To increase the number of points, different depth of neutral axis (c) should be considered; the smallest is the incremental values of (c), the

more accurate is the F-M diagram. Consequently, for each value of (c), the axial load (P_n) and the bending moment (M_n) are calculated employing Eq.2.34 through Eq.2.42. To calculate the F-M diagrams for cross sections with more than two layers of steel reinforcement, we can compute the general coordinates of the points by the following equations.

$$P_n = C_c + \sum_{i=1}^n F_{si} \quad \text{Eq. 2. 44}$$

$$M_n = C_c \left(\bar{x} - \frac{a}{2} \right) + \sum_{i=1}^n (F_{si} (\bar{x} - d_i)) \quad \text{Eq. 2. 45}$$

In these equations, C_c is defined in Eq.2.34, a is defined in Eq. 2.35, \bar{x} is the distance between centroid of gross cross section to the most compressed edge of the cross section, F_{si} is the force in the steel reinforcement, and it is defined as:

$$F_{si} = \varepsilon_i \cdot E \cdot A_{si} \leq f_y \cdot A_{si} \quad \text{Eq. 2. 46}$$

Where ε_i is the strain in the layer (i) of the steel reinforcement; ε_i that is positive for compression and negative for tension is computed based on Eq.2.39 ; and A_{si} is the area of reinforcement of the i^{th} layer of reinforcement.

Preceding paragraphs discussed the computation of axial force-bending moment (F-M) diagrams for rectangular cross sections. Now, the (F-M) diagrams for RC columns with circular cross sections can be constructed similarly. Incremental values for neutral axis depth are selected while the compressive strain at the extreme fiber is set equal to 0.003. The only differences are the area of compressive stress block and the distance from the centroid of the cross section to the center of this stress block area.

Having the depth of the neutral axis c, the depth of the compressive stress block, a, can be obtained using Eq.2.35. Then, following equations are used to calculate the area of the compressive stress block and the distance from the centroid of the cross section to the center of this stress block area^[5].

$$A = h^2 \left(\frac{\theta - \sin \theta \cdot \cos \theta}{4} \right) \quad \text{Eq. 2. 47}$$

$$A \cdot \bar{y} = h^3 \left(\frac{\sin^3 \theta}{12} \right) \quad \text{Eq. 2. 48}$$

Parameters θ and \bar{y} are shown in Figure 2. 11.

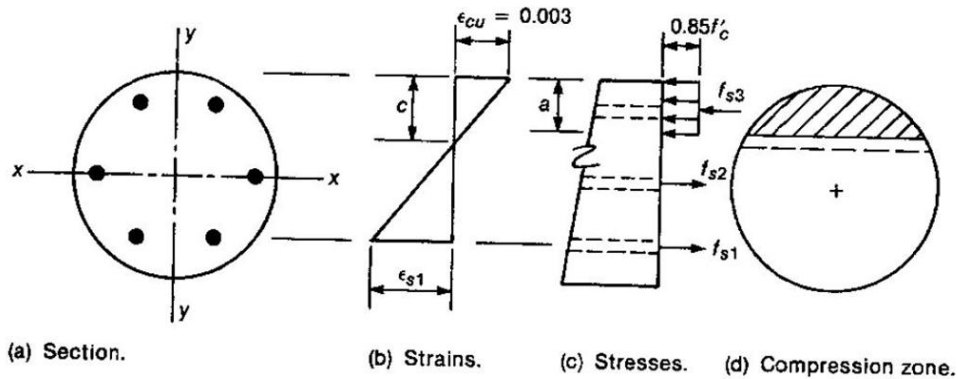


Figure 2.11a- Strain and stress distribution of circular column. Adopted from [7]

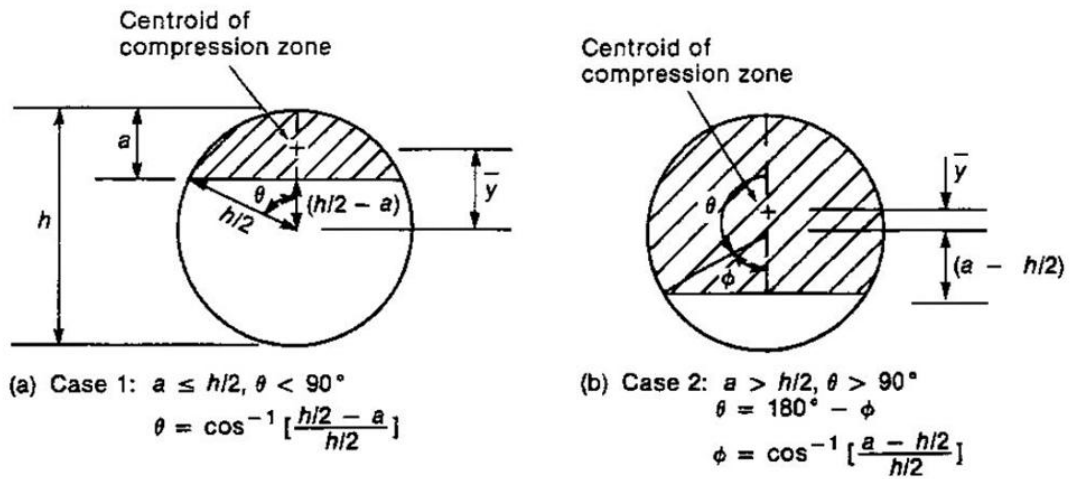


Figure 2. 11.(b). θ and \bar{y} . Adopted from [7]

Notably, the preceding discussion and formulation are applicable only to RC columns under axial loads with/without uniaxial bending moment; throughout this report, the F-M diagrams that are constructed using on this method are called *simplified-unconfined F-M diagrams*. The procedure of analysis of those columns supporting the bending moment in two directions (biaxially loaded in bending) is quite different and is not covered in this study.

2.4.2 – Simplified method for confined concrete:

This method also uses the concept of “equivalent rectangular stress block”; however, the parameters of this stress block are different from those of the ACI equivalent stress block since confinement is considered in this method. In this method, the ultimate compressive strain is found from the stress-strain model used for confined concrete, and the other parameters of equivalent rectangular stress block are obtained from figure 2.4. With the confined equivalent stress block, the procedure employed in previous method is applicable for this method to obtain F-M diagrams.

However, to compute confined F-M diagrams based on this method, some parameters of the cross sections are different from those used in unconfined (plain) concrete sections. The ultimate compressive strain of confined concrete (ϵ_{cu}) is much higher than for the unconfined one, and its value is given by Eq.2.16. In this method, we assume that the cover concrete does not exist; thus, only the core concrete is considered to be effective. Figure 2.12 shows the parameters of core concrete used in the analysis procedure.

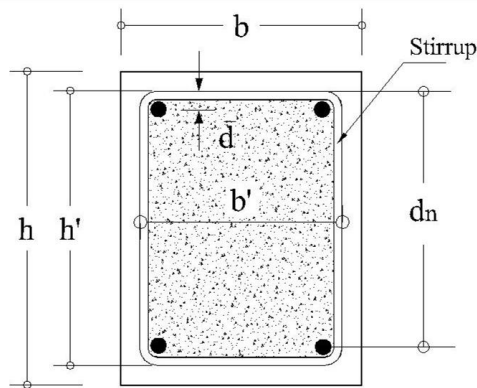


Figure 2. 12. Parameter of the cross section for the confined concrete.

Since in this method the concrete cover is considered to be crushed, the height and the width of the cross section will be changed. The shaded area in figure 2.12 is the confined core concrete and its dimensions, h' and b' , are shown in the figure; these are the effective dimensions of the cross sections.

We should also change the rectangular stress block parameters; that is to find the relevant stress block for confined concrete. Considering the equivalent stress block as shown in figure 2.4, we can find the compressive force of confined concrete as:

$$C_c = \alpha \cdot K \cdot f'_c \cdot \beta \cdot c \cdot b' = \alpha \cdot f'_{cc} \cdot \beta \cdot c \cdot b' \quad \text{Eq. 2. 49}$$

In this equation, f'_{cc} is the maximum compressive stress of confined concrete given in Eq.2.15 for circular sections and from Figure 2. 3 for rectangular cross sections, β and α can be found from Figure 2. 4, b' is the width of the core concrete indicated in Figure 2. 12, and (c) is the depth of the neutral axis obtained by the following formula.

$$c = \left(\frac{\varepsilon_{cc}}{\varepsilon_{cc} - \varepsilon_{st}} \right) d_n \quad \text{Eq. 2. 50}$$

Similarly, the pure compressive axial force of the confined concrete cross section can be computed as:

$$P_n = \left[\alpha \cdot f'_{cc} (A_e) + A_{st} f_y \right] \quad \text{Eq. 2. 51}$$

Where A_e is the effective area of the cross section.

Thus, to find the F-M diagrams for confined concrete columns, the equations 2.49 through 2.51 are employed to include the core concrete dimensions and the confinement effects into the computations. Also, the computation procedure is the same as for unconfined cross sections; the F-M diagrams obtained using this method are called *simplified-confined F-M diagrams* within this report. Figure below shows three different stages of strain distribution in a confined cross section.

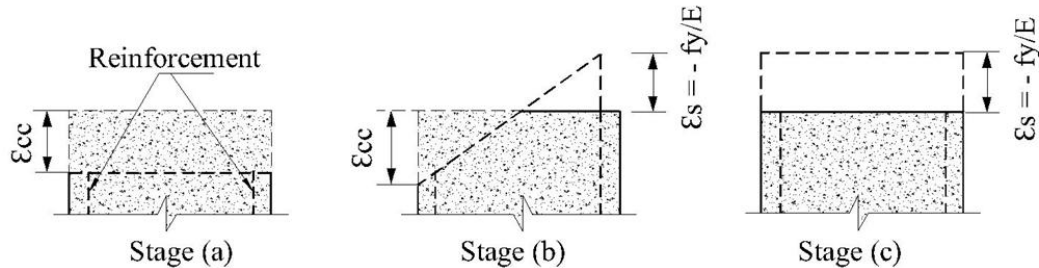


Figure 2. 13. Strain distribution for confined concrete cross section.

In stage (a), the section is under pure compression; stage (b) is the balance situation, and stage (c) is the pure tension state of the section. From stage (a) to stage (b), the strain in the reinforcement decreases from ε_{cc} to the $-f_y / E$ while from stage (b) to stage (c) the compression strain in the concrete decreases from ε_{cc} to $-f_y / E$. This procedure works best by selecting small incremental values of strain in the bottom layer of reinforcement to generate a more accurate F-M diagram. For each value of the depth of the neutral axis, the values of nominal axial force (P_n) and nominal bending moment (M_n) of the cross section are computed using the confined equivalent stress block and the procedure given in section 2.4.1.

2.4.3- Simplified curvature-based method:

As discussed, F-M diagrams based on the simplified method are constructed by assuming that the strain at extreme compression fiber is constant and equal to the ultimate strain. Then, several values of the depth of the neutral axis help render a graph representing the axial force-bending moment response of concrete columns. However, the axial load-bending moment diagram for concrete columns can be constructed in a way that the compressive strain at the extreme compressed fiber is not constant but variable; this is done by using the M-C diagrams for obtaining the F-M diagrams. For each axial load level for a concrete column, there is a unique M-C diagram for the columns. Having the axial load level of the cross section, the corresponding maximum bending moment and the corresponding maximum compressive strain are obtained from the M-C diagram.

The Moment-Curvature (M-C) responses of RC columns are more realistic than the F-M responses; this is because deriving the M-C diagrams requires no pre-assumed compressive strain for the cross section. Consequently, the maximum compressive strain in M-C diagrams that are computed by equilibrium of forces in the cross section can have different values for different axial load levels.

This section explains the procedure of obtaining the F-M diagrams based on M-C diagrams. The F-M diagrams derived using this method are called *simplified curvature-based F-M* diagrams in this text.

2.4.3.1- Moment-curvature (M-C) diagrams for columns:

The basic equation for obtaining the curvature of a concrete cross section is given as^[7]:

$$\phi = \frac{\varepsilon_c}{x} \quad \text{Eq. 2. 52}$$

In this formula, ε_c is the compressive strain at the extreme compressed fiber, and x is the corresponding depth of the neutral axis.

Equation 2.52 can be written in terms of bending moment and flexure rigidity of the section as^[7]:

$$\phi = \frac{M}{EI} \quad \text{Eq. 2. 53}$$

Equations 2.52 and 2.53 are valid as long as the behavior of the cross section is linear. Having the values of ε_c and x , curvature, ϕ , is obtained from Eq.2.52; then, the corresponding bending moment can be calculated using Eq.2.53.

As Eq.2.53 shows, the bending moment is dependent on two parameters; the curvature ϕ and the flexure rigidity, EI , of the cross section. For a linear and elastic material, such as steel, it is assumed that the EI is constant through the analysis procedure; however, for a material, such as concrete, whose analysis goes very far from its elastic limit, EI is not constant. The flexure rigidity of the concrete cross section has different values through its M-C response; this is so because throughout the M-C diagram, the value of compressive strain goes up to the ultimate limit. Therefore, the flexure rigidity (EI) of the cross section is large before cracking of the concrete, and afterwards, its value decreases drastically.

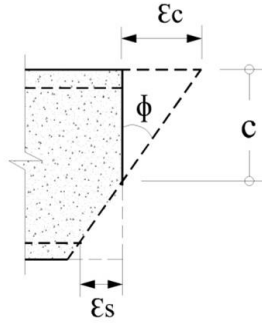


Figure 2. 14. Curvature of a cross section.

The general procedure for development of a M-C diagram for a concrete column under a given axial load is as follows: first a value for compressive strain at the top of the section is selected; then, the depth of the neutral axis (c) is assumed. After assuming the value for (c), curvature can be obtained; after obtaining the curvature, we can find the strains in concrete and steel reinforcement layers. Having the strains in the concrete and steel reinforcement, we can find corresponding internal forces of the cross section. After computing the forces in concrete and steel, we should check the depth of the neutral axis by equilibrium of forces; if the forces induced on the cross section were not in equilibrium, another depth of the neutral axis must be assumed and so on until the equilibrium of internal forces is met. Then, the value of c , at which the equilibrium of the cross section was met, along with the selected value of strain, are used to compute the bending moment and curvature of the cross section. This procedure is continued for other compressive strains; the procedure should be continued until the compressive strain is equal to the ultimate strain (or any intended value) of the concrete. The smaller the increment of the compressive strain, the more precise the M-C diagram^[34].

For a concrete cross section, there are four important points in the moment-curvature diagram. The first point is the point just before cracking point; the second is the point just after cracking; the third point is the yielding point (the point where the bottom layer of reinforcement yields), and the fourth point is the ultimate point. From the first point to the second there is a jump in the M-C diagram; this is because the moment of inertia of the section reduces when the first crack happens. This jump can occur either in the moment or in the curvature. If the moment is kept constant, the jump occurs in the curvature value; if the curvature is kept constant, the jump takes place in the moment

value. If, in a M-C diagram, the moment has the same value in the first and second points, the diagram called force-controlled M-C diagram while if the curvature has the same value in these two points, the diagram is said to be displacement-controlled M-C diagram.

Figure 2. 15 shows the simplified force-controlled and displacement-controlled M-C diagrams. There, the nonlinear behavior of concrete is simplified to linear; that is the diagrams consist of four straight lines.

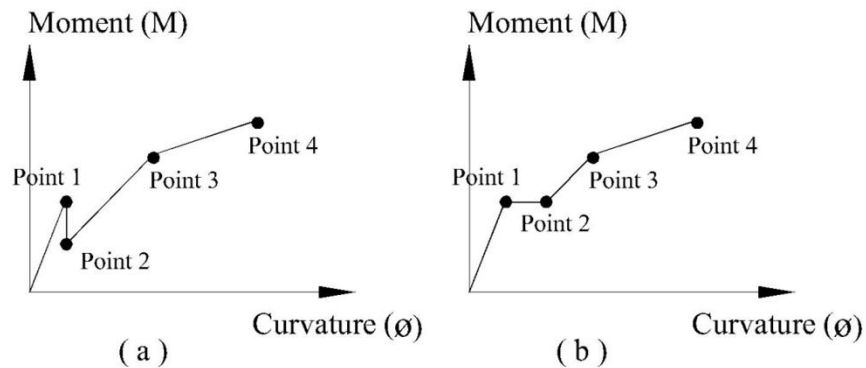


Figure 2. 15. Simplified M-C diagrams. (a) Displacement-controlled (b) force-controlled.

The simplified M-C diagrams are usually plotted by knowing the coordinates of four important points. The procedure for computing the coordinates of these points is described next. The coordinates of point one through point three are the same for confined and unconfined concrete because the lateral confining pressure is assumed to be negligible in this region^[5]. However, the coordinate of the fourth point is different for confined and unconfined concrete; this is because the fourth point is the point where the ultimate compressive strain occurs, and so the property of the cross section and the strength of the cross section are different for confined concrete compared to unconfined concrete at this point. Below is the computation procedure for obtaining the coordinates of these four points.

Starting point:

The start point is a point with zero coordinates.

Coordinates of the first point:

This point is right before cracking of the cross section; here, the maximum stress in the concrete should be equal to the modulus of rupture, f_r , of the concrete. The cross section is uncracked at this point, and the moment of inertia is equal to the moment of inertia of the gross cross section. The coordinate of this point is calculated for a given axial load (P_n) using the following formulas^[6].

$$M_1 = \frac{\left(f_r + \frac{P_n}{bh + (n-1)A_{st}} \right) I_g}{h - \bar{y}} \quad \text{Eq. 2. 54}$$

$$\phi_1 = \frac{M_1}{E_c \cdot I_g} \quad \text{Eq. 2. 55}$$

$$n = \frac{E_s}{E_c} \quad \text{Eq. 2. 56}$$

$$f_r = 7.5 \sqrt{f'_c} \quad \text{Eq. 2. 57}$$

Where I_g is the moment of inertia of the gross cross section (including the reinforcement), f_r is the modulus of rupture of the concrete, E_s is the modulus of elasticity of steel reinforcement, E_c is the modulus of elasticity of the concrete, \bar{y} is the distance from the bottom tension fiber to the neutral axis, b is the width of the cross section, h is the height of the cross section, and P_n is the axial load applied on the cross section.

Coordinates of the second point:

Since we intend to construct a force-controlled M-C diagram, for this point, the bending moment is equal to the moment of the first point, M_1 , and the curvature is computed by the following equations^[6].

$$P_n = \frac{1}{2} E_c \cdot \phi_2 \cdot c^2 \cdot b + E_c \cdot \phi_2 (c - d')(n-1)A'_s - E_c \cdot n \cdot \phi_2 (d - c)A_s \quad \text{Eq. 2. 58}$$

$$M_1 = \frac{1}{3} E_c \cdot \phi_2 \cdot c^3 \cdot b + E_c \cdot \phi_2 (c - d')^2 (n-1) A'_s - E_c \cdot n \cdot \phi_2 (d - c)^2 A_s - P_n \left(\frac{h}{2} - c \right) \quad \text{Eq. 2. 59}$$

Solving these two equations (Eq. 2.58 and 2.59) simultaneously, renders the depth of the neutral axis, c , and the curvature for the second point, ϕ_2 . Note that these equations are just for two layers of reinforcement, top and bottom. If several layers of reinforcements are used within the cross section, the general formulas are:

$$P_n = \frac{1}{2} E_c \cdot \phi_2 \cdot c^2 \cdot b + \sum E_c \cdot \phi_2 (c - d_i) (n-1) A'_{si} - \sum E_c n \cdot \phi_2 (d_i - c) A_{si} \quad \text{Eq. 2. 60}$$

$$M_1 = \frac{1}{3} E_c \cdot \phi_2 \cdot c^3 \cdot b + \sum E_c \cdot \phi_2 (c - d_i)^2 (n-1) A'_{si} - \sum E_c \cdot n \cdot \phi_2 (d_i - c)^2 A_{si} - P_n \left(\frac{h}{2} - c \right) \quad \text{Eq. 2. 61}$$

Where d_i is the distance of the i^{th} layer of reinforcement from top edge of the cross section, A'_{si} is the area of i^{th} reinforcement layer that is in compression, and A_{si} is the i^{th} reinforcement layer that is in tension. Figure 2. 16 shows more details about these parameters.

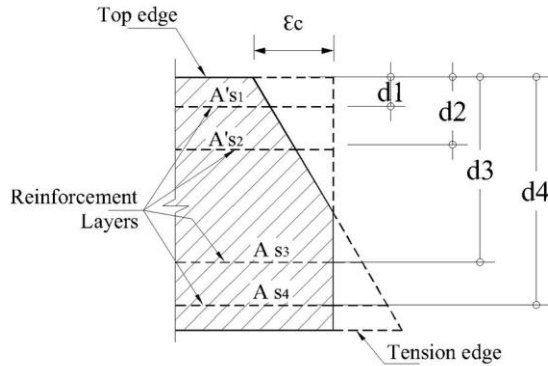


Figure 2. 16. Parameters of the generalized formula.

Coordinates of the third point:

For this point, the tensile steel in the extreme tension fiber has yielded; the tensile strain

at this location is $\varepsilon_y = \frac{f_y}{E_s}$; following are the equations^[6].

$$\phi_3 = \frac{\varepsilon_y}{d-c} \quad \text{Eq. 2. 62}$$

$$P_n = \frac{1}{2} E_c \cdot \phi_3 \cdot c^2 \cdot b + E_c \cdot \phi_3 (c-d')(n-1)A'_s - f_y \cdot A_s \quad \text{Eq. 2. 63}$$

$$M_3 = \frac{1}{3} E_c \cdot \phi_3 \cdot c^3 \cdot b + E_c \cdot \phi_3 (c-d')^2 (n-1)A'_s - E_c \cdot n \cdot \phi_3 (d-c)^2 A_s - P_n \left(\frac{h}{2} - c \right) \quad \text{Eq. 2. 64}$$

Where M_3 and ϕ_3 are the coordinates of the third point.

Coordinates of the fourth point for unconfined concrete:

For this point, the strain at the extreme compressed fiber is equal to the ultimate strain of the concrete, that is $\varepsilon_c = 0.003$.

$$\phi_4 = \frac{0.003}{c} \quad \text{Eq. 2. 65}$$

$$P_n = 0.85 f'_c \cdot \beta_1 c \cdot b + E_s \frac{c-d'}{c} 0.003 A'_s - E_s \left(\frac{d-c}{c} \right) \cdot 0.003 A_s \quad \text{Eq. 2. 66}$$

$$M_4 = 0.85 \cdot f'_c \cdot \beta_1 c \cdot b \left(\frac{h}{2} - \frac{\beta_1 c}{2} \right) + E_s \left(\frac{c-d'}{c} \right) * 0.003 \cdot A'_s \left(\frac{h}{2} - d' \right) + E_s \left(\frac{d-c}{c} \right) \cdot 0.003 \cdot A_s \left(d - \frac{h}{2} \right) \quad \text{Eq. 2. 67}$$

If the steel in top and bottom has yielded, instead of $E_s \left(\frac{d-c}{c} \right) \cdot 0.003$ and

$E_s \frac{c-d'}{c} 0.003$, f_y is used. Solving Eq.2.66 through Eq.2.67 the coordinates of the

fourth point, the ultimate moment and corresponding curvature, are obtained.

A general form for above formulas can be written as follows.

$$P = 0.85 * f'_c \cdot \beta_1 c \cdot b + \sum E_s \frac{c-d_i}{c} 0.003 * A'_{si} - \sum E_s \left(\frac{d_i-c}{c} \right) \cdot 0.003 A_{si} \quad \text{Eq. 2. 68}$$

$$M_4 = 0.85 \cdot f'_c \cdot \beta_1 c \cdot b \left(\frac{h}{2} - \frac{\beta_1 c}{2} \right) + \sum E_s \left(\frac{c-d_i}{c} \right) * 0.003 \cdot A'_{si} \left(\frac{h}{2} - d_i \right) + \sum E_s \left(\frac{d_i-c}{c} \right) \cdot 0.003 \cdot A_{si} \left(d_i - \frac{h}{2} \right) \quad \text{Eq. 2. 69}$$

As mentioned, the confinement effect is only considered for the fourth point. Also, the computation procedure for the coordinates of the fourth point for confined concrete is the same as for unconfined concrete; however, instead of using parameters of unconfined concrete, we use the parameters and properties of confined concrete.

Coordinates of the fourth point for confined concrete:

At this point, the strain at the most compressed fiber of the cross section is equal to the ultimate compressive strain of the confined concrete, ε_{cu} . Also, for this point, no concrete cover is considered^[6]:

$$\phi_4 = \frac{\varepsilon_{cu}}{c} \quad \text{Eq. 2. 70}$$

$$P_n = \alpha \cdot f'_{cc} \cdot \beta \cdot c \cdot b' + E_s \frac{c - \bar{d}}{c} \varepsilon_{ccu} \cdot A'_s - E_s \left(\frac{d_n - c}{c} \right) \cdot \varepsilon_{cu} \cdot A_s \quad \text{Eq. 2. 71}$$

$$M_4 = \alpha \cdot f'_{cc} \cdot \beta \cdot c \cdot b' \cdot \left(\frac{h'}{2} - \frac{\beta c}{2} \right) + E_s \left(\frac{c - \bar{d}}{c} \right) \cdot \varepsilon_{cu} \cdot A'_s \left(\frac{h'}{2} - \bar{d} \right) + E_s \left(\frac{d_n - c}{c} \right) \cdot \varepsilon_{cu} \cdot A_s \left(d_n - \frac{h'}{2} \right) \quad \text{Eq. 2. 72}$$

If the steel in top and bottom has yielded, instead of $E_s \left(\frac{d_n - c}{c} \right) \cdot \varepsilon_{ccu}$ and $E_s \frac{c - \bar{d}}{c} \varepsilon_{ccu}$,

f_y is used. In the above equations, f'_{cc} and ε_{cu} are obtained from equations 2.15 and 2.16, α and β are shown in figure 2.4, h' , b' , d_n , and \bar{d} are shown in Figure 2. 12.

Solving Eq.2.70 through Eq.2.72 gives us the coordinates of fourth point for the confined concrete cross section.

So far in this section has explained the procedure for constructing the simplified M-C diagram. The next section presents the process for obtaining the M-F diagram from M-C diagrams.

2.4.3.2- Obtaining the F-M diagram from M-C diagrams:

Here, the intention is to obtain the axial force-moment (F-M) diagram for RC columns based on its moment-curvature diagrams. In general, for each axial force, a maximum moment is obtainable from M-C diagram. The plot of the axial forces versus these moments is said to be the axial force-moment (F-M) diagram based on M-C diagrams. Here, a simplified F-M is obtained using M-C diagrams considering at least four different axial load levels.

Since for high level of axial loads the moment-curvature of the section is small, we assume that for pure compression and tension forces, the moment and curvature is zero. Thus, the axial load corresponding to the second point, third point, fourth point, and the fifth point of interaction diagram is first obtained. Then, for each of these axial forces, a moment-curvature (M-C) diagram is drawn; each of these M-C diagrams has a maximum moment, which is comes from the fifth point of the M-C diagram. This is illustrated in figure 2.17.

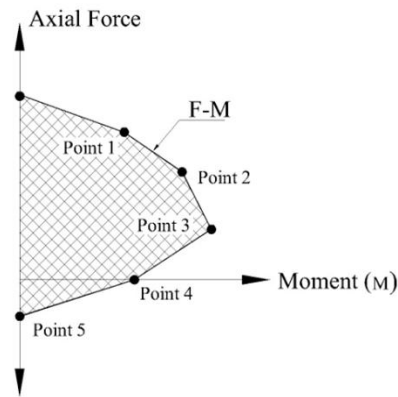


Figure 2. 17. Axial force-Moment diagram based on M-C diagrams.

Finally, the graph of the axial force versus maximum moment is plotted; this graph is called the *curvature-based* F-M diagram within this study.

2.4.4- Detailed method:

So far, section 2.4 has presented the simplified methods for obtaining the axial force-bending moment diagrams and moment-curvature diagrams for a RC column; these methods were called simplified methods since the exact distribution of compression stress was simplified to an equivalent rectangular stress block. Next, this section discusses the detailed method. The only difference between the detailed and the simplified method is that in the detailed method, the exact distribution of compressive stress within the cross section is used; by exact stress distribution, we mean the stress distribution that is directly derived from stress-strain curves. Therefore, in the detailed method, the role of the material model is evident; this is because the exact distribution of stress comes from the material model used in the analysis.

Several methods, such as the finite element method and the fiber-element model, can be used to find the exact stress distribution over the cross section^[35]. The fiber-element method is one of those methods that are used to construct this exact stress distribution. In the fiber-element model, the cross section is divided into thin strips; these strips can be either in one or two directions, depending on whether the bending moment is uniaxial or biaxial. Figure 2.18 illustrates a concrete column cross section divided into strips; figure 2.18a, which shows the strips are in two directions, is used for a column under biaxial bending moment; figure 2.18b that indicates the strips in one direction can be used for a column cross section under uniaxial bending.

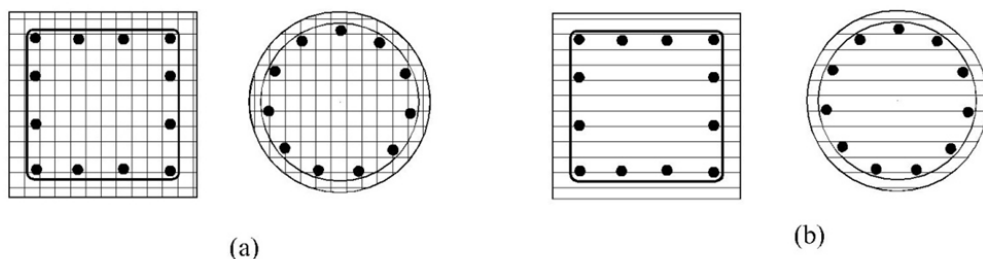


Figure 2. 18. The cross section discretization in fiber-element model.

Once the cross section is divided into thin fibers, the compressive strain for the extreme fiber is selected (as in the simplified method). With the number of strips within the cross

section and strain at the most compressed strip, the strain in each strip is obtained using the flexure theory. Next, having the strain distribution over the cross section, a computational algorithm, such as Monte Carlo stimulation^[36], along with a material model, such as Mander model^[26], is used to obtain the stress distribution over the cross section. Then, numerical integration is used to calculate the compression force under the compression stress distribution; the internal forces for steel reinforcement are simply determined by multiplying the stress in each reinforcement layer by the corresponding steel area. Once the internal forces are derived, axial load and bending moment of the cross section are computed using the equilibrium concept.

In this report, the fiber-element method is implemented by KSU-RC software^[37] developed by Dr. Asad Esmaily, associated professor in the Civil Engineering Department at Kansas State University. The KSU-RC software uses the fiber-element model for constructing the confined and unconfined F-M and M-C diagrams for both circular and rectangular cross sections under uniaxial bending; the software has other capabilities, though. In the current version of the software, the Mander model is used for both unconfined and confined concrete and also the user is able to use the custom model. Therefore, this software uses three different strain-stress models for analyzing concrete cross sections; steel, unconfined and confined concrete.

To find the axial force-bending moment diagrams for a RC column using this software, some inputs should be assigned to the software: the properties of the cross section is assigned, the number of the strips of the cross section is selected, and also the compressive strain at the extreme fiber is given. Then, using these input data, the software plots the F-M diagram. These outputs should also be given to derive the M-C diagram; however, since M-C diagrams are not constructed for a constant compressive strain, a limiting value for strain is given instead.

Figure 2. 19 shows the interface of the KSU-RC software.

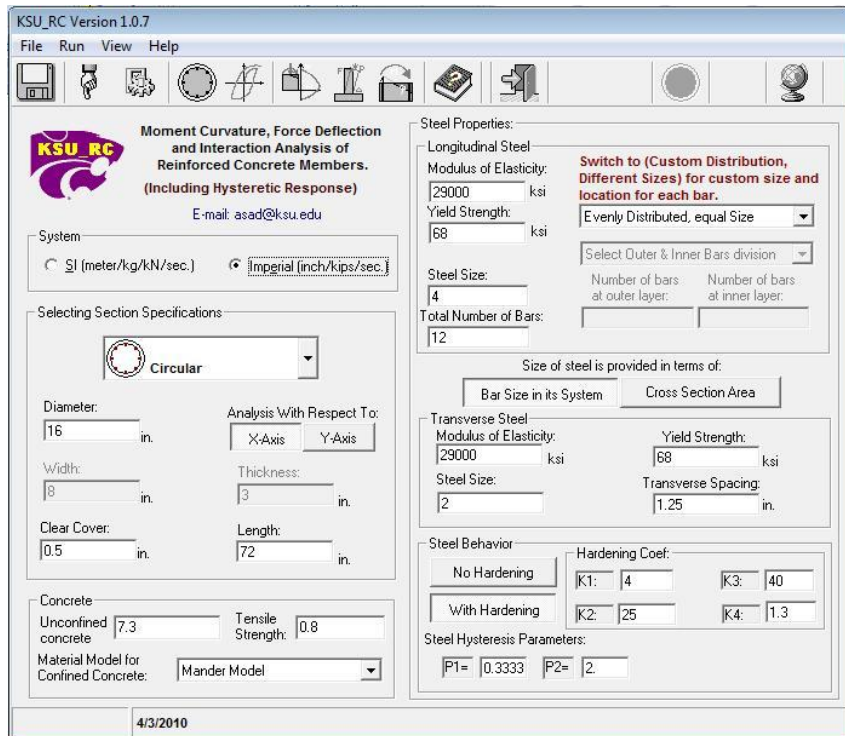


Figure 2. 19. KSU-RC interface [37].

In this research, the detailed F-M diagrams and the detailed M-C diagrams for both confined and unconfined RC columns are obtained directly with the KSU-RC software. Finally, the detailed curvature-based F-M diagrams are derived by using the detailed M-C diagrams.

Chapter Three- Exploring Analytical Methods

3.1- Chapter opening:

In chapter two, different analytical methods for obtaining the F-M diagrams were discussed. In this chapter, these methods are used to construct F-M diagrams for two RC columns, one with circular and the other with square cross section.

In section 3.2, the aforementioned analytical methods are used to obtain the F-M diagrams for unconfined cross sections. Next, in section 3.3, these methods are employed to construct the F-M diagrams for confined cross sections. These analytical methods will be compared in the next chapter. The methods will, then, be validated against the existing experimental results to spot the best method that can provide a realistic, yet conservative prediction of the strength and behavior of a reinforced concrete column.

3.2- Computation of F-M diagrams for unconfined RC columns:

As it was pointed out, two concrete columns are chosen to be analyzed. Here, in this section, confinement is not considered; both simplified and detailed methods are used to obtain the unconfined F-M diagrams. Following is the detail for column cross sections.

$f'_c = 4000$ psi.
 $f_y = 60000$ psi.
clear cover = 2 in.
 $E_s = 29000$ Ksi.
12 # 9 longitudinal bars
3 @ 4 in. stirrups

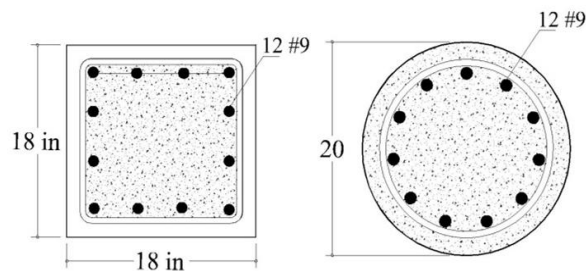


Figure 3. 1. Columns' cross sections.

3.2.1- Computation of F-M diagram based on the simplified method:

To find the simplified-unconfined F-M diagram, the procedure of section 2.4.1 is used. Following is the procedure for a square cross section.

Coordinates for the first point:

$$\text{Gross cross section area} = A_g = 18 \cdot 18 = 324 \text{ in}^2.$$

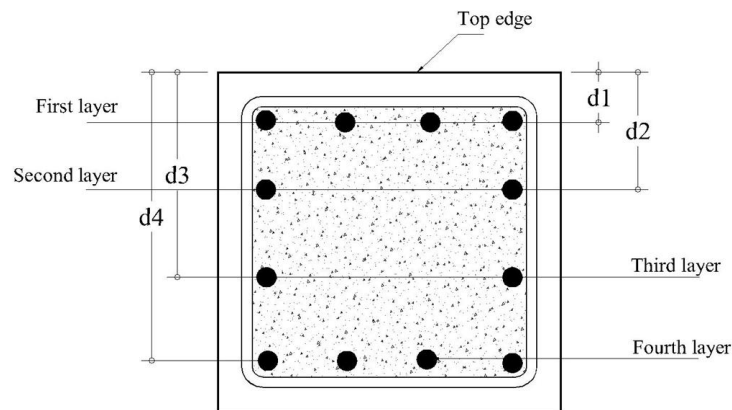
$$\text{Area of steel reinforcement} = A_s = 12 \cdot \left(\frac{3.14}{4}\right) \cdot \left(\frac{9}{8}\right)^2 \approx 12 \text{ in}^2.$$

$$P_{O_n} = 0.85 f'_c \cdot (A_g - A_s) + f_y \cdot A_s = 0.85 \cdot 4 \cdot (324 - 12) + 60 \cdot 12 = 1781 \text{ kips}.$$

So, the coordinates of this point are (0, 1781).

Coordinates for the second point:

At this point, the tensile strain at the bottom layer of reinforcement is zero; therefore, the depth of the neutral axis is equal to d_4 ; the depth of all the layers of reinforcement is shown below.



$$\text{Depth of the neutral axis} = c = d_4 = 18 - 2 \cdot \left(\frac{3}{8}\right) - \left(\frac{9}{16}\right) = 15.1 \text{ in}.$$

$$\text{Depth of the ACI stress block} = a = \beta \cdot c = 0.85 \cdot 15.1 = 12.83 \text{ in}.$$

$$\text{Strain in the first layer} = \varepsilon_1 = \frac{0.003}{c} (c - d_1) = \frac{0.003}{15.1} (15.1 - 2.94) = 0.00242$$

$$\text{Strain in the second layer} = \varepsilon_2 = \frac{0.003}{c} (c - d_2) = \frac{0.003}{15.1} (15.1 - 6.98) = 0.00161$$

$$\text{Strain in the third layer} = \varepsilon_3 = \frac{0.003}{c}(c - d_3) = \frac{0.003}{15.1}(15.1 - 11) = 0.00082$$

$$\text{Strain in the fourth layer} = \varepsilon_4 = \frac{0.003}{c}(c - d_4) = \frac{0.003}{15.1}(15.1 - 15.1) = 0.00$$

$$\text{Stress in the first layer} = f_1 = \varepsilon_1 \cdot E = 0.00242 \cdot 29000 = 70.18 \text{ ksi}$$

Since this value is greater than $f_y=60$ kis, use $f_1=60$ ksi.

$$\text{Stress in the second layer} = f_2 = \varepsilon_2 \cdot E = 0.00161 \cdot 29000 = 46.7 \text{ ksi}$$

$$\text{Stress in the third layer} = f_3 = \varepsilon_3 \cdot E = 0.00082 \cdot 29000 = 23.8 \text{ ksi}$$

$$\text{Stress in the fourth layer} = f_4 = \varepsilon_4 \cdot E = 0.00 \cdot 29000 = 0.00 \text{ ksi}$$

$$\text{Force in the first layer} = F_1 = f_1 \cdot A_1 = 60 \cdot 4 = 240 \text{ kips}$$

$$\text{Force in the second layer} = F_2 = f_2 \cdot A_2 = 46.7 \cdot 2 = 93.4 \text{ kips}$$

$$\text{Force in the third layer} = F_3 = f_3 \cdot A_3 = 23.8 \cdot 2 = 47.6 \text{ kips}$$

$$\text{Force in the fourth layer} = F_4 = f_4 \cdot A_4 = 0 \cdot 4 = 0.00 \text{ kips}$$

$$\text{Force in the concrete} = C_c = 0.85 \cdot f'_c \cdot ab = 0.85 \cdot 4 \cdot 18 \cdot 12.83 = 785.2 \text{ kips}$$

$$\text{Total nominal Axial force} = P_n = C_c + F_1 + F_2 + F_3 + F_4 = 1166.2 \text{ kips}$$

$$\text{Nominal bending moment} = M_n = C_c \left(\bar{x} - \frac{a}{2} \right) + \sum_{i=1}^n (F_{si} (\bar{x} - di))$$

$$M_n = 785.2 \left(\frac{18}{2} - \frac{12.83}{2} \right) + 240(9 - 2.94) + 93.4(9 - 6.98) + 47.6(9 - 11) = 3577.6 \text{ kip.in}$$

Thus, the nominal coordinates of the second point are (**3577.6** , **1166.2**).

Coordinates for the third point:

At this point, the strain at the lower layer of reinforcement is equal to the yield strain of steel reinforcement.

Strain in the fourth layer =

$$\varepsilon_4 = \frac{0.003}{c}(c - d_4) = \frac{0.003}{c}(c - 15.1) = -60/29000 = -0.00207$$

$$c = 8.94 \text{ in.}$$

Depth of neutral axis =

$$\text{Depth of compression block} = a = \beta \cdot c = 0.85 \cdot 8.94 = 7.6 \text{ in..}$$

$$\text{Strain in the first layer} = \varepsilon_1 = \frac{0.003}{c}(c - d_1) = \frac{0.003}{8.94}(8.94 - 2.94) = 0.0020$$

$$\text{Strain in the second layer} = \varepsilon_2 = \frac{0.003}{c}(c - d_2) = \frac{0.003}{8.94}(8.94 - 6.98) = 0.00066$$

$$\text{Strain in the third layer} = \varepsilon_3 = \frac{0.003}{c}(c - d_3) = \frac{0.003}{8.94}(8.94 - 11) = -0.0007$$

$$\text{Stress in the first layer} = f_1 = \varepsilon_1 \cdot E = 0.0020 \cdot 29000 = 58 \text{ ksi.}$$

$$\text{Stress in the second layer} = f_2 = \varepsilon_2 \cdot E = 0.00066 \cdot 29000 = 19.14 \text{ ksi.}$$

$$\text{Stress in the third layer} = f_3 = \varepsilon_3 \cdot E = -0.0007 \cdot 29000 = -20.3 \text{ ksi.}$$

$$\text{Stress in the fourth layer} = f_4 = \varepsilon_4 \cdot E = -0.00207 \cdot 29000 = -60 \text{ ksi.}$$

$$\text{Force in the first layer} = F_1 = f_1 \cdot A_1 = 58 \cdot 4 = 232 \text{ kips.}$$

$$\text{Force in the second layer} = F_2 = f_2 \cdot A_2 = 19.14 \cdot 2 = 38.3 \text{ kips.}$$

$$\text{Force in the third layer} = F_3 = f_3 \cdot A_3 = -20.3 \cdot 2 = -40.6 \text{ kips.}$$

$$\text{Force in the fourth layer} = F_4 = f_4 \cdot A_4 = -60 \cdot 4 = -240 \text{ kips.}$$

$$\text{Force in the concrete} = C_c = 0.85 \cdot f'_c \cdot a \cdot b = 0.85 \cdot 4 \cdot 18 \cdot 7.6 = 465 \text{ kips.}$$

$$\text{Total nominal Axial force} = P_n = C_c + F_1 + F_2 + F_3 + F_4 = 455 \text{ kips.}$$

$$\text{Nominal bending moment} = M_n = C_c \left(\bar{x} - \frac{a}{2} \right) + \sum_{i=1}^n (F_{si}(\bar{x} - di))$$

$$M_n = 465 \left(\frac{18}{2} - \frac{7.6}{2} \right) + 232(9 - 2.94) + 38.3(9 - 6.98) - 40.6(9 - 11) - 240(9 - 15.1)$$

$$M_n = 5446.5 \text{ Kip.in.}$$

Thus, the coordinates of the third point is (**5446.5 , 455**).

This process can be employed to get the coordinates of the other points.

Coordinates of Fourth point = (4578 , 61)

Coordinates of Fifth Point = (4325 , 0.00)

Coordinates of Sixth point = (0.00 , - 720)

Finally, the simplified-unconfined F-M diagram for this cross section is plotted as in figure 3.2(a) .

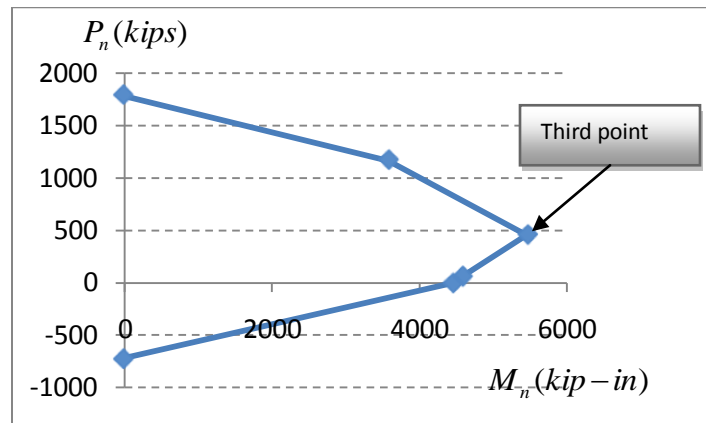


Figure 3. 2 (a). Simplified-unconfined F-M diagram for square cross section.

As the graph shows, the maximum moment occurs approximately at the third point, where the strain in the steel is just equal to the yielding steel strain (-0.00207). At this point the moment is 5446.5 kip-in. For a more accurate diagram, increase the number of data points; figure 3.2(b) presents the simplified-unconfined F-M diagram for this cross section with more data points.

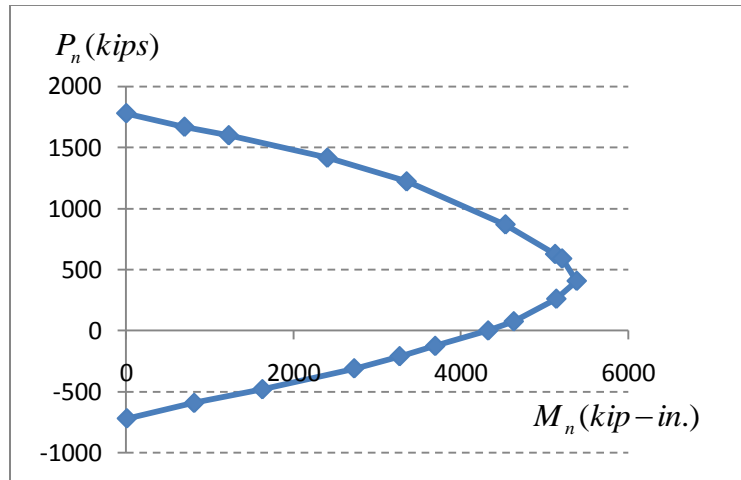


Figure 3.2(b). Simplified-unconfined F-M diagram for square cross section with more data points.

A similar procedure can be used to obtain the simplified F-M diagram for an unconfined circular cross section. Figure 3. 3 shows the simplified-unconfined F-M diagram for the proposed circular cross section.

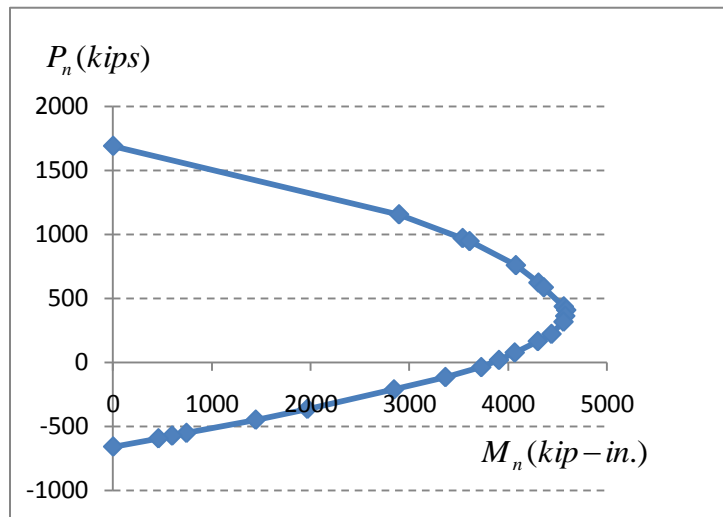


Figure 3. 3. Simplified-unconfined F-M for circular concrete column

3.2.2- Obtaining F-M diagram based on simplified-curvature-based method:

Moment-curvature diagrams for concrete columns are computed based on a given axial load; for each axial load level, there is a specific M-C diagram for a column. For the columns given in section 3.2, to find the F-M diagram from M-C diagrams' data, we should have one M-C diagram for each axial load; these axial loads can be those that are calculated for each point of the F-M diagram. For illustration, the axial force in the third point of the simplified-unconfined F-M diagram, which is shown in figure 3.2a, is considered; meanwhile, the simplified moment-curvature diagram for the square cross section is obtained using the procedure in section 2.4.3. Below is the procedure for obtaining the simplified M-C diagram for square cross section.

Concrete modulus of elasticity = $E_c = 57000 (f'_c)^{1/2} = 3605$ ksi.

Steel modulus of elasticity = $E_s = 29000$ ksi.

Concrete modulus of fracture = $f_r = 7.5\sqrt{f'_c} = 0.4743$ ksi.

$$n = E_s / E_c = 8.044$$

$$P_n = 455 \text{ Kips.}$$

Coordinates for the starting point :

The coordinates of this point is (0.00 , 0.00)

Coordinates for the first point:

$$f_r = \frac{M_1 \cdot \bar{y}_t}{I_g} - \frac{P_n}{b \cdot h + (n-1)A_{st}} = 0.4743$$

Where $\bar{y}_t = 9$ in. is the distance from the centroid of the cross section to the tensile fiber,

$$I_g = \frac{18^4}{12} + 2183 \text{ (} I_g \text{ is the transformed moment of inertia); } A_{st} \text{ is the total reinforcement}$$

area within the cross section.

$$M_1 = 1928.5 \text{ kip.in.}$$

$$\phi_1 = \frac{M_1}{E_c \cdot I_g} = \frac{1928.5}{3605 \cdot 10931} = 0.000049 \quad \text{in}^{-1}.$$

So, the coordinates of the first point are (**0.000049 ; 1928.5**).

Coordinates for the second point:

We will plot the displacement-controlled M-C diagram; therefore, the curvature at this point is the same as the curvature at the first point.

From the equilibrium of forces within the cross section we have:

$$P_n = (1/2)E_c \cdot \phi_1 \cdot c^2 \cdot b + E_c \cdot \phi_1(n-1)(c-d_1)A_{s1} + E_c \cdot \phi_1(n-1)(c-d_2)A_{s2} \\ + E_c \cdot \phi_1(n)(c-d_3)A_{s3} + Ec \cdot \phi_1(n)(c-d_4)A_{s4}$$

In the above equation the only unknown term is the depth of the neutral axis, c . So:
c =15.12 in.

Having c, we can get the bending moment at this point as:

$$M_2 = (1/3)E_c \cdot \phi_1 \cdot c^3 \cdot b + E_c \cdot \phi_1 \cdot (n-1)(c-d_1)^2 A_{s1} + E_c \cdot \phi_1(n-1)(c-d_2)^2 A_{s2} \\ + E_c \cdot \phi_1(n)(c-d_3)^2 A_{s3} + E_c \cdot \phi_1(n)(c-d_4)^2 A_{s4} - P_n(c-h/2)$$

$$M_2 = 1824 \quad \text{kip-in.}$$

Therefore, the coordinates of the second point are (**0.000049 ; 1824**) .

Note that the points are shown in figure below.

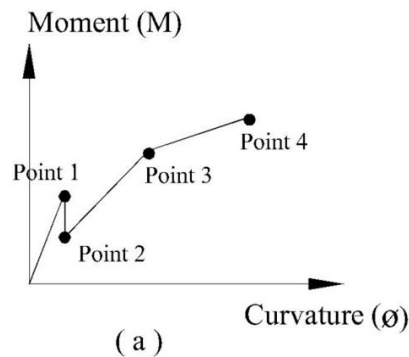


Figure 3. 4. M-C diagram Point labeling.

Coordinates for the third point:

This is the point at which the bottom reinforcement layer yields. The curvature and moment at this point are computed as follows:

$$\phi_3 = \frac{\varepsilon_y}{d_4 - c} = \frac{f_y / E_s}{d_4 - c} = \frac{0.00207}{15.1 - c}$$

$$P_n = (1/2)E_c \cdot \phi_3 \cdot c^2 \cdot b + E_c \cdot \phi_3 \cdot (n-1)(c-d_1)A_{s1} + E_c \cdot \phi_3(n-1)(c-d_2)A_{s2} \quad c = 7.92 \text{ in.} \\ + E_c \cdot \phi_3(n)(c-d_3)A_{s3} - 60 \cdot A_{s4} = 455$$

$$\phi_3 = \frac{0.00207}{15.1 - 7.92} = 0.000288 \text{ in}^{-1}.$$

$$\text{Compressive strain in the top fiber of concrete} = \varepsilon_c = c \cdot \phi_3 = 0.00228$$

Since at this strain the concrete is not linear, the concept of equivalent stress block should be employed. So;

$$\text{Compression force in the concrete} = C_c = 0.85 f'_c \cdot 0.85 \cdot c \cdot b$$

$$P_n = 0.85 f'_c \cdot 0.85 \cdot c \cdot b + E_c \cdot \phi_3(n-1)(c-d_1)A_{s1} + E_c \cdot \phi_3(n-1)(c-d_2)A_{s2} \\ + E_c \cdot \phi_3(n)(c-d_3)A_{s3} - 60 \cdot A_{s4} = 455 \text{ kips.}$$

Thus, the depth of the neutral axis is $c = 8.93$ in.

$$\phi_3 = \frac{0.00207}{15.1 - 9} = 0.000335 \text{ in}^{-1}.$$

$$\varepsilon_c = c \cdot \phi_3 = 0.00299 \approx 0.003$$

So, the compressive strain at the top edge of the concrete is equal to the ultimate strain 0.003.

$$\text{Strain in the first layer} = \varepsilon_1 = 0.000335(c-d_1) = 0.000335(8.93-2.94) = 0.00201$$

$$\text{Strain in the second layer} = \varepsilon_2 = 0.000335(c-d_2) = 0.000335(8.93-6.98) = 0.000653$$

$$\text{Strain in the third layer} = \varepsilon_3 = 0.000335(c-d_3) = 0.000335(8.93-11) = -0.000693$$

$$\text{Strain the fourth layer} = -\frac{f_y}{E_s} = -0.00207$$

$$\text{Stress in the first layer} = f_1 = \varepsilon_1 \cdot E = 0.00201 \cdot 29000 = 58.3 \text{ ksi.}$$

$$\text{Stress in the second layer} = f_2 = \varepsilon_2 \cdot E = 0.000653 \cdot 29000 = 18.94 \text{ ksi.}$$

$$\text{Stress in the third layer} = f_3 = \varepsilon_3 \cdot E = -0.000693 \cdot 29000 = -20.1 \text{ ksi.}$$

$$\text{Stress in the fourth layer} = f_4 = \varepsilon_4 \cdot E = -0.00207 \cdot 29000 = -60 \text{ ksi.}$$

$$\text{Force in the first layer} = F_1 = f_1 \cdot A_1 = 58.3 \cdot 4 = 233.2 \text{ kips.}$$

$$\text{Force in the second layer} = F_2 = f_2 \cdot A_2 = 18.94 \cdot 2 = 37.9 \text{ kips.}$$

$$\text{Force in the third layer} = F_3 = f_3 \cdot A_3 = -20.1 \cdot 2 = -40.2 \text{ kips.}$$

$$\text{Force in the fourth layer} = F_4 = f_4 \cdot A_4 = -60 \cdot 4 = -240 \text{ kips.}$$

$$\text{Force in the concrete} = C_c = 0.85 f'_c a \cdot b = 0.85 \cdot 4 \cdot 18 \cdot 0.85 \cdot 8.93 = 464.5 \text{ kips.}$$

$$M_3 = 464.5 \left(\frac{18}{2} - \frac{0.85 \cdot 8.93}{2} \right) + 233.2(9 - 2.94) + 37.9(9 - 6.98) - 40.2(9 - 11) - 240(9 - 15.1)$$

$$M_3 = 5447.7 \text{ kip-in.}$$

Thus, the coordinates of the third point are (**0.000339 ; 5451.7**) .

Coordinates for the fourth point:

This is the point where the compressive strain at the top concrete fiber reaches the ultimate value, 0.003. For this particular axial load level, the coordinates are equal to the coordinates of the third point. This is so because the given axial load corresponds to the balance point of the simplified F-M diagram; at the balance point, the compressive strain at the top edge of the cross section is equal to the ultimate value (0.003), and the tensile strain at the bottom layer of reinforcement is equal to the yielding strain. So, in a simplified M-C diagram for this axial load both yielding of the steel and ultimate strain of the concrete occur simultaneously.

Therefore, the coordinates of the fourth point are (**0.000339 ; 5451.7**) .

Figure 3. 5 shows the simplified-unconfined M-C diagram for this cross section under 455 kips axial load.

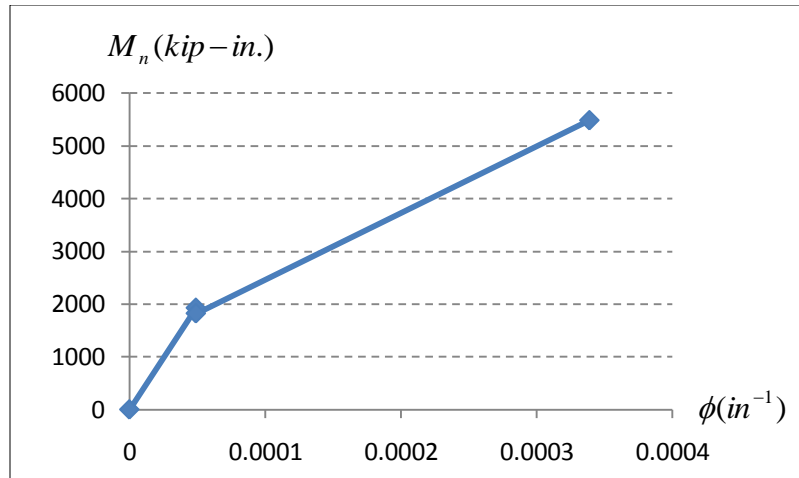


Figure 3. 5- Simplified-unconfined Moment-Curvature diagram for axial load of 455 kips.

The same procedure applies to compute the M-C for all other axial load levels.

As the figure shows, the maximum bending moment based on the simplified-unconfined M-C diagram for an axial load of 455 kip is 5447.7 kip-in. Also, based on the simplified-unconfined F-M diagram for this column, the bending moment corresponding to this axial load is 5446.5 kip-in; this little change (5447.7-5446.5) in bending moment value is negligible. So, these two moments are approximately equal to each other. If the computations are done for the other points, the same result will be obtained. This is because at the ultimate point (fourth point in simplified M-C diagram) it is assumed that the maximum bending moment occurs at the ultimate strain (0.003 for unconfined concrete); in F-M diagrams it is also assumed that at the ultimate strain the bending capacity of the cross section is maximum for any axial load level. Therefore, in both simplified F-M and simplified M-C diagrams the same assumptions are employed, and, consequently, the results of these two diagrams are the same.

Thus, we can say that the simplified-unconfined moment-force diagrams are exactly the same as the simplified- unconfined curvature-based F-M diagrams.

3.2.3- Constructing the F-M diagrams based on detailed methods:

In this section, we will derive the unconfined F-M and unconfined M-C diagrams by detailed methods. Computations of these diagrams are done using the KSU-RC software.

Figure 3.6 shows F-M diagrams for circular and square columns that were already detailed. For obtaining these F-M diagrams, a constant compressive strain of 0.003 was considered at the most compressed fiber of the cross section.

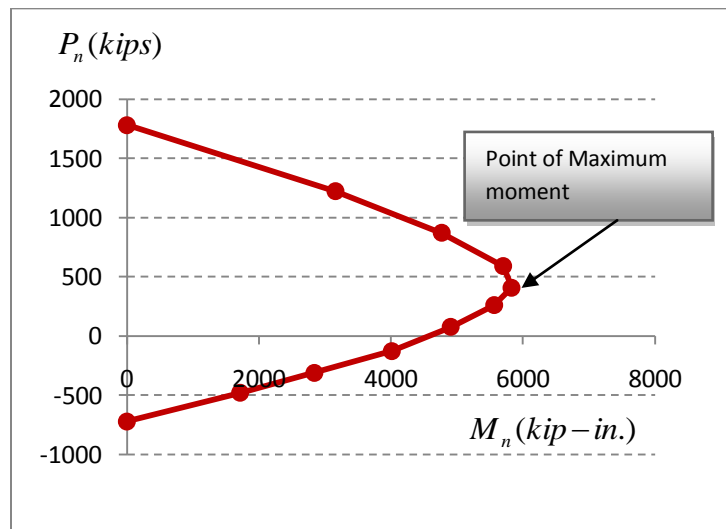


Figure 3. 6 (a). Detailed-unconfined F-M diagram for square cross section.

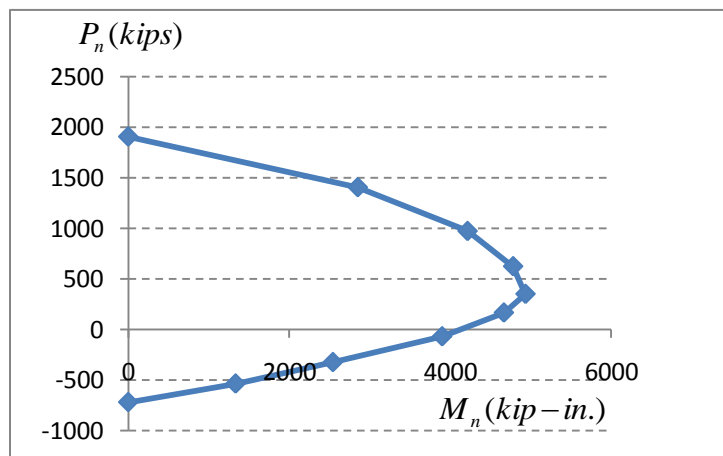


Figure 3.6b- Detailed-unconfined F-M diagram for circular cross section.

Based on Figure 3. 6(a) , the maximum moment is 5828 kip-in., and the corresponding axial force is 407.2 kips. At the point of maximum moment, the depth of the neutral axis is 8.08 in. and corresponding curvature is 0.00037 in^{-1} .

Figure 3. 6 shows unconfined-detailed F-M diagrams for concrete columns. To draw the unconfined F-M diagrams based on the detailed-curvature-based method, it is needed to obtain the M-C diagram for these cross sections for a limiting compressive strain of 0.003 (unconfined concrete). To draw the F-M diagram by using M-C diagrams, we need to have the M-C diagram for the axial load of each point on figure 3.6; then, for each axial load, we will choose the maximum moment from the corresponding M-C diagram. Finally, the plot of these axial loads versus the corresponding maximum bending moments gives us the detailed-unconfined curvature-based F-M diagram.

Figure 3.7 shows the detailed moment-curvature diagram for an unconfined square cross section for an axial load of 407.2 kips. This graph is produced by the software using a limiting compressive strain of 0.003.

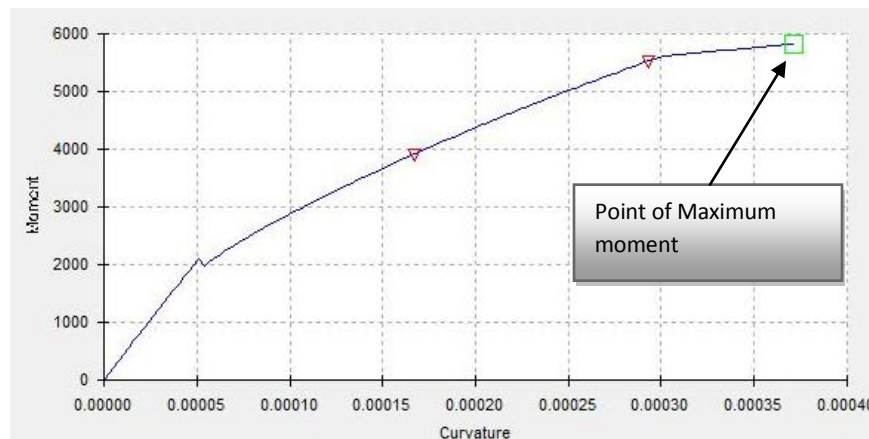


Figure 3.7. Detailed-unconfined M-C diagram for axial load of 407.2 kips.

Figure 3.7 shows that the maximum bending moment is exactly 5828 kip-in; the corresponding compression strain is exactly 0.003.

Therefore, this bending moment is equal to the one that was determined from the detailed-unconfined F-M diagram; this result can be shown also for other axial load

levels. So, if the detailed-unconfined curvature-based F-M diagram were to be plotted, it would be the same as the detailed-unconfined F-M diagram.

Thus, we can say that the detailed-unconfined F-M diagram is exactly the same as the detailed-unconfined curvature-based F-M diagram.

3.3- Computation of F-M diagrams for confined cross sections:

In section 3.2, simplified and detailed methods were used to obtain the F-M diagrams for unconfined concrete. In this section we intend to do the same but for confined concrete columns; for simplicity, the aforementioned column's cross sections will be used. Following are the details of the square cross section repeated.

Height of the section $h = 18$ in

Width of the section $b = 18$ in.

Concrete cover = 2 in.

Compressive strength of the concrete $f'_c = f'_{co} = 4$ ksi.

Steel yield strength $f_y = 60$ ksi.

Elastic modulus of elasticity of steel $E_s = 29000$ ksi.

Modulus of elasticity of concrete $E_c = 3605$ Ksi.

Transverse reinforcement = #3 @ 4 in.

Longitudinal reinforcement = 12 # 9 bars evenly distributed.

Confined core concrete dimensions:

$$h' = 18 - 2 - (3/8) - 2 - (3/8) = 13.25 \text{ in.} \quad b' = h'$$

$$d_1 = (3/16) + (9/16) = 0.75 \text{ in.} \quad d_2 = d_1 + 4.04 = 4.79 \text{ in.}$$

$$d_3 = d_2 + 4.04 = 8.83 \text{ in.} \quad d_4 = d_3 + 4.04 = 12.87 \text{ in.}$$

Before starting the computations of confined F-M and M-C diagrams, it is needed to find the properties and parameters of confined concrete; this is done using the Mander model for confined concrete. Following is the procedure.

$$\rho_{cc} = \frac{A_{st}}{A_g} = \frac{12}{h' \cdot b'} = \frac{12}{(13.25)^2} = 0.0684$$

$$k_e = \frac{\left(1 - \sum_{i=1}^n \frac{(w'_i)^2}{6b'_c \cdot d'_c}\right)}{(1 - \rho_{cc})} \left(1 - \frac{s'}{2b'_c}\right) \left(1 - \frac{s'}{2d'_c}\right) \quad \text{where } w'_i = 4.04 - (9/8) = 2.92 \text{ in.}$$

$$s' = 4 - (3/8) = 3.625 \text{ in.} \quad b'_c = b' \quad \text{and} \quad d'_c = h'$$

$$k_e = \frac{\left(1 - 12 \frac{2.92}{6 \cdot 13.25 \cdot 13.25}\right)}{(1 - 0.0684)} \left(1 - \frac{3.625}{2 \cdot 13.25}\right) \left(1 - \frac{3.625}{2 \cdot 13.25}\right) = 0.773$$

$$k_e = \frac{A_e}{A_{cc}} \Rightarrow A_e = A_{cc} \cdot k_e = 13.25 \cdot 13.25 \cdot 0.773 = 135.7 \text{ in}^2.$$

$$\text{Area of the transverse reinforcement } A_{sx} = 4 \cdot (\pi/4)(3/8)^2 = 0.221 \text{ in}^2. \quad A_{sy} = A_{sx}$$

$$\rho_x = \frac{Asx}{s \cdot b'_c} = \frac{0.221}{4 \cdot 13.25} = 0.00417 \quad \rho_y = \rho_x$$

$$\rho_s = \rho_x + \rho_y = 0.00834$$

$$f_{lx} = \rho_x \cdot f_y = 0.00417 \cdot 60 = 0.2502 \text{ ksi.} \quad f_{ly} = \rho_y \cdot f_y = f_{lx} = 0.2502 \text{ ksi.}$$

$$f'_{lx} = k_e \cdot f_{lx} = 0.773 \cdot 0.2502 = 0.193 \text{ ksi.} \quad f'_{ly} = k_e \cdot f_{ly} = f'_{lx} = 0.193$$

$$\frac{f'_{lx}}{f'_{co}} = \frac{f'_{ly}}{f'_{co}} = \frac{0.193}{4} = 0.0484 \cong 0.05$$

$$\text{From figure 2.3: } K = \frac{f'_{cc}}{f'_{co}} = 1.4 \Rightarrow f'_{cc} = 1.4 \cdot f'_{co} = 1.4 \cdot 4 = 5.6 \text{ ksi.}$$

$$\varepsilon_{cc} = \varepsilon_{co} \left[1 + 5 \left(\frac{f'_{cc}}{f'_{co}} - 1 \right) \right] = 0.002 \left[1 + 5 \left(\frac{5.6}{4} - 1 \right) \right] = 0.006$$

$$\varepsilon_{cu} = 0.004 + 1.4 \rho_s \frac{f_y \cdot \varepsilon_{sm}}{f'_{cc}} = 0.004 + 1.4 \cdot 0.00834 \frac{60 \cdot 0.1}{5.6} = 0.0165$$

(The value of ϵ_{sm} is 0.1 for steel grade 60 and 0.15 for steel grade 40 ksi.)

$$\frac{\epsilon_{cu}}{\epsilon_{cc}} = \frac{0.0165}{0.006} = 2.75$$

From figure 2.4 we can find $\beta = 0.95$ and $\beta\alpha = 0.9$ and, thus, $\alpha = 0.95$.

3.3.1- Confined F-M diagrams based on simplified method:

Now that we have the compressive strength of confined concrete f'_{cc} , the maximum strain for confined concrete ϵ_{cc} , and the ultimate strain for confined concrete ϵ_{cu} , we can draw the F-M diagram for confined cross section. To do so, we consider a strain equal to the ultimate strain ϵ_{cu} at the extreme compressed edge of the cross section and select different values for tensile strain at the bottom layer of reinforcement; this process is continued until a reasonable value of tensile strain at the bottom layer is reached, say (0.008). Then we assume the tensile strain at the bottom layer of reinforcement to be constant; next, the compressive strain is decreased from ϵ_{cu} to a tensile strain equal to, at least, the yielding strain of the reinforcement. Following is the procedure for a few points for the square cross section.

Coordinates for the first point (pure compression):

$$P_n = \alpha \cdot \beta \cdot f'_{cc} \cdot (b' \cdot h' - 12) + 60 \cdot 12 = 0.95 \cdot 0.95 \cdot 5.6 \cdot (13.25^2 - 12) + 720 = 1547 \text{ Kips.}$$

The bending moment at this point is zero. So, the coordinates of this point on F-M diagram is (0.0 ; 1547).

Coordinates for the second point (where the strain at the bottom layer of reinforcement is zero):

At this point the depth of the neutral axis is equal to d_4 ; that is $c = d_4 = 12.87$ in. having the depth of the neutral axis and the compressive strain at the top, the strain in other reinforcement layers can be calculated.

$$\frac{\varepsilon_{cu}}{d_4} = \frac{\varepsilon_{cu}}{c} = \frac{0.0165}{12.87} = \frac{\varepsilon_{s1}}{c - d_1} = \frac{\varepsilon_{s1}}{12.87 - 0.75}$$

$$\varepsilon_{s1} = \frac{0.0165}{c} (c - d_1) = 0.016$$

$$\varepsilon_{s2} = \frac{0.0165}{c} (c - d_2) = 0.0104$$

$$\varepsilon_{s3} = \frac{0.0165}{c} (c - d_3) = 0.0052$$

$$\varepsilon_{s4} = \frac{0.007}{c} (c - d_4) = 0.00$$

Stresses in the reinforcement:

$f_{s1} = \varepsilon_{s1} \cdot 29000 = 464$ ksi. since this is more than the yielding stress 60, we take it as 60 ksi.

$f_{s2} = \varepsilon_{s2} \cdot 29000 = 302$ ksi. > 60 ; use $f_{s2} = 60$ ksi.

$f_{s3} = \varepsilon_{s3} \cdot 29000 = 151$ ksi. > 60 ; use $f_{s3} = 60$ ksi.

$f_{s4} = \varepsilon_{s4} \cdot 29000 = 0.00$ Ksi.

Forces in concrete and in the steel:

Concrete force: $C_c = \alpha \cdot f'_{cc} \cdot \beta \cdot c \cdot b' = 0.95 \cdot 5.6 \cdot 0.95 \cdot 12.87 \cdot 13.25 = 861$ kips.

Force in first layer: $F_1 = (f_{s1} - \alpha \cdot f'_{cc}) \cdot A_{s1} = 54.6 \cdot 4 = 218.4$ kips.

Force in second layer: $F_2 = (f_{s2} - \alpha \cdot f'_{cc}) \cdot A_{s2} = 54.6 \cdot 2 = 109.2$ kips.

Force in third layer: $F_3 = (f_{s3} - \alpha \cdot f'_{cc}) \cdot A_{s3} = 54.6 \cdot 2 = 109.2$ kips.

Force in fourth layer: $F_4 = f_{s4} \cdot A_{s4} = 0 \cdot 4 = 0.00$ kips.

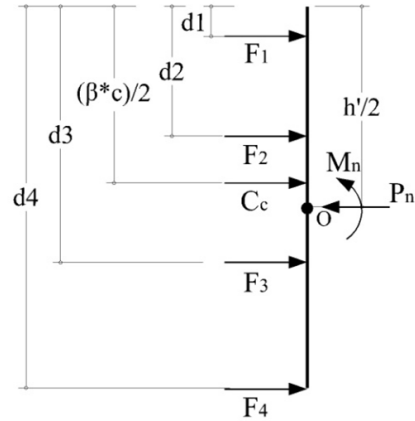
Note that the compressive strains and compressive forces are assumed to be positive.

Nominal axial load (P_n):

$$P_n = C_c + F_1 + F_2 + F_3 + F_4 = 1297 \quad \text{kips.}$$

Nominal moment:

The bending moment shall be computed with respect to the center of rigidity of the cross section since the axial force at the cross section is not zero. Because the cross section and its reinforcement is symmetric, the center of rigidity of the cross section is located at its geometric centroid; therefore, the bending moment should be taken about the point (O) as indicated in the figure.



$$M_n = C_c \cdot \left(\frac{h'}{2} - \frac{\beta \cdot c}{2} \right) + F_1 \cdot \left(\frac{h'}{2} - d_1 \right) + F_2 \cdot \left(\frac{h'}{2} - d_2 \right) + F_3 \cdot \left(\frac{h'}{2} - d_3 \right) + F_4 \cdot \left(\frac{h'}{2} - d_4 \right)$$

$$M_n = 861 \cdot \left(\frac{13.25}{2} - \frac{0.95 \cdot 12.87}{2} \right) + 218.4 \cdot \left(\frac{13.25}{2} - 0.75 \right) + 109.2 \cdot \left(\frac{13.25}{2} - 4.79 \right) + 109.2 \cdot \left(\frac{13.25}{2} - 8.83 \right) + 0 \cdot \left(\frac{13.25}{2} - 12.87 \right)$$

$$M_n = 1417.7 \quad \text{Kip-in.}$$

So, the coordinates of the second point are (1417.7 ; 1297).

Coordinates for the third point:

For this point, the strain at the bottom steel layer is

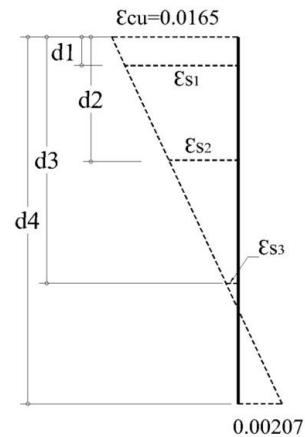
$$-0.00207 = -\frac{f_y}{E_s} \quad (\text{yielding strain}). \text{ Having employed}$$

the process for the second point, we can find the coordinates of this point:

$$P_n = 820 \text{ kips. and } M_n = 4085 \text{ kip-in.}$$

Therefore, the coordinates of the third point are (4085

; 820); note that the units are kip-in. and kips for moment and axial force, respectively.



Coordinates for the fourth point (strain equal to the -0.0065):

At this point, we select the strain in the bottom layer of reinforcement to be -0.0065 (tensile). Following the procedure above, we can get the coordinates of the this point (4807;439.7).

Coordinates for the fifth point:

For this point the tensile strain at the bottom layer of steel remains constant (-0.0065), but the compressive strain decreases; supposing the compressive strain is selected to be equal to 0.004, we can determine the coordinates of this point as (4500 ; 203.7) using the above procedure.

Coordinates for the sixth point:

At this point also, the tensile strain remains as -0.0065(strain at the bottom), but the strain at the top decreases to 0.001; the coordinates for this point are (2537.6; -297.4).

Coordinates for the seventh point(pure tension):

For this point, the strain at the top steel layer is -0.00207 (tensile yielding), and the strain at the bottom steel layer is -0.0065 (as before). Thus, all the cross section is in tension.

$$P_n = -60 \cdot 12 = -720 \text{ kips (tension).}$$

Having the coordinates of points above, the simplified-confined F-M diagram can be plotted; this is shown in Figure 3. 8.

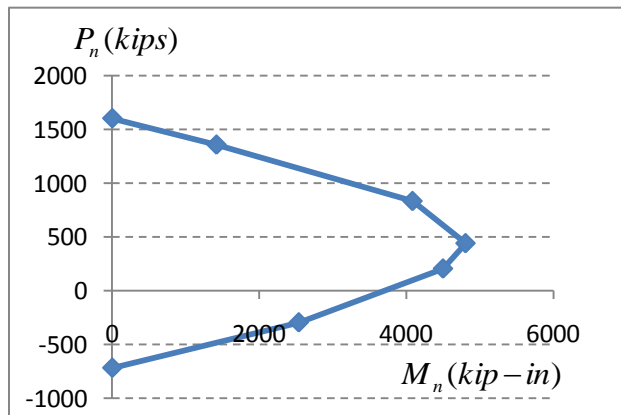


Figure 3. 8. Simplified-Confined F-M diagram for square cross section.

3.3.2- Confined F-M diagram based on simplified curvature-based method:

The procedure for constructing the M-C diagram for a confined concrete cross section is, generally, the same as for unconfined concrete; neither the coordinates of cracking points nor the yielding point changes at all since the confinement is considered just after ultimate status. However, for the ultimate point, the confinement effects should be taken into account.

Here, the coordinates of the ultimate point (shown as point four in Figure 3. 3) are computed, and the other points are directly taken from section 3.2.2.

Coordinates of ultimate point considering confinement:

For this point, the strain at the top fiber of concrete is equal to $\varepsilon_{cc} = 0.007$ and the curvature is $\phi = \frac{\varepsilon_{cc}}{c} = \frac{0.0165}{c}$. We assume that the first, the third and the fourth layer of reinforcement have yielded. The axial load is considered to be the axial load of the fourth point of the F-M diagram in figure 3.8; so, the axial load is equal to $P_n = 439.7$ kips.

To find the coordinates of this point on M-C diagram, the first step is to calculate the depth of the neutral axis.

$$P_n = \alpha \cdot f'_c \cdot \beta \cdot c \cdot b' + E_c (n-1)\phi(c-d_1)A_{s1} + E_c (n-1)\phi(c-d_2)A_{s2} + E_c (n-1)\phi(c-d_3)A_{s3} + E_c (n-1)\phi(c-d_4)A_{s4}$$

$$P_n = 0.95 \cdot 5.6 \cdot 0.95 \cdot c \cdot 13.25 + (60 - 0.9 \cdot 6)4 + 3605(8.04 - 1)\left(\frac{0.007}{c}\right)(c - 4.79)2 - 60 \cdot 2 - 60 \cdot 4 = 439.7$$

Solving this equation, we get $c = 6.73$ in.

Having the depth of the neutral axis, the nominal moment (M_n) for this point is computed as follows:

Strains:

$$\varepsilon_{s1} = \frac{0.0165}{c}(c - d_1) = 0.0146$$

$$\varepsilon_{s2} = \frac{0.0165}{c}(c - d_2) = 0.00475$$

$$\varepsilon_{s3} = \frac{0.0165}{c}(c - d_3) = -0.0051$$

$$\varepsilon_{s4} = \frac{0.0165}{c}(c - d_4) = -0.014$$

Stresses:

$$f_{s1} = \varepsilon_{s1} \cdot 29000 = 423 \text{ ksi} > 60; \text{ use } f_{s1} = 60 \text{ ksi.}$$

$$f_{s2} = \varepsilon_{s2} \cdot 29000 = 138 \text{ ksi} > 60, \text{ use } f_{s2} = 60 \text{ ksi.}$$

$$f_{s3} = \varepsilon_{s3} \cdot 29000 = -145, \text{ ksi} < -60; \text{ use } f_{s3} = -60 \text{ ksi.}$$

$$f_{s4} = \varepsilon_{s4} \cdot 29000 = -406 \text{ ksi} < -60; \text{ use } f_{s4} = -60 \text{ ksi}$$

Forces:

$$\text{Concrete force: } C_c = \alpha \cdot f'_{cc} \cdot \beta \cdot c \cdot b' = 0.95 \cdot 5.6 \cdot 0.95 \cdot 6.73 \cdot 13.25 = 451 \text{ kips.}$$

$$\text{Force in first layer: } F_1 = (f_{s1} - \alpha \cdot f'_{cc}) \cdot A_{s1} = 54.6 \cdot 4 = 218.4 \text{ kips.}$$

$$\text{Force in second layer: } F_2 = (f_{s2} - \alpha \cdot f'_{cc}) \cdot A_{s2} = 54.6 \cdot 2 = 109.2 \text{ kips.}$$

$$\text{Force in third layer: } F_3 = (f_{s3}) \cdot A_{s3} = -60 \cdot 2 = -120 \text{ kips.}$$

$$\text{Force in fourth layer: } F_4 = f_{s4} \cdot A_{s4} = -60 \cdot 4 = -240 \text{ kips.}$$

Nominal moment:

$$M_n = C_c \cdot \left(\frac{h'}{2} - \frac{\beta \cdot c}{2} \right) + F_1 \cdot \left(\frac{h'}{2} - d1 \right) + F_2 \cdot \left(\frac{h'}{2} - d2 \right) + F_3 \cdot \left(\frac{h'}{2} - d3 \right) + F_4 \cdot \left(\frac{h'}{2} - d4 \right)$$

$$M_n = 451 \cdot \left(\frac{13.25}{2} - \frac{6.73}{2} \right) + 218.4 \cdot \left(\frac{13.25}{2} - 0.75 \right) + 109.2 \cdot \left(\frac{13.25}{2} - 4.79 \right) \\ - 120 \cdot \left(\frac{13.25}{2} - 8.83 \right) - 240 \cdot \left(\frac{13.25}{2} - 12.87 \right)$$

$$M_n = 4807 \text{ kip-in.}$$

Next, another axial load is considered to find the coordinates of the ultimate point. This time, the axial load is $P_n=1297$ kips; this axial load corresponds to the second point of figure 3.8. Having employed the above procedure, the bending moment corresponding to this axial load is 1419 kip-in.

Therefore, for an axial load of 439.7 kips, the maximum bending moment based on the simplified-confined M-C diagram is 4807 kip-in; the same bending moment was obtained from the simplified-confined F-M diagram. Also, for an axial load of 1297 kips, the maximum moment that was obtained from the simplified-confined M-C diagram was 1419 kip-in. while for this axial load (1297 kips) the bending moment based on the simplified-confined F-M diagram was 1417.7 kip-in; these two bending moments are also very close to each other.

Thus, we can conclude that the result from the simplified-confined F-M diagram is the same as the result from the simplified-confined curvature-based F-M diagram.

3.3.3- Computation of F-M diagram based on detailed method:

As determined, the axial load-bending moment (F-M) diagram for the confined cross section developed by the simplified-confined method was the same as the F-M diagram that was obtained using the simplified-confined curvature-based method. Now, we will derive the F-M diagrams by the detailed method; as already mentioned, the detailed method is implemented by KSU-RC software. First, detailed-confined F-M diagrams are constructed; the RC columns which are detailed in section 3.3 are used in the analysis. Table 3. 1 shows some data points for the confined square cross section.

Table 3. 1- Coordinates of points for confined- detailed F-M diagram

Point #	Axial force (kips)	Moment (kips-in)
Pure Comp.	1813	0.00
First point	1540	1624
Second point	1200	3282
Third point	914	4387
Fourth point	669	5091
Fifth point	523.8	5107
Sixth point	394.5	5070
Seventh point	124	4665
Eight point	-92	3881

Ninth point	-325	2531
Tenth point	-550.7	1170
Pure tension	-720	0.00

Figure 3.9a is the plot for Table 3. 1. Also, the circular cross section was analyzed by KSU-RC, and its detailed-confined F-M diagram is shown in figure 3.9b.

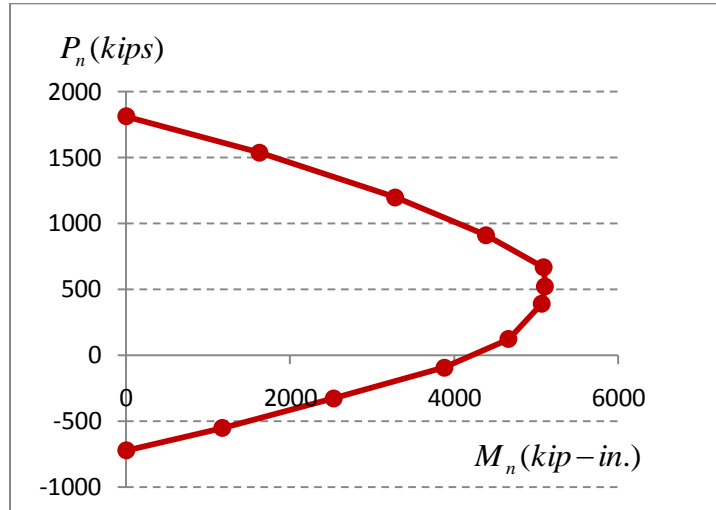


Figure 3. 9(a). Detailed-confined F-M diagram for square cross section.

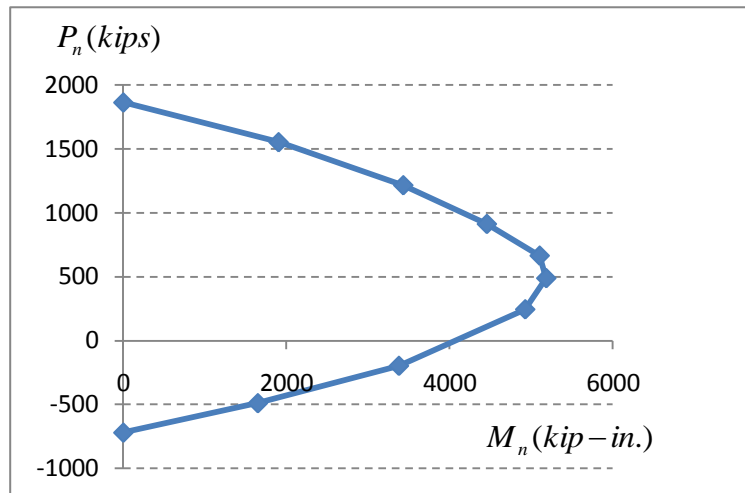


Figure 3.9b- Detailed-confined F-M diagram for circular cross section.

3.3.4- Obtaining the F-M diagrams based on detailed curvature-based method:

In section 3.3.3, the F-M diagram was derived by the detailed method, but now we intend to obtain the F-M diagrams for these confined concrete cross sections using the detailed curvature-based method. To do so, requires the axial load of each point which is indicated in figure 3.9; then, for each of these axial forces, the software generates one M-C diagram. Having the maximum moment from these M-C diagrams, we can plot the F-M diagram for each cross section. These F-M diagram are called the detailed-confined curvature-based F-M diagrams.

Following is the procedure.

We will start from the pure compressive point; based on table 3.1, the value of the axial load at this point is 1813. Having this axial load level, the detailed M-C diagram is constructed by KSU-RC, which is shown below.

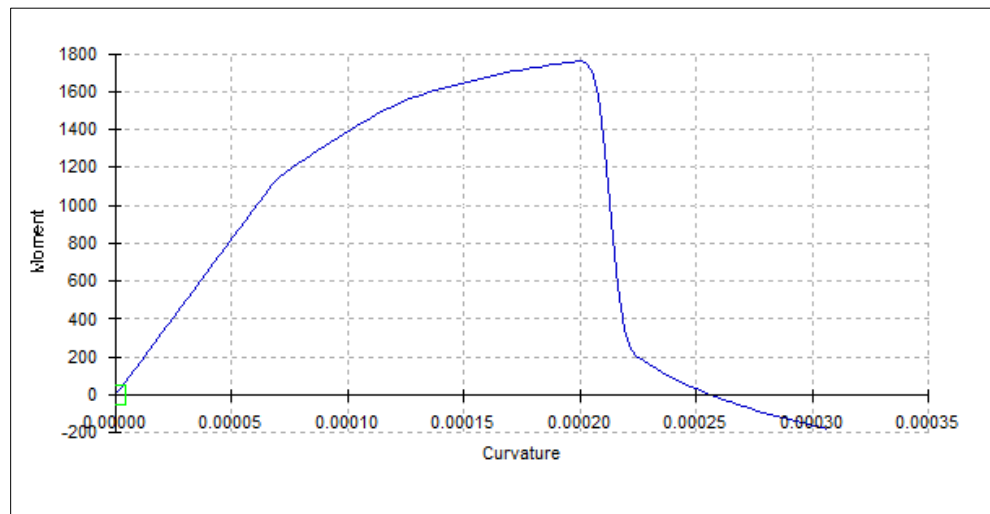


Figure 3. 10. detailed-confined M-C diagram for axial load 1813 kips.

Based on Figure 3. 10, the maximum moment is 1760 kip-in.

Now, we will consider some other points and construct their M-C diagrams. The next point is the first point indicated in figure 3.9a. At this point, the axial load is 1540 kips. Figure 3. 11 shows the M-C diagram for this axial load (note that all the axial loads are considered to be monotonic).

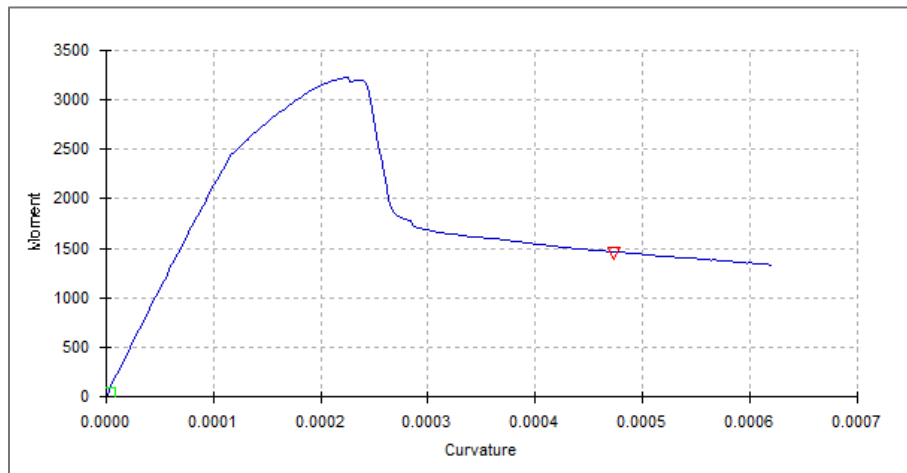


Figure 3. 11. Detailed-confined M-C diagram for axial load of 1540 kips.

The software renders the diagram above showing that the maximum moment is 3229 kip-in, and corresponding curvature is 0.000225 in^{-1} . This moment and curvature occur at a compressive strain of 0.00384 and a tensile strain of 0.000238.

Figure 3. 12 presents the detailed M-C diagram for the confined square cross section under an axial load of 1200 kips. Based on this diagram, the maximum moment is 4552 kip-in, and the corresponding curvature is 0.000395 in^{-1} . This moment and curvature occur at a tensile strain of 0.00067 at the lowest steel layer and the compressive strain at the top section of 0.00404.

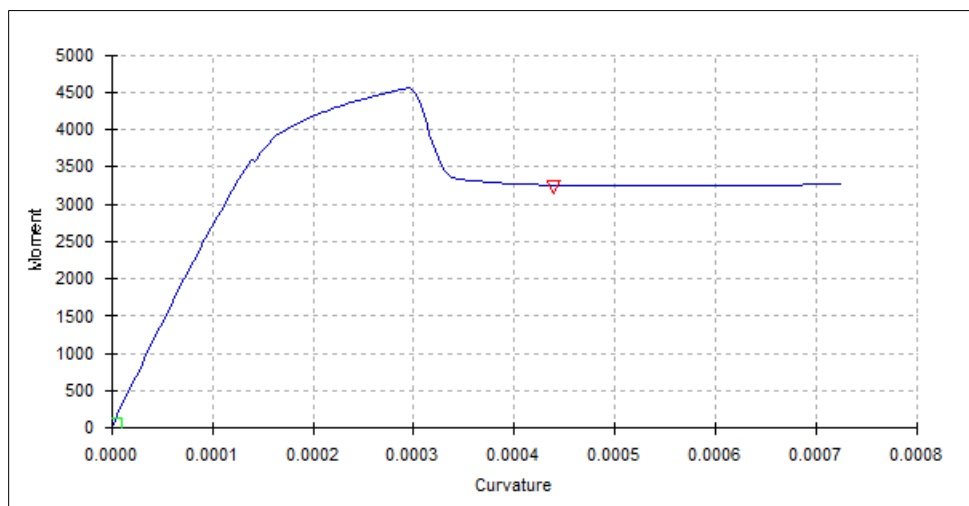


Figure 3. 12. Detailed-confined M-C diagram for axial load of 1200 kips.

Let's consider an axial load of 523.8 Kips (this corresponds to the fifth point on figure 3.9a). Figure 3. 13 shows the M-C diagram that is obtained using the KSU-RC program.

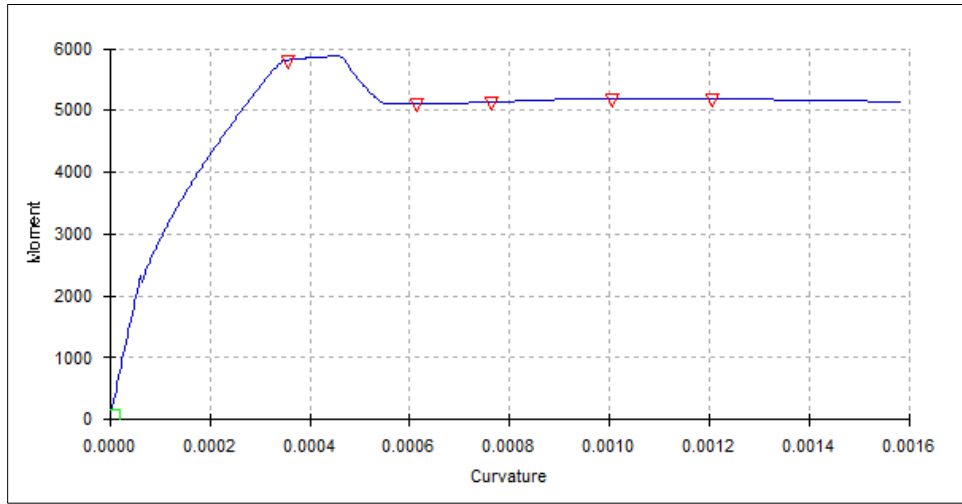


Figure 3. 13. detailed-confined M-C diagram for axial load of 523.8 kips

According to Figure 3. 13, the maximum moment is 5884 kip-in, and the corresponding curvature is 0.000455 in^{-1} . At this moment and curvature, the compressive strain is 0.00402 and the tensile strain at the bottom layer of reinforcement is 0.00326.

Similarly, the maximum moments for the other axial loads are computed. Once all the maximum moments are defined, the *curvature-based* F-M diagram can be derived by plotting the axial forces versus the corresponding maximum moments obtained from detailed-confined M-C diagrams. Table 3. 2 shows axial loads and corresponding maximum moment, compressive strain, and tensile strain; these data are obtained from the detailed-confined M-C diagrams.

As mentioned, Table 3. 2 shows the data obtained from detailed-confined M-C diagrams. With the axial load level and the corresponding maximum bending moment from table 3.2, we can plot them in a graph to obtain the detailed-confined curvature-based F-M diagram for this cross section.

Table 3. 2: confined-detailed M-C data.

Point #	Axial force (kips)	Maximum Moment (kip-in)	Depth of the N.A (in)	Compressive strain at top	strain at bottom layer
Pure Comp.	2100	0			
Point 1	1813	1760	19.94	0.00402	0.0008
Point 2	1540	3229	17	0.00384	0.000238
point 3	1200	4552	13.7	0.004	-0.00068
point 4	914	5335	11.6	0.00403	-0.00154
point 5	669	5905	10.1	0.00406	-0.00239
point 6	523.8	5883	8.83	0.00402	-0.00326
point 7	394.5	5769	7.8	0.00403	-0.00424
point 8	124	5033	5.54	0.00405	-0.00765
point 9	-92	4060	4.23	0.00403	-0.011
point 10	-325	2664	2.9	0.00285	-0.0129
point 11	-550.7	1249	2	0.00343	-0.024
Pure tension	-720	0			

Figure 3.14a shows the detailed-confined curvature-based F-M diagram for the square cross section. Also, the same procedure as for the square cross section is employed for the circular cross section; figure 3.14b shows the resulting detailed-confined curvature-based F-M diagram.

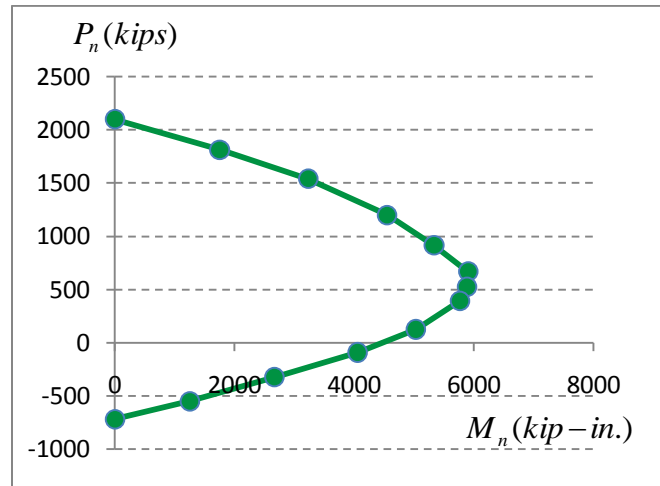


Figure 3.14a- detailed-confined curvature-based F-M diagram for the square section.

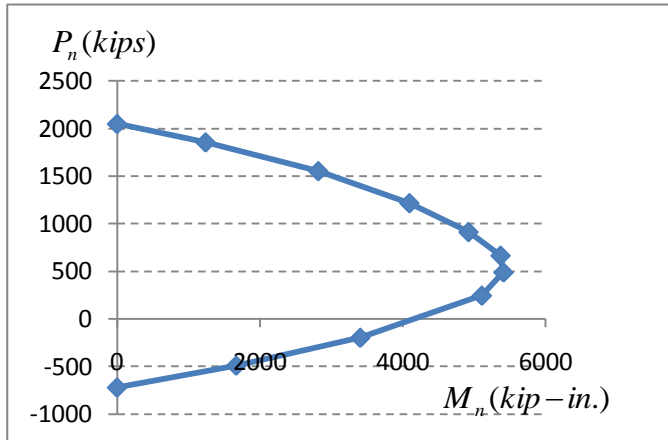


Figure 3. 14(b). detailed-confined curvature-based F-M diagram for the circular section.

3.4- Chapter summary:

In this chapter, we constructed F-M diagrams for two concrete columns. Specifically, in section 3.2, the unconfined F-M diagrams were derived using both simplified and detailed methods. Then, in section 3.3, these methods were used to obtain confined F-M diagrams for concrete columns.

Next, in chapter four the results of each method will be compared to each other and also will be validated against the existing experimental data.

Chapter four- Validation of Analytical Methods Against the Experimental Data

4.1- Chapter Opening:

In chapter 3, two RC columns, one with a square cross section and the other with a circular cross section, were analyzed. The confined and unconfined F-M diagrams for these columns were obtained using different analytical methods. In this chapter, the results of these analytical methods are compared to each other. First, in section 4.2, the simplified and detailed methods for unconfined cross sections are compared with each other while in section 4.3, the unconfined detailed F-M diagrams are compared to the confined detailed F-M diagrams. Next, section 4.4 of this chapter compares the detailed and detailed-curvature-based axial force-bending moment (F-M) diagrams. Finally, section 4.5 validates the detailed and detailed-curvature-based methods against the existing experimental data^[11].

4.2- Comparison of unconfined simplified and unconfined detailed F-M diagrams:

In section 3.2.1 of chapter three, the unconfined F-M diagrams for square and circular cross sections were derived by using the simplified method as the diagrams are shown in figures 3.2 and 3.3. Also, in section 3.2.3, the unconfined F-M diagrams for these columns were obtained using the detailed method; these diagrams are shown in figure 3.6. Now, in this section, the F-M diagrams based on these methods are compared to each other. For instance, Figure 4. 1 shows the simplified-unconfined F-M and detailed-unconfined F-M diagram for the square cross section.

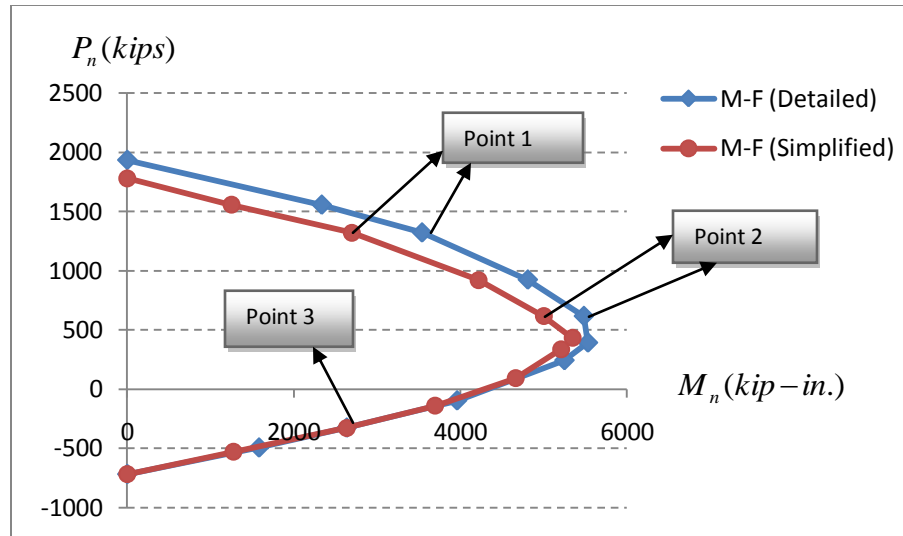


Figure 4. 1. Unconfined F-M diagrams based on Simplified and Detailed methods

As it can be seen from figure above, the difference between these two F-M diagrams occurs within the compression controlled zone. So, what will be the reason for this divergence at this region? Following is the description for this question.

Recall from chapter two that the stress-strain model was described for unconfined (plain) concrete; this model is shown in figure 2.1. Based on this figure, the maximum compressive stress ($f'_c = f'_{co}$) occurs at a strain equal to ϵ_{co} , which is taken usually to be equal to 0.002 for plain concrete. However, the concrete crashes at strain equal to ϵ_{ult} , which is equal to 0.003 for unconfined concrete; for this strain, the concrete compressive stress decreases to a lower value than f'_c . Therefore, when the strain in the plain concrete is equal to 0.002, it experiences maximum stress; for strain values less than or more than 0.002, the compressive stress in the concrete cross section decreases.

ACI code recommends a strain equal to ultimate strain (ϵ_{ult}) for analyzing the plain concrete sections. So, no matter what method is employed, the strain at the extreme compressed fiber of a concrete section should be taken equal to $\epsilon_{ult} = 0.003$. This is applied in our case as well; for both simplified and detailed methods, we assumed a constant compressive strain of 0.003 at the top of the column section. Figure 4. 2 shows the *exact* strain stress distribution for an unconfined concrete cross section. As it can be seen from the figure, at the top edge of the section the compressive strain is 0.003, and

this strain is assumed to decrease linearly from the top edge to the bottom; at the neutral axis, the compressive and tensile strains are zero while in the regions below the neutral axis (N.A) the strain distribution is negative. Since the tensile strain in the concrete is negligible, the tensile forces are provided only by steel reinforcement layers.

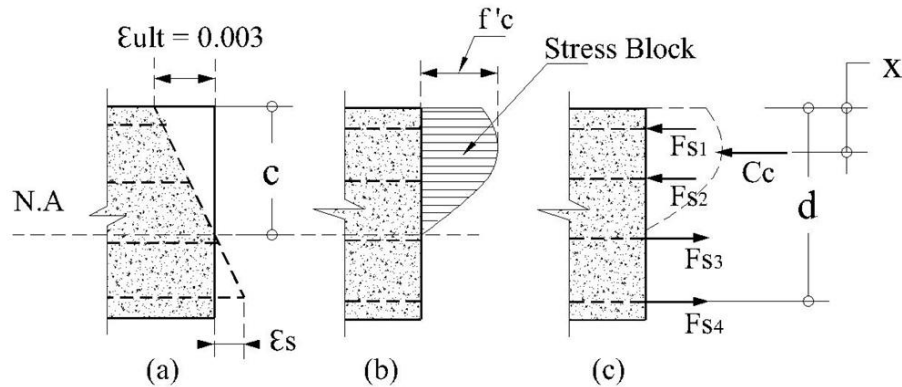


Figure 4. 2. Exact strain-stress distribution for unconfined concrete column section.

Figure 4. 2(a) shows the strain distribution, and Figure 4. 2(b) indicates the corresponding compressive stress block. As Figure 4. 2 (a) shows that the maximum stress (f'_c) does not occur at the top edge (where the strain is 0.003); rather, it happens between the neutral axis (N.A) and the top edge; the stress block shown in the figure has, exactly, the shape of the strain-stress model for plain concrete.

Although in the simplified method the ultimate compressive strain of plain concrete at the extreme compressed fiber is taken as 0.003, and it varies linearly from the top of the section to its bottom, the exact stress distribution is not used in this method. ACI code recommends using an equivalent rectangular stress block for concrete cross sections. The depth of this rectangular stress block is equal to $a = \beta_1 \cdot c$ (see chapter two); the width of this stress block is equal to $(0.85 \cdot f'_c)$. Figure 4. 3(b) presents more details.

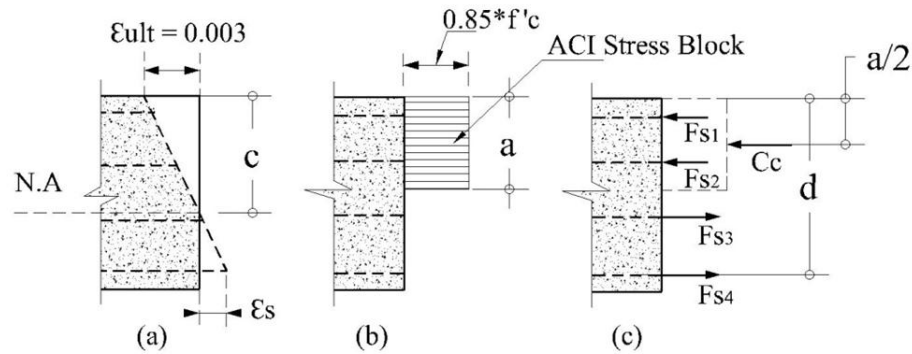


Figure 4. 3. ACI stress block.

Considering Figure 4. 2 and Figure 4. 3, several observations can be made; if the depth of the neutral axis is the same in these two figures, the strain and stress in reinforcement layers are the same as well in these two cases; this is so because the strain is assumed to vary linearly in both cases. Consequently, the forces in steel layers in figure 4.2 are equal to those in figure 4.3. However, the compressive force C_c and its line of action don't have to be the same in these two figures; depending on the value of the N.A depth they can be either different or equal.

Thus, if the depth of the neutral axis (c) is equal in both cases, there are two possibilities for concrete compressive forces C_c ; the first possibility is that the compressive forces may be either equal in each case or different from each other. The second possibility is that the line of action of compressive forces may be either equal (that is $x=(a/2)$) or unequal ($x \neq (a/2)$); where, x and $(a/2)$ are shown in Figure 4. 2 and Figure 4. 3.

For instance, in pure axial load, the whole cross section undergoes a compressive strain of 0.003 in both methods. However, based on the simplified method at this strain, which is the ultimate strain, the compressive stress in concrete is $0.85f'_c$. On the contrary, based on the detailed method, for a strain of 0.003 the compressive force is not $0.85 \cdot f'_c$; it is computed directly from the strain-stress model for unconfined concrete. For this column the compressive stress for a strain of 0.003 is 3.75 ksi, which is $0.94f'_c$. So, for this cross section, the compressive stress, which is obtained using the detailed method, is 9 percent ($0.94-0.85=0.09$) more than the compressive stress assigned by ACI code. Therefore, this increase in compressive stress increases the pure axial load of the cross

section; this is clear in Figure 4. 1. Note that the compressive stress in reinforcement layers is the same for both of these methods since there is no approximation in steel stress-strain distribution.

Next, assume that the compressive forces in the concrete and the depth of the N.A. in these two cases (Figure 4. 2 and Figure 4. 3) are equal to each other, but the line of action of concrete compressive forces may be different. This means that for a given axial load, the moment capacity obtained by the simplified method will differ from the moment capacity computed by the detailed method; this is so because the lever arm of the concrete compressive force is different in these two cases. The following figure offers more explanation.

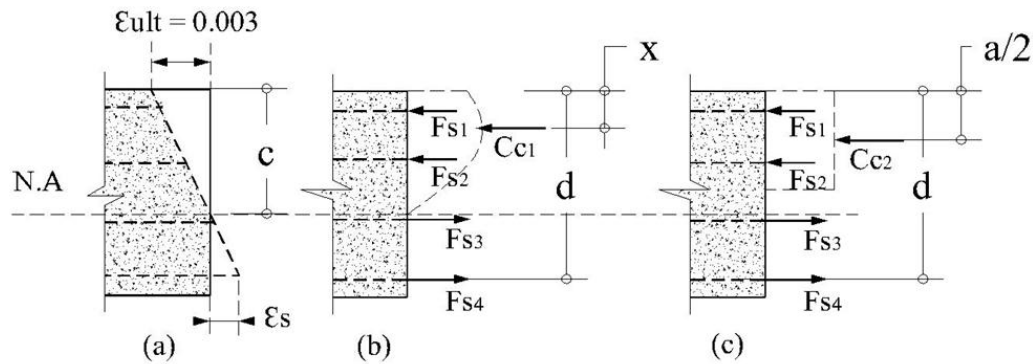


Figure 4. 4. Line of action of compressive forces.

Figure 4. 4 (b) shows the cross section internal forces obtained using the detailed method, and Figure 4. 4 (c) indicates the cross section internal forces derived employing the simplified method. In figure 4.4, it is assumed that for a given depth of the neutral axis (c), the compressive forces obtained by both methods (simplified and detailed) are equal to each other; that is $C_{c1} = C_{c2}$. Notably, this assumption does not guarantee that the lever arms of these concrete compressive forces and the depth of N.A. are equal; that is the value of x is not necessarily equal to $(a/2)$.

For further illustration, let's consider point (1) in figure 4.1 where the axial force is equal for both F-M diagrams and its value is 1321 kips; from the simplified F-M diagram the corresponding bending moment and depth of the neutral axis are 2629 kip-in and 17.42 in, respectively. From the detailed F-M diagram, the moment and the

neutral axis depth are 3539 kip-in and 16.2 in, respectively. As it can be seen, a big difference ($17.42-16.2=1.22$) exists between the depths of N.A of both diagrams and a big difference ($3539-2695=844$ kip-in.) between bending moments. Following is the calculation of C_{C1} , C_{C2} , x , and $(a/2)$.

$$226.4 + 92 + 48.5 + 10 + C_{C1} = 1321 \quad C_{C1} = 944 \text{ kips.}$$

$$C_{C1}(9 - x) + 226.4(9 - 2.937) + 92(9 - 6.98) + 48.5(9 - 11) + 10(9 - 15.1) = 3539$$

Solving the above equation, we can have: $x = 6.72$ in.

Likewise, using Figure 4. 5. Internal forces for point (1)., we will have: $C_{C2} = 906.5$ kips. and $(a/2) = 8.71$ in.

So, for this point, the concept of ACI rectangular stress block underestimates the compressive force in concrete as well as the lever arm of this force. This, in turn, is the cause of the reduction in bending moment based on the simplified method.

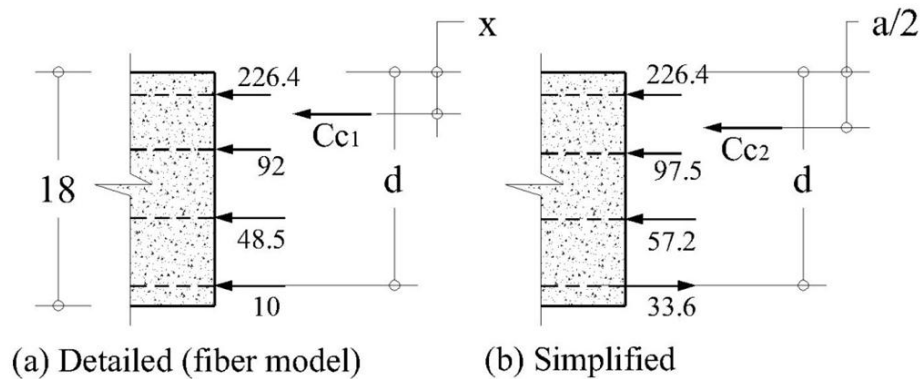


Figure 4. 5. Internal forces for point (1).

Now, let's consider point (2) of Figure 4. 1; at this point, the axial load is 615.5 kips for both diagrams; however, the bending moments and depth of N.A are different for each diagram. For the simplified F-M diagram, the bending moment and the depth of N.A are 5001 kip-in and 10.13 in, respectively; but for the detailed F-M diagram, the moment and the depth of the N.A are 5482 kip-in and 9.7 in. respectively. Again, we see a difference between the depth of N.A (i.e. $10.13-9.7=0.43$ in.) and between bending moments ($5001-5482=481$). Having the depth of the neutral axis, the strain at the top

edge of the cross section (0.003), and the axial force (615.5), we can find the value of ($a/2$) and (x) as follows.

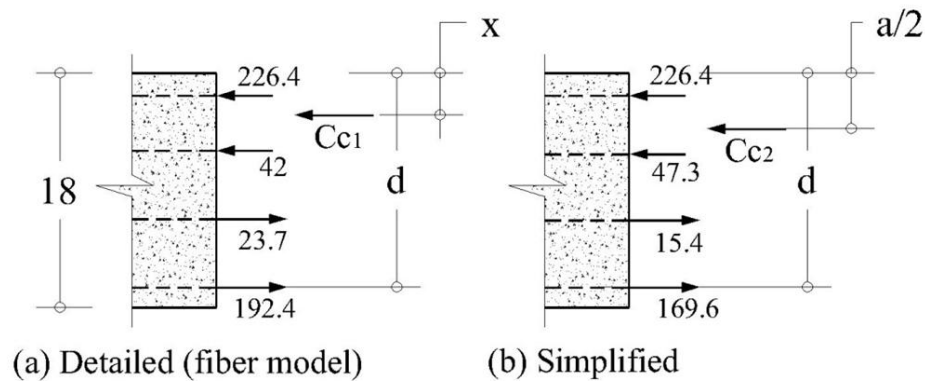


Figure 4.6. Internal forces for point (2).

$$226.4 + 42 + C_{C1} = 192.4 + 23.7 + 615.5$$

$$C_{C1} = 563.2 \text{ kips.}$$

$$C_{C1}(9 - x) + 226.4(9 - 2.937) + 42(9 - 6.98) - 23.7(9 - 11) - 192.4(9 - 15.1) = 5482$$

So, $x = 3.74$ in.

Likewise, for Figure 4.6(b) we have: $C_{C2} = 526.8$ Kips. and $(a/2) = 5.06$ in.

Although the difference between the depths of neutral axis is small, the concrete compressive forces (C_{C1} and C_{C2}) and their lines of action (x and $(a/2)$) are not the same. On one hand, the concrete compressive force (C_{C1}) in the detailed F-M diagram is larger than the concrete compressive force (C_{C2}) that occurs in the simplified F-M diagram ($C_{C1} = 563.2 > C_{C2} = 526.8$). On the other hand, the lever arm of C_{C1} is larger than that of C_{C2} ($x < (a/2)$). These two factors have caused the big difference (481 kips-in.) between the moment values. Thus, we can conclude that the ACI equivalent stress block concept underestimates both the concrete compressive force in the section and its lever arm.

Now let's consider point (3) on the F-M diagrams; this point is shown in Figure 4. 1. At this point the axial force is -328 kips. for both diagrams. For the simplified F-M diagram the bending moment and depth of the neutral axis corresponding to this axial load are 2634 kip-in. and 3.0 in. respectively. Likewise, for the detailed F-M diagram, the

moment and depth of the neutral axis at this point are 2635 kip-in and 2.85 in, respectively.

Figure 4.7 presents the internal cross section forces of the cross section for this point. Since the depth of neutral axis is a little bit different in these two cases, the internal forces are also different. Note that for both F-M diagrams, the axial force is the same and equal to -328 kips.

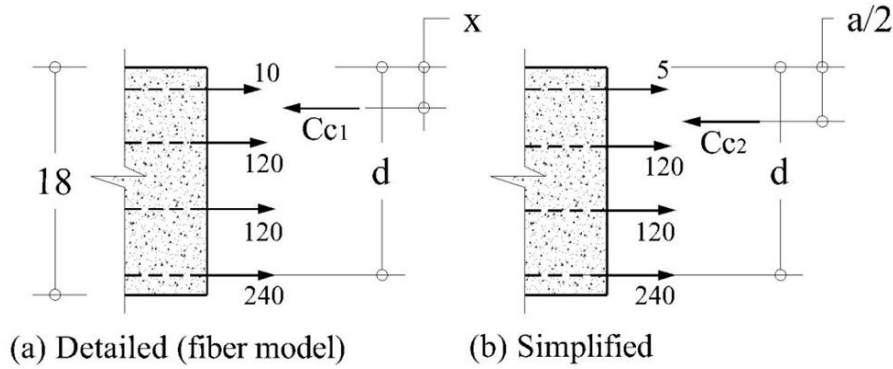


Figure 4.7. Internal cross section forces for axial force of -328 kips.

For this point, the difference between bending moments is $(2635-2634 = 1 \text{ kip-in})$; as we can see the difference has reduced much compared to the other two points; these two moments are approximately equal. Based on the information given above, we can find the values for C_{C1} , C_{C2} , x , and $(a/2)$.

$$C_{C1} = 120 + 120 + 240 + 10 - 328 \qquad C_{C1} = 162 \text{ kips.}$$

$$C_{C1}(9 - x) - (10(9 - 2.94)) - (120(9 - 6.98)) - (120(9 - 11)) - (240(9 - 15.1)) = 2635$$

Solving the above equation, we find $x = 1.32 \text{ in.}$

Similarly, considering figure 4.7b we will have: $C_{C2} = 157 \text{ kips}$ and $(a/2) = 1.5 \text{ in.}$

So, the value of x is slightly smaller than $(a/2)$, and compressive force C_{C1} is slightly greater than C_{C2} . Although the moment due to forces in steel layers only, in figure 4.7b, is greater than the moment due to forces in steel layers in figure 4.6a, the difference of compressive force and its lever arm offset this effect. Therefore, at this point the simplified method underestimates the compressive force of concrete and its lever arm;

however, it also underestimates the tensile force in the top reinforcement layer. This caused the bending moment at this point to be equal to each other, for both the simplified method and the detailed method.

Ultimately, for this cross section, we can conclude that the ACI equivalent stress block model underestimates, for any depth of the neutral axis, the concrete compressive force and overestimates the depth of the neutral axis under any axial loading compared to the detailed method. Consequently, overall, the simplified method underestimates the strength of this unconfined concrete column cross section compared to the detailed method by the maximum difference of about 14 percent.

To check the validity of this conclusion for other unconfined cross sections, another unconfined column cross section is considered to be analyzed; this cross section is a square cross section with dimensions of 25x25in, and it has the same reinforcement and cover as the previous cross section. Both simplified and detailed F-M diagrams are plotted for this cross section and are presented in figure 4.8.

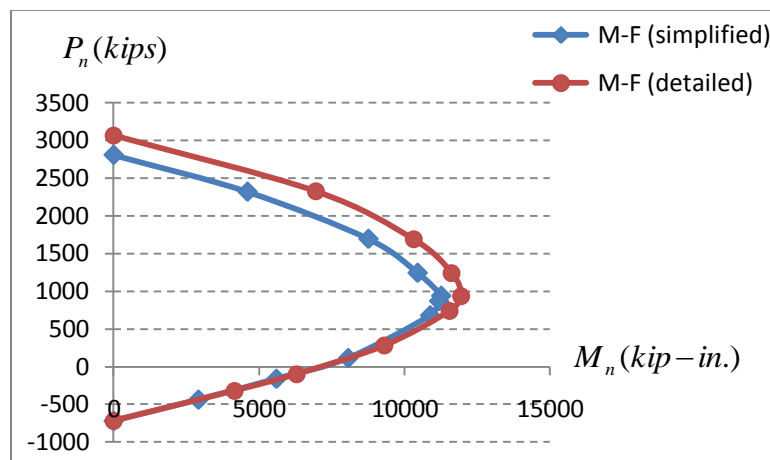


Figure 4.8. F-M diagrams for 25x25 in. unconfined square cross section.

As it can be seen from figure 4.8, the unconfined detailed F-M diagram is larger, mostly, in the compressive controlled zone than the simplified one; the maximum percent increase in bending moment in the detailed F-M diagram is about 40 percent when the axial load is 1800 kips.

Thus, for any rectangular unconfined cross section, the simplified method underestimates the moment capacity of the section compared to the detailed method;

again, this occurs mostly in the compression controlled zone. Also, this conclusion can be shown for unconfined circular cross sections; figure 4.9 shows the diagrams for a circular cross section with 20 in diameter, 2in. cover, and 12 #9 longitudinal bars.

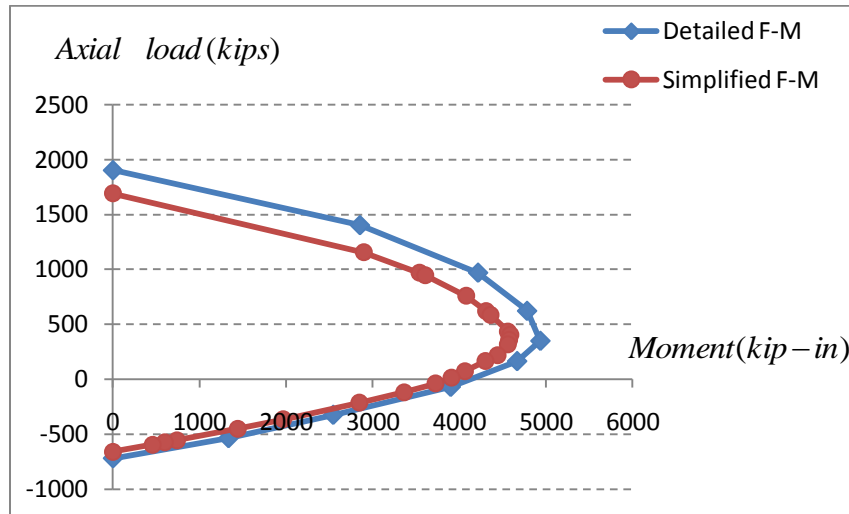


Figure 4.9. Simplified and Detailed F-M diagrams for unconfined circular cross section.

4.3-1. Comparison of unconfined and confined F-M diagrams based on detailed method:

In section 3.2.3 of chapter three, the unconfined axial force-bending moment (F-M) diagrams for square and circular cross sections were constructed using the detailed method; these diagrams are shown in figure 3.6. Also, in section 3.3.3 the detailed method was used to obtain the confined F-M diagrams for these columns; these diagrams are shown in figure 3.9. For obtaining the unconfined F-M diagrams (figure 3.6) the compressive strain at the extreme fiber of the cross section was taken to be 0.003 while this compressive strain is equal to ϵ_{cc} for confined F-M diagrams (figure 3.9).

Now, this section compares these confined and unconfined F-M diagrams for a square cross section, which are derived using the detailed method, as Figure 4.10 demonstrates. As the figure shows, the unconfined F-M diagram is larger, in some regions, than the confined one. This section explores the reason for this difference.

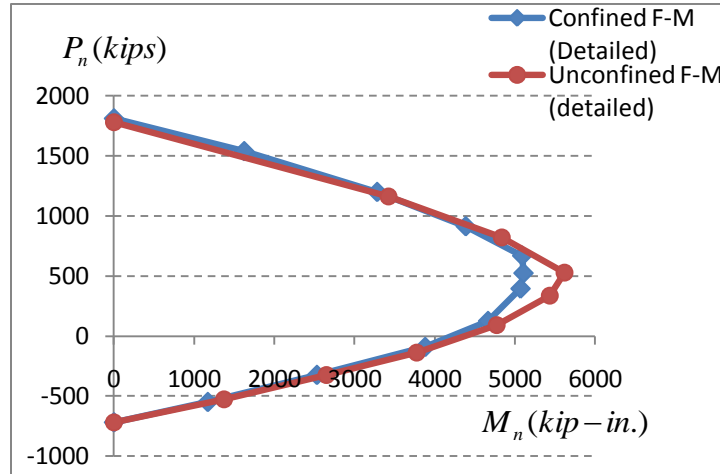


Figure 4.10. Confined and Unconfined detailed F-M diagrams for square cross section.

Various parameters of the concrete cross section can affect the strength and capacity of confined core concrete; the size and the spacing of the stirrups, the size and the numbers of longitudinal steel bars within the cross section, and the concrete cover of the cross section are some of these factors, the most prominent of which is the concrete cover of the cross section; decreasing the cover concrete, the effective depth of the section is increased and also the area of the core concrete get enlarged.

To show the effects of concrete cover on the confined F-M diagram, we will decrease the cover of this square cross section by one inch and redraw its confined F-M diagram; then, we will compare this F-M diagram with its unconfined F-M diagram. This is presented in figure 4.11. As it is seen from the figure, the confined F-M diagram is now larger than the unconfined F-M diagram; this is because the concrete cover was decreased from two inches to one inch. Consequently, the depth of the core concrete was increased by two inches, and also the area of the unconfined concrete was decreased.

The confined F-M diagram is larger than the unconfined one mostly within the compression controlled zone since within this region, the concrete compressive force dominates the bending capacity of the cross section.

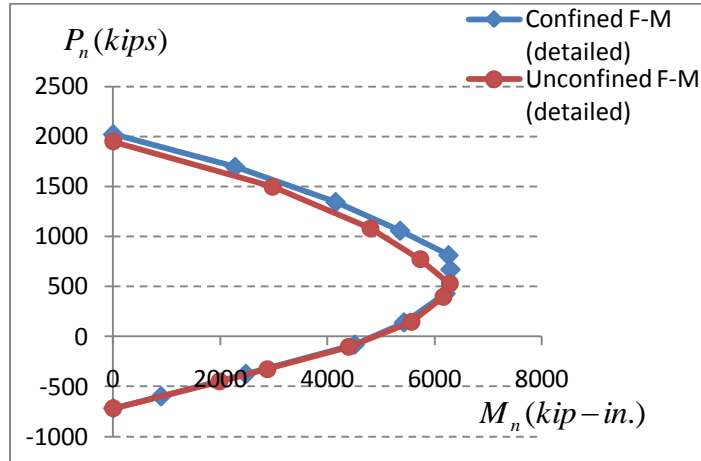


Figure 4.11. Confined and unconfined F-M diagram for one inch cover.

As stated, the compressive strain for unconfined concrete was taken to be 0.003 at the top edge of the section, and for confined concrete, the compressive strain was equal to ϵ_{cc} at the top edge. Now, we will plot both confined and unconfined F-M diagrams for the same compressive strain; this strain should be taken at most equal to 0.003 to construct the unconfined F-M diagram. Figure 4.12 shows the unconfined and confined detailed F-M diagrams for a compressive strain of 0.003. Note that the square cross section with 2 in. cover was used and also the detailed method is employed.

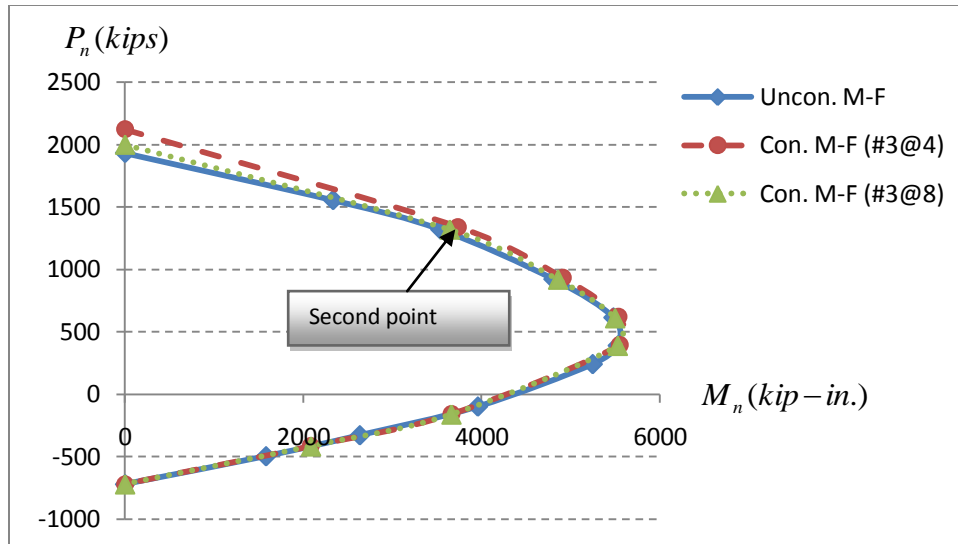


Figure 4.12. Detailed F-M diagrams for compressive strain of 0.003.

In figure 4.12, three detailed F-M diagrams are plotted; one of these diagrams is for unconfined concrete, and another is for confined concrete with #3 stirrups at 4 in; the third one is also for a confined section but with # 3 stirrups at 8 in. In all of these diagrams, the compressive strain at extreme compressed fiber is 0.003, and the same cross section (the cross section details are shown in figure 3.1) is used for all three.

From figure 4.12, we can see that below the second point the difference between these three diagrams is very small; in this range the maximum increase in moment is about 0.9 percent, which is negligible. However, at the pure axial load, the difference is large; the pure axial load is 1934 kips for the unconfined section while this force is 2123 kips for confined section with # 3 @4 in. stirrups. As we move from the pure axial load toward the second point, this difference decreases for two reasons. First, as the depth of the neutral axis decreases, the effect of core concrete on the concrete compressive force (C_c) decreases. The other reason is the strain and strain distribution within the cross section.

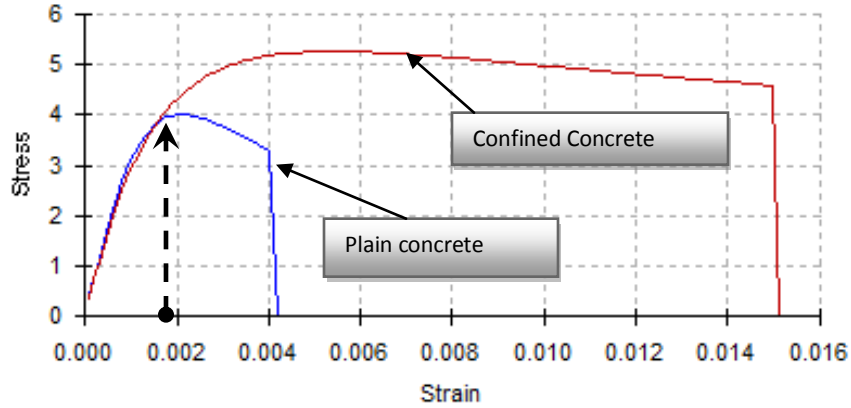


Figure 4.13. Stress-strain curve for cover and core concrete for #3@4 in. stirrups.

Figure 4.4a shows the strain variation within the depth of the neutral axis; the strain starts from a maximum of 0.003 at the top edge and decreases to zero at the N.A. In figure 4.13 the strain-stress model for this cross section is plotted both for cover (unconfined) concrete and for core (confined) concrete; the lateral reinforcement is #3@4in. for this graph. As it can be seen from the figure, as the strain decreases below 0.003, the difference between the confined concrete stress (f'_{cc}) and unconfined concrete stress (f'_c) decreases too; at the strain of 0.0016 these two stress are the same (as shown in figure 4.13). Consequently, based on the fact that the compressive strain decreases from top edge to bottom of the cross section, and the fact that for strain smaller than 0.0016 the confined and unconfined stresses are the same, the confined F-M diagram and unconfined F-M diagram are approximately the same; this is true when the depth of the neutral axis is within the cross section. However, for when the depth of the neutral axis, c , is greater than the height of the cross section, the confined F-M diagram is larger than the unconfined F-M diagram.

Now let's consider the circular cross section to find out the difference between its confined and unconfined detailed F-M diagrams for a compressive strain of 0.003 (the ultimate strain of unconfined concrete). Figure 4.14 illustrates three detailed F-M diagrams for a circular cross section of 20 in. diameter, 12 # 9 longitudinal bars, and 2 in. clear cover. One of these diagrams is obtained for the unconfined cross section; the second one is developed considering the confinement effects of #3 stirrups at 2in.

spacing, and the third F-M diagram is derived for confined section with #3 stirrups at 4 in. spacing.

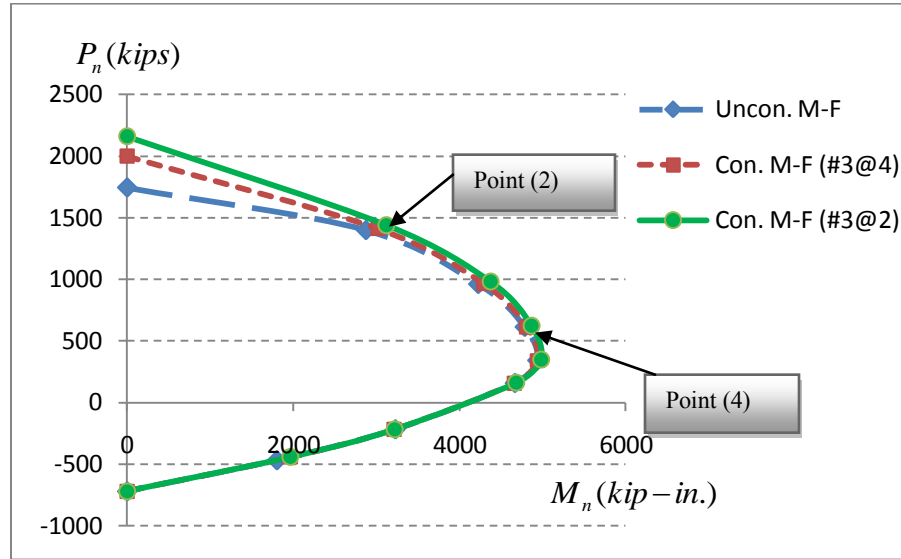


Figure 4.14. F-M diagrams of circular column for compressive strain of 0.003.

As figure 4.14 shows, the difference between these diagrams is large at the point where the bending moment is zero (pure axial load); at this point the percentage increase of the axial load in confined (#3@2) and unconfined diagrams is about 20%. However, this difference decreases to 8% at point (2) and 1.5% at point (4). Therefore, as the depth of the neutral axis decreases, the difference between confined and unconfined F-M diagrams decreases as well.

Thus, for both square and circular concrete column cross sections the difference between the unconfined-detailed F-M diagram and the confined-detailed F-M diagram is big at the zero moment point while this difference decreases as the depth of the neutral axis decreases; this is true only when the compressive strain at the top edge is less than or equal to 0.003. Ultimately, although the difference between these two diagrams is small, it is advisable to use the confined F-M diagram when the cross section is subjected to axial load only.

4.4- Comparison of detailed method and detailed-curvature-based method for confined cross sections:

In section 3.3.3 of chapter three, the confined F-M diagrams were obtained using the detailed method (see figure 3.9). Next, in section 3.3.4, the confined F-M diagrams were derived by employing the detailed-curvature-based method; these diagrams are presented in Figure 3. 14. Now, this section intends to compare these F-M diagrams. Figure 4.15 shows the comparison of these two diagrams (detailed and detailed-curvature-based) for the confined square cross section. As can be seen from the figure, the detailed-curvature-based F-M diagram is larger than the detailed F-M diagram. In this section, the reason for this difference will be explored.

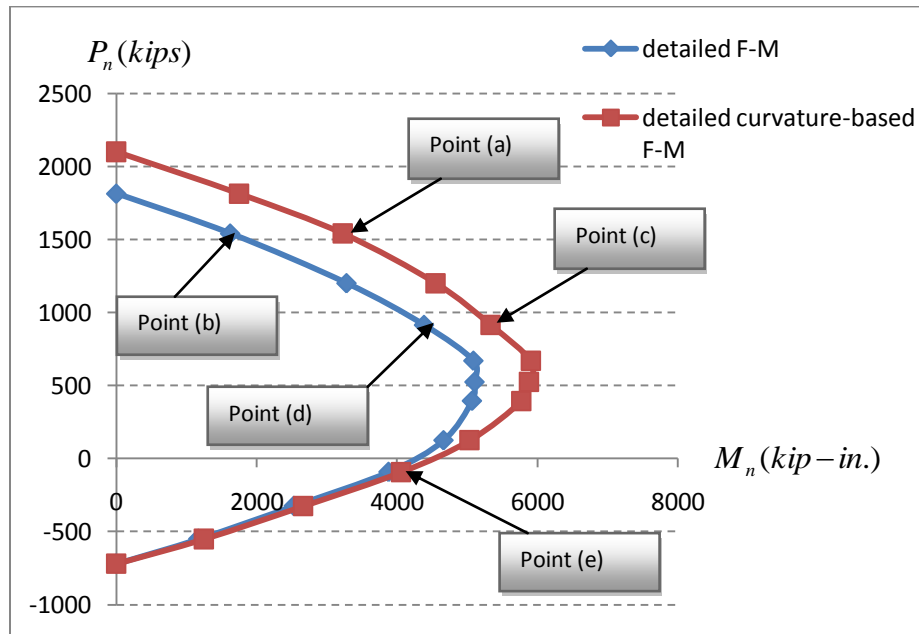


Figure 4.15. detailed and “detailed curvature-based” F-M diagrams

In the figure above, the value of the pure axial load is different for each of the two diagrams; the pure axial load from the curvature-based F-M diagram is 2100 kips while the pure axial load is 1813 for the detailed F-M diagram. Based on the M-C diagrams for

this cross section under 2100 kips axial load, this pure axial load occurs when the maximum compressive strain is 0.0042; this strain is smaller than $\varepsilon_{cc} = 0.00541$.

Also, based on the Figure 4.15, point (a) and point (b) have the same axial load but different bending moments; point (a) is located on the detailed-curvature-based F-M diagram while point (b) is located on the detailed F-M diagram.

The axial load at point (a) is 1540 kips and the bending moment is 3230 kip-in; this moment is the maximum moment obtained from confined-detailed M-C diagram of the confined cross section under an axial load of 1540 kips. The corresponding compressive strain at the extreme fiber and the neutral axis depth are 0.00385 and 17.05 in. respectively; these data are also found from detailed M-C diagram.

The axial load for point (b) is also 1540 kips but the moment is 1624 kip-in; based on the confined detailed F-M diagram, the depth of the neutral axis is 17.02 in. Since in the detailed F-M diagram the strain at extreme compressed fiber is taken to be constant, the compressive strain for all of the points in this F-M diagram is equal to the ε_{cc} ; that is 0.00541. However, it is seen from M-C diagram data that the maximum moment for this section under the axial load of 1540 Kips happens at a compressive strain of 0.003846.

Likewise, the compressive axial load level for points (c) and (d) is the same and is equal to 914 kips; however, the moments and corresponding strains are not equal for these two points. The moment in point (c) is 5335 kip-in. and corresponding compressive strain is 0.00402. Also, point (d) has a moment of 4378 kip-in. and corresponding strain of 0.00541. This tells us that based on the confined-detailed M-C diagram for an axial load of 914 kips, the maximum moment occurs at a strain of 0.00402, which is still different from 0.00541. In other words, the detailed-curvature-based F-M diagram uses a compressive strain of 0.00402 to compute the coordinates of this point.

At point (e), the axial force is the same for both diagrams and it is -92 kips; however, the moments are, still, a little bit different. At this point, the moment corresponding to the detailed-curvature-based F-M diagram is 4063 kip-in, and the corresponding compressive strain at the extreme compressed fiber is 0.00359. Also, the moment corresponding to the detailed F-M diagram is 3881 kip-in. Therefore, for this point, the strain at which the moment is maximum is 0.00359.

Thus, according to the detailed-curvature-based F-M diagram, all the moments on this diagram, regardless of the axial load level, occur at a compressive strain of 0.0036 to 0.00402; this range is less than the peak compressive strain of confined concrete ($\epsilon_{cc} = 0.00541$) for this cross section (the cross section is shown in figure 3.1).

Recall from second chapter that in obtaining the M-C diagram the compressive strain at the extreme compressed fiber is not taken constant. For obtaining the M-C diagram, the first step is to select a compressive strain at the top edge of the section; then, the depth of the neutral axis is assumed. Having the depth of the neutral axis, c , and the compressive strain, the strains and stresses on the steel reinforcement layers are computed; after this, the axial force for the cross section can be calculated. This axial force which is the summation of internal cross section forces is compared to the given axial load. If these two forces are the same, the bending moment with respect to the center of the section is computed; if these forces are different, then another depth of the neutral axis is assumed, and previous steps are taken again. Then, another value of compressive strain is selected and the same steps are taken to find the bending moment and the depth of the neutral axis corresponding to the equilibrium of forces at the cross section. This procedure is repeated until the compressive strain at the top edge reaches its intended value (such as ϵ_{cu}).

Therefore, for a given axial load and for a selected value of compressive strain, a bending moment is calculated. Since several values of compressive strain are chosen, different values of moments can be obtained for the same axial load; the maximum value of these bending moments is the maximum moment that the section can carry under the assigned axial force level. Notably, this bending moment does not have to occur at either (ϵ_{cc}) or (ϵ_{cu}); this is explained further in Figure 4.16.

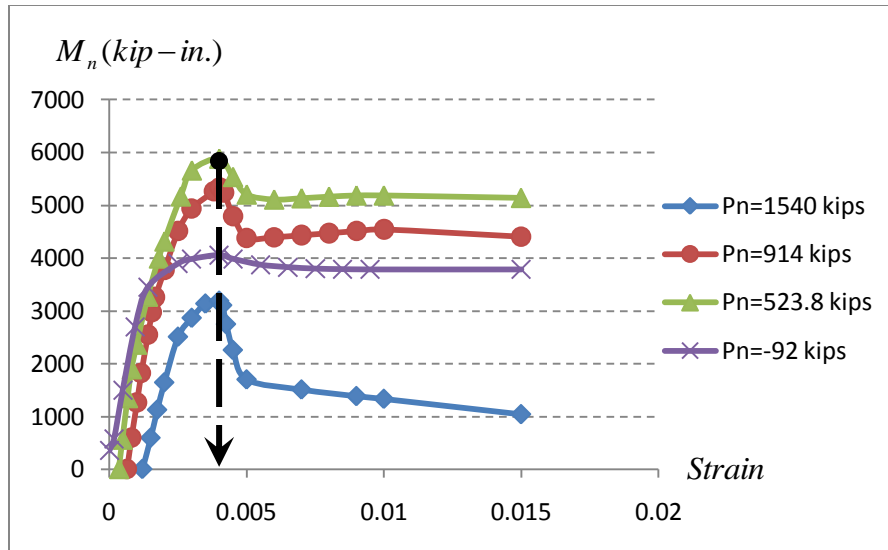


Figure 4.16. Moment versus compressive strain for different axial loads.

Figure 4.16 shows the graphs of moment versus compressive strain for the confined concrete square cross section; each of these diagrams is for a specific axial load. The data used in these diagrams are taken from confined-detailed M-C diagram of the cross section under the given axial loads. As it can be seen from the figure, for *all* the given axial load levels, for this cross section, the maximum moment occurs at a compressive strain approximately around 0.004 (the exact values of this strain are 0.0036 to 0.00402). This means that when the compressive strain is equal to 0.004, under any axial load, the bending moment is the maximum for this cross section.

Since under all the axial load levels the maximum bending moment occurs at a compressive strain of, roughly, 0.004, we can obtain a confined F-M diagram based on this strain; this F-M diagram will be exactly the same as the detailed-curvature-based F-M diagram.

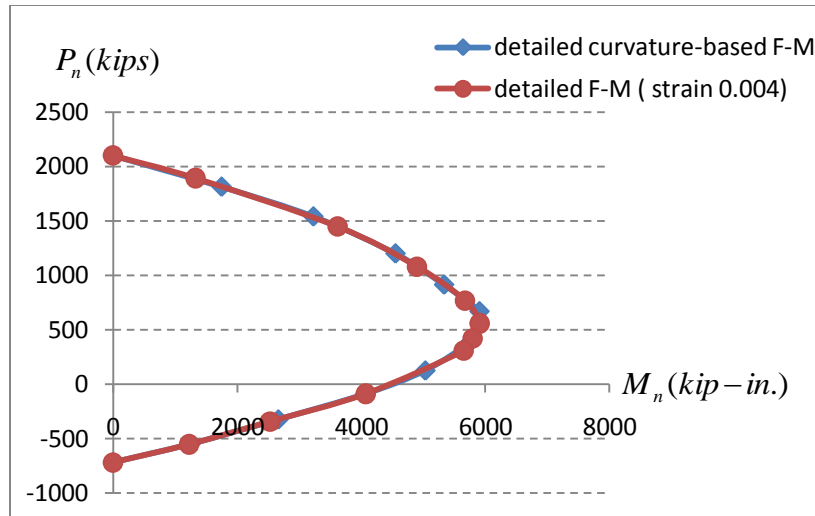


Figure 4.17. Confined F-M diagrams

Two confined F-M diagrams are shown in Figure 4.17; one of them is the detailed-curvature-based diagram, and the other is the detailed F-M diagram which is obtained using a compressive strain of 0.004. As it can be seen from the figure, both of these diagrams are exactly the same. Figure 4.16 along with Figure 4.17 tell us that the F-M diagram that is derived based on a compressive strain of 0.004 is larger than the F-M diagram that is obtained using any other compressive strain; remember this conclusion is valid for this cross section with 2in. concrete cover, and may or may not be true for other cross section's properties.

The preceding discussion was for the square confined concrete cross section (figure 3.1); now, the circular confined concrete cross section is considered to be analyzed. The properties of the section are as followings:

Column cross section type: Circular
 Cross section's diameter : 20 in.
 Longitudinal steel bars : 12 # 9
 Transverse reinforcement : #3 @ 4 in.
 Concrete cover : 2 in.
 Plain concrete strength : 4 ksi.
 Steel grade : 60 ksi.

For this cross section, the strain at pick stress is $\epsilon_{cc} = 0.00501$, and the confined ultimate strain is $\epsilon_{cu} = 0.0154$.

As for the square cross section, we will obtain two confined F-M diagrams for this circular cross section. One of these F-M diagrams is the detailed diagram; for this diagram the compressive strain is taken to be equal to $\epsilon_{cc} = 0.00501$. The other diagram is the detailed-curvature-based F-M diagram.

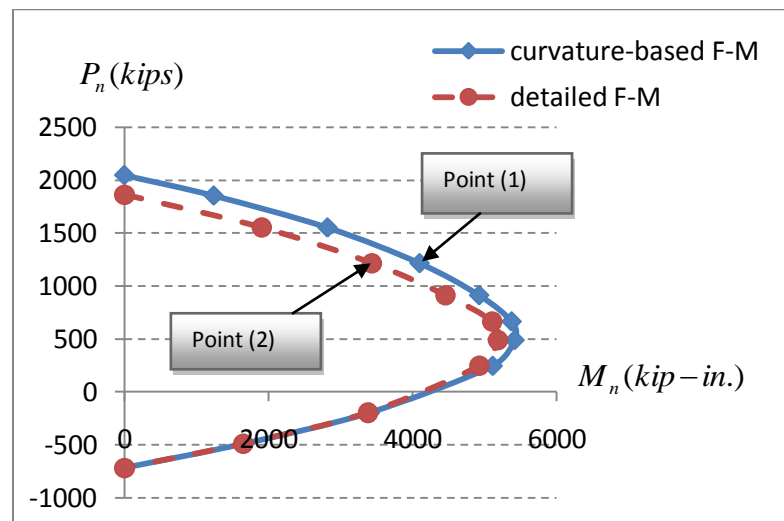


Figure 4.18. Confined F-M diagrams for circular cross section.

Figure 4.18 presents two F-M diagrams for the confined circular cross section. The one which is drawn in dashed line is the detailed diagram, and the solid line shows the detailed-curvature-based F-M diagram. These diagrams are different in some regions, mostly in the compression controlled zone; the detailed-curvature-based F-M diagram is larger than the other one.

Based on the Figure 4.18, the pure axial load level is not the same for these two diagrams; this load is 2050 kips for the detailed-curvature based diagram, and it is 1865 kips for the other one. From M-C diagram for the axial load of 2050 kips, the compressive strain at the extreme compressed fiber is 0.0035, and the corresponding moment is about zero.

Also, at point (1), the axial load is 1217.2 kips; the moment at this point is 4094 kip-in. and corresponding compressive strain is 0.00406. Point (2) also has an axial force of 1217.2 kips, but the moment and corresponding compressive strain are 3430 kip-in and 0.00501, respectively.

Using the detailed M-C diagrams, we can find the moment and corresponding compressive strain for each axial load level by plotting the moment versus compressive strain for each axial load level by plotting the moment versus compressive strain for each axial load of each point. Below are the graphs for a few data points.

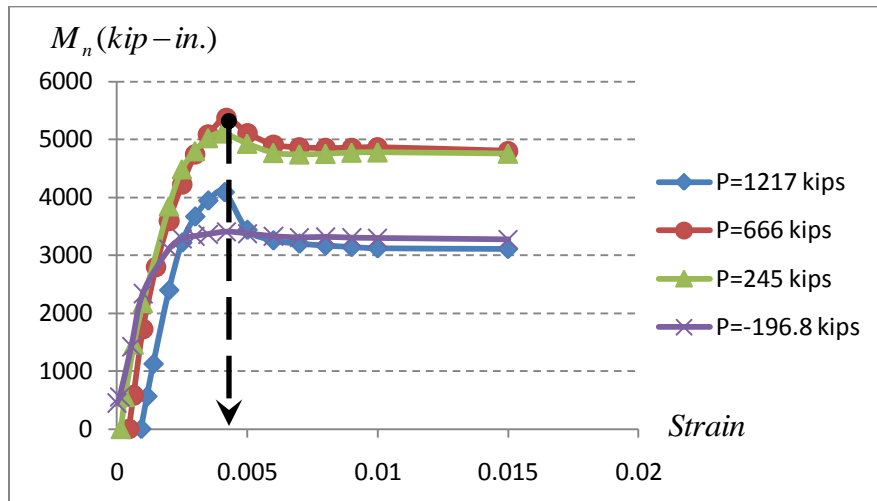


Figure 4.19. Moment versus compressive strain for circular cross section.

As it can be seen from above figure, the maximum moments for the circular confined concrete section under indicated axial loads occur at a compressive strain of approximately 0.004 (from 0.0039 to 0.0042). It is also obvious that there is an abrupt change in moment capacity at a strain of more than 0.004; this is because at this strain the concrete cover spalls off. Therefore, for this circular cross section, the maximum bending moment under any allowable axial load occurs at a compressive strain of around 0.004.

Based on Figure 4.16 and Figure 4.19, the moments corresponding to the compressive strain of 0.00541 are equal to the moments in the detailed F-M diagrams (see Figure 4.15 and Figure 4.18). This means that if the same compressive strain is used for both detailed and detailed-curvature-based F-M diagrams, both of these diagrams will be exactly the same.

Thus, from Figure 4.16 and Figure 4.19 it can be concluded that for the aforementioned square and circular cross sections, the confined F-M diagram has the maximum size for a compressive strain of about 0.004, meaning that for these cross sections, the maximum bending moment under any axial load occurs at a compressive strain of 0.004.

Now, we will discuss why the detailed F-M diagram is large at a compressive strain of around 0.004 for these cross sections. Several factors are involved; the concrete cover, the depth of the neutral axis, the confinement level, and, consequently, the forces in concrete and steel reinforcements are among those factors. For our case, the concrete cover and the confinement level play the dominant role in causing the F-M to be large at the mentioned strain. It should be noted that this strain is at the extreme compressed fiber of the cross section. According to the Mander model for unconfined concrete, the concrete cover spalls at a compressive strain of 0.004 ($2\varepsilon_{co}$); see figure 2.1. The confined and unconfined concrete models for the square cross section are shown in figure below; this figure is plotted using KSU-RC software.

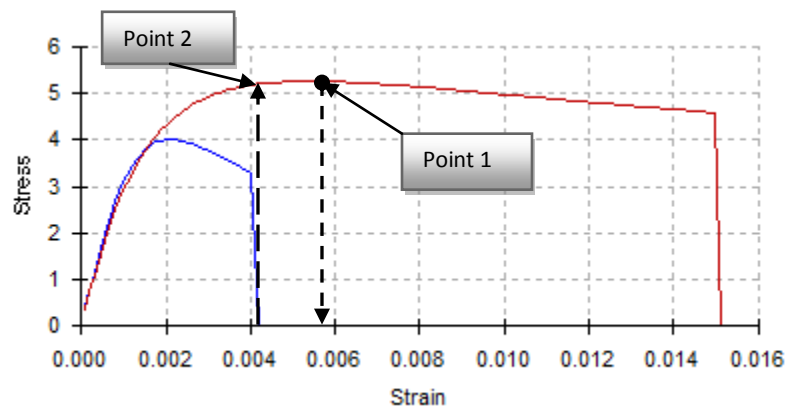


Figure 4.20. Confined and unconfined stress-strain curve for square cross section

These models represent the Mander model for this cross section. In Figure 4.20, the smaller diagram is the unconfined concrete model and the larger diagram is the model for the confined concrete. As it is seen from the figure, for the unconfined concrete the maximum strain is 0.004 and the maximum compressive stress is 4 ksi, and for confined concrete the maximum stress is about 5.26 ksi and corresponding strain is 0.0054. In Figure 4.19, point (1) is the point where stress is 5.26 ksi while at point (2) the stress is

5.16 ksi. Since the difference between these two stresses is very little ($5.26-5.16=0.1$), if the compressive strain of 0.004 is used, the compressive force at the confined concrete (core concrete) will show a very slight decrease. However, since based on the Mander model, the ultimate strain for unconfined concrete is 0.004, at this strain the cover concrete exists and contributes to the compressive force of the cross section. Consequently, the bending moment in the cross section is increased; this increase of bending moment is mostly dependent on the area of the cover concrete; the larger the cover concrete, the larger the compressive force due to cover.

The same result can be shown for circular section. As determined, for any allowable axial force the bending moment is maximum at the compressive strain ranging from 0.0039 to 0.0042; let's say it is 0.004. Therefore, if we look at the strain-stress models for unconfined and confined concrete for this circular cross section, we can see that $\varepsilon_{cc} = 0.005014$ and $\varepsilon_{cu} = 0.0154$. Figure 4.21 shows the confined and unconfined concrete strain-stress curves. Again, for this cross section, the difference between the confined stress at 0.004 strain and the confined stress at 0.005014 strain is very small. So, in order to increase the compressive force of the concrete, the compressive strain needs to be around 0.004 so that the cover concrete can be included in the calculations.

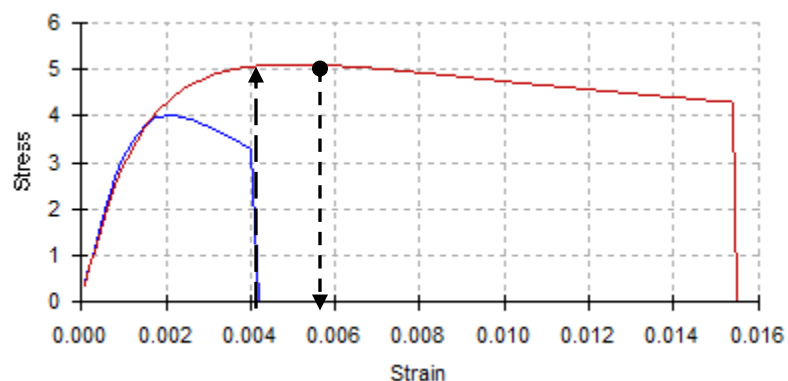


Figure 4.21. Confined and unconfined concrete models for circular cross section

Although the maximum compressive strain for cover concrete is 0.004, for some axial load levels, the strain is more than 0.004; this can be figured out from Figure 4.16 and Figure 4.19. Note that this strain is considered at the extreme compressed fiber of the

cross section. So, for strain more than 0.004, some concrete covers will collapse and some may not. It will not be confusing if the maximum bending moment for a given axial load occurs at a strain of more than 0.004; this is because to construct the M-C diagrams, different values of compressive strains are selected to find the maximum bending moment. In this optimization process, not only the concrete compressive force plays an important role, but the forces in steel reinforcements and the depth of the neutral axis have a significant effect on determining this maximum moment.

Thus, for these two cross sections, since the difference between the peak confined stress (f'_{cc}) and the stress at the 0.004 strain is very little, and also because the cover concrete is large, the maximum bending moment under any axial load happens at the compressive strain of 0.004.

In previous cross sections, the cover concrete was two inches and the transverse reinforcement was #3 @4 inches. Now, the analysis will be done for cross sections with different properties; the cross sections with different transverse reinforcement will be used to magnify the confined concrete model. We will increase the amount of transverse reinforcement to #3 @ 2 in. while the other section properties remain unchanged. Below are the properties for the new columns cross sections.

Square cross section:

Height = 18 in.

Longitudinal bars = 12 #9 bars

Transverse reinforcement = #3 at 2 in.

Cover concrete = 2 in.

Steel yield stress = 60 ksi.

Concrete compressive stress = 4 ksi

Circular cross section:

Diameter = 20 in.

Longitudinal bars = 12 #9 bars

Transverse reinforcement = #3 at 2in.

Cover concrete = 2 in.

Steel yield stress = 60 ksi.

Concrete compressive stress = 4 ksi

First the square cross section is considered, and as before, the detailed and detailed-curvature-based confined F-M diagrams are constructed for this column cross section; then, based on confined-detailed M-C diagram data, the compressive strains at which the moments are maximum are obtained. Figure 4. 22 illustrates the detailed and detailed-curvature-based confined F-M diagrams for the confined square cross section which is detailed above. As it can be seen from Figure 4. 22, still the detailed-curvature-based F-M diagram is larger than the detailed F-M diagram. Remember that Figure 4. 22 is constructed for the same square cross section as in Figure 4.15 but with different transverse reinforcement; in Figure 4. 22, the lateral reinforcement is # 3 @ 2in while in Figure 4.15 it is # 3 @ 4 in. The percent of moment increase varies from 34 to 8. Now, from M-C diagram data, under a given axial load, the moment-strain (M-S) diagram can be constructed; from moment-strain (M-S) diagrams, at any compressive strain the corresponding bending moment can be obtained.

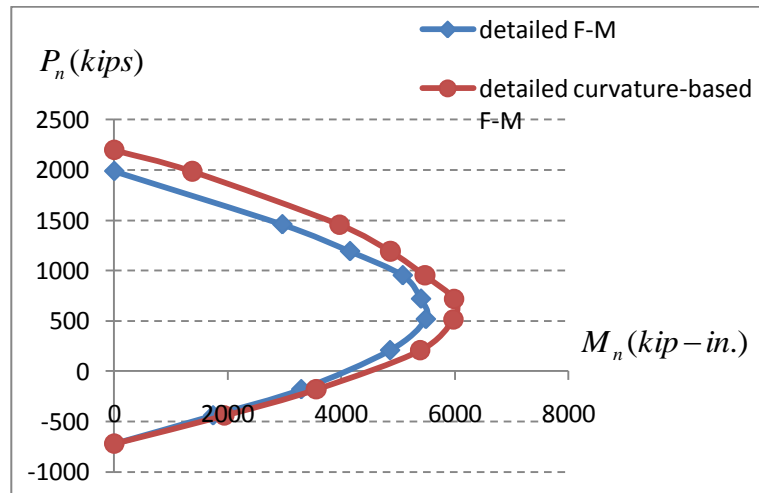


Figure 4. 22. Confined F-M diagrams for square cross section with #3@2 in. stirrups.

Therefore, we can find the maximum moment and corresponding compressive strain for a given axial load. Following are M-S diagrams for some axial loads for the aforementioned confined square cross section. It should be stated that the confined compressive strain (ϵ_{cc}) at the pick stress is 0.00875, and the ultimate confined strain (ϵ_{cu}) is 0.0248.

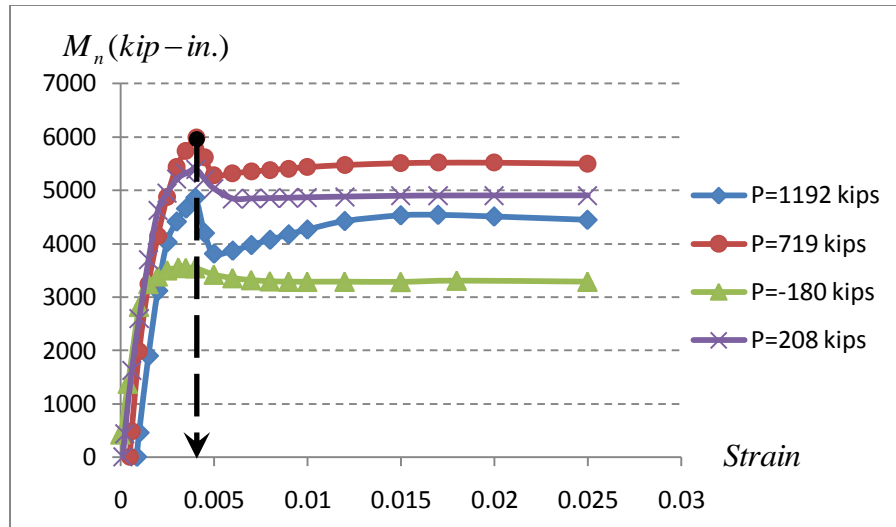


Figure 4. 23. M-S diagrams for confined square section with 2 in. cover.

The M-S diagrams are constructed using the data of moment-curvature diagrams; based on these data, the maximum moments under allowable axial forces occur in a compressive strain range of 0.0032 to 0.0041. However, for positive axial loads, this strain can be approximated to 0.004; this is shown in Figure 4. 23. Also, this figure clarifies that at a strain of 0.00875 (ϵ_{cc}) the moments are less than the moments that correspond to a strain of 0.004. This is because of the cover concrete cover; the cover concrete still provides a large concrete area.

Although the compressive stress at a compressive strain of 0.004 is less than the compressive stress at $\epsilon_{cc} = 0.00875$, the concrete compressive force is larger at 0.004 strain than at $\epsilon_{cc} = 0.00875$ strain; this is because the area of cover concrete is still dominant.

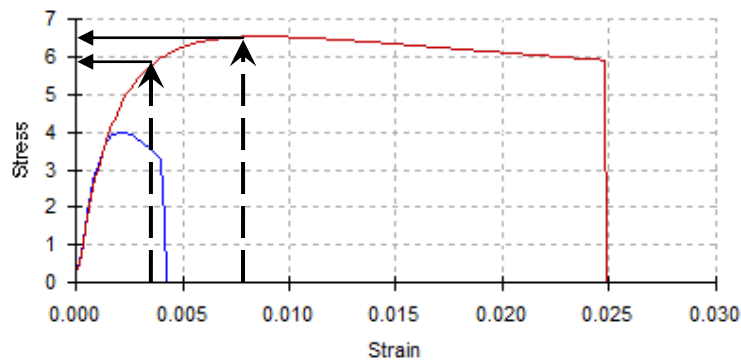


Figure 4. 24. Stress-strain model for square cross section with #3@2 in. stirrups.

As it is shown in Figure 4. 24 , the compressive stress at 0.004 strain is equal to approximately 6 ksi while the pick (at 0.00875 strain) compressive stress is 6.53 ksi. Accordingly, this increase in stress (6.53-6=0.53) seems not to be enough to overcome the effects of the area of the cover concrete. So, using cover concrete along with 6 ksi gives a larger compressive force (C_c) at the concrete stress block than the compressive force that comes from only the core concrete whose stress is 6.53 ksi. Thus, having larger values of concrete compressive force (C_c), the values of bending moments will increase as well.

Next, the new circular cross section (transverse reinforcement at 2 in. spacing) will be considered. For this cross section, we will again construct the detailed F-M and detailed-curvature-based F-M diagrams, taking into account the confinement effect due to transverse reinforcement. Figure 4. 25 shows the confined F-M diagrams for the circular cross section; in this column cross section, the spacing of stirrups has been decreased to 2 in. From this figure, it can be seen that the detailed-curvature-based F-M diagram is larger than detailed F-M diagram. The reason for this difference can be the fact that has been discussed in preceding paragraphs.

For this cross section, the confined strain at pick stress is $\epsilon_{cc} = 0.0081$, and the ultimate confined strain is $\epsilon_{cu} = 0.025$.

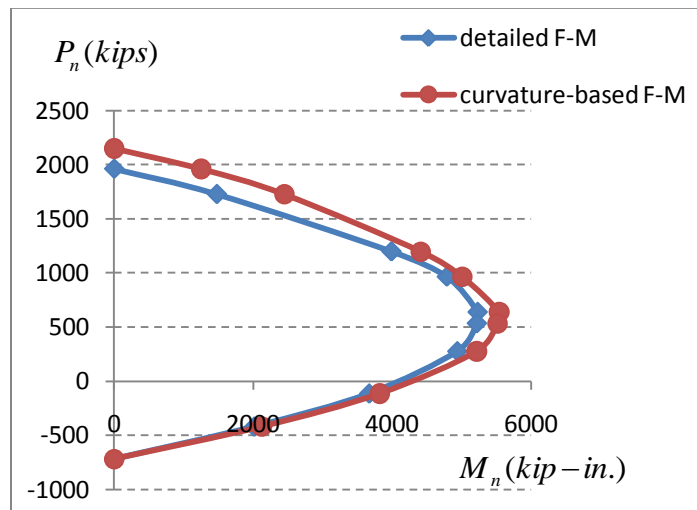


Figure 4. 25. Confined F-M diagrams for circular cross section with #3@2 in. stirrups

Also, Figure 4.26 presents the moment-strain (M-S) diagrams for different axial load levels. Again, the maximum bending moment occurs at the compressive strain of around 0.004. At this strain, the confined concrete compressive stress is 5.25 ksi while the maximum confined compressive stress is 6.3 ksi. However, for cover concrete the compressive stress is not 5.25; it is less than this as obtained from the unconfined strain-stress model. Therefore, a larger concrete compressive force will be achieved if the cover concrete along with the confined compressive stress of 5.25 are used rather than only confined core concrete. Consequently, at a strain of 0.004, the F-M diagram is larger than any F-M diagram that is obtained for any other values of compressive strain.

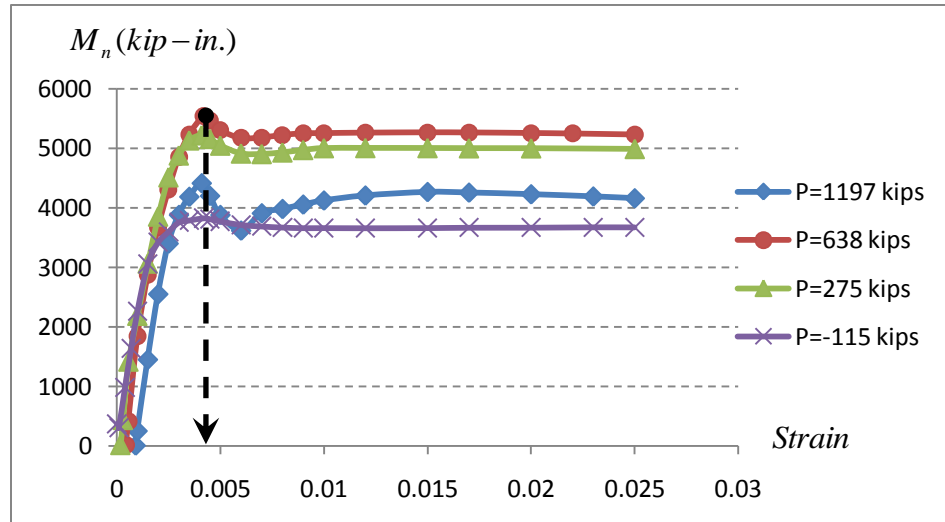


Figure 4.26. M-S diagrams for circular cross section with #3@2 in. stirrups

As a result, for both of these circular and square column cross sections, the maximum moment for any allowable axial load value occurs at a strain of 0.004; this is the compressive strain at the most compressed edge of the cross section. The same result has been already obtained for these two column cross sections with different lateral reinforcement (#3 @ 4 in.). Although in Figure 4. 23 and Figure 4.26 the stirrups spacing was decreased to 2 in. (#3 @ 2in), it was not decreased sufficiently to overcome the effect of cover concrete; consequently, the confined F-M diagrams are still larger at compressive strain of 0.004 than at any other compressive strain value.

The preceding discussion concluded that cover concrete plays an important role in confined F-M diagrams. Next, we need to disregard the effect of the cover concrete in analysis. To do so, we will use the same cross sections, but this time the concrete cover will be taken as zero to eliminate the effects of cover concrete on the confined F-M diagrams; meanwhile, the spacing of transverse reinforcement is 4 inches (#3@4).

Figure 4. 27 illustrates confined F-M diagrams for the square cross section with zero concrete cover and #3 @4 in. stirrups; as indicated, one of diagrams is the detailed F-M diagram and the other is the detailed-curvature-based F-M diagram (obtained using the detailed- confined M-C diagrams data). In this figure, the difference between these two diagrams has been decreased drastically compared to those in Figure 4.15 (which were obtained for the same cross section, but with 2 in. cover); however, these two diagrams are not exactly equal to each other. The maximum percent increase in the curvature-based diagram is 12 %.

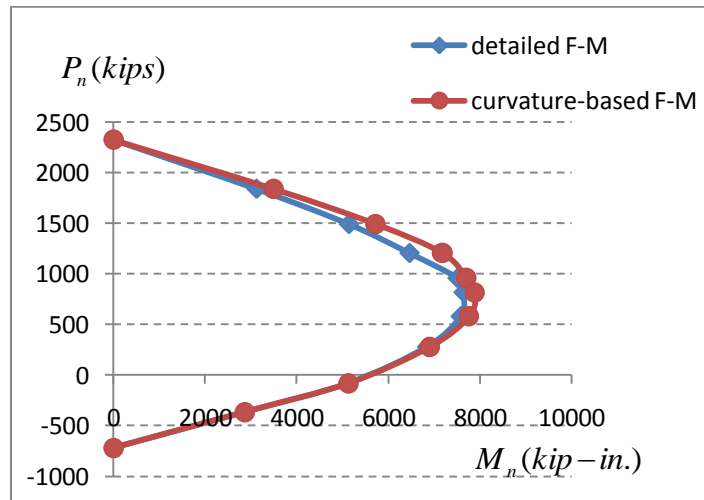


Figure 4. 27. Confined F-M diagrams for square cross section with zero cover.

Since the concrete cover was taken as zero, the difference between these two diagrams has been reduced. Now, let's see at what values of compressive strain these maximum bending moments occur. As it has been already stated, the detailed F-M diagram is obtained by considering a constant value of compressive strain (ϵ_{cc}) at the most compressed edge of the cross section; for this cross section, $\epsilon_{cc} = 0.00468$. However, the

detailed-curvature-based F-M diagram is not constructed based on a constant value of strain because the detailed M-C diagram is derived by selecting different values of compressive strain. For each axial load, the strain versus bending moment is plotted in Figure 4. 28. As it is seen, for each value of strain there is a corresponding value of bending moment. And so, to construct the curvature-based F-M diagram, we should find the maximum moment for each axial load level; these diagrams are shown in Figure 4. 28. Here, we are looking for strain at which the maximum moments occur.

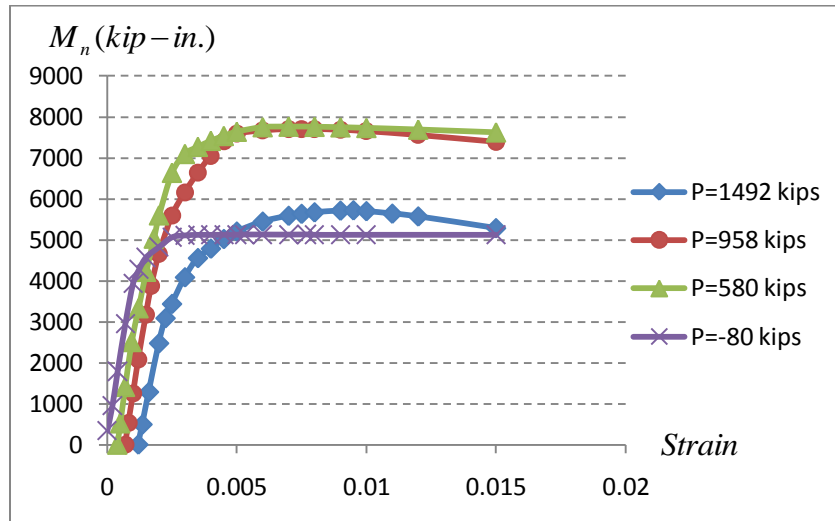


Figure 4. 28. M-S diagrams for square cross section with zero cover

Unlike for the other two square cross sections (see figures 4.18 and 4.25), for this square cross section the maximum moments do not occur at a strain of 0.004 (see figure 4.30). As it can be seen from figure 4.30, all the maximum moments happen at a compressive strain of more than 0.004; this is because the cover concrete does not exist in the cross section. Also, all of the maximum moments under different axial loads don't occur at the same strain; this means that for different axial loads, there are different strains at which the bending moment is maximum. For this cross section, the maximum moments occur at compressive strain of 0.0075 to 0.0095; this range is more than the $\epsilon_{cc} = 0.00468$ and less than $\epsilon_{cu} = 0.015$. Therefore, to find the largest possible confined F-M diagram for this section, the confined M-S diagrams which are obtained based on M-C diagrams should be used. This is so because these diagrams give the plot of bending moment

versus compressive strain; consequently, it is possible to find the maximum moment under each axial load level and also the compressive strain at which this moment occurs. Next, the circular cross section will be considered; this time, the cover is zero and the spacing of transverse reinforcement is 4 inches (#3@4 in.). Figure 4. 29 shows the confined F-M diagrams for this cross section.

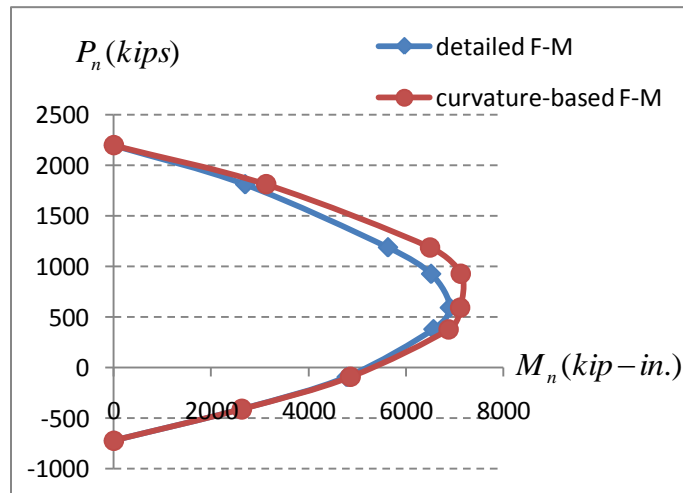


Figure 4. 29. Confined F-M diagrams for circular cross section with zero cover.

From this figure, it is obvious that the difference between the two F-M diagrams has been reduced compared to the Figure 4.20. However, the difference between these diagrams has not become zero; the maximum percent increase in bending moment in the curvature-based diagram is about 15 %. This decrease of difference between the diagrams happens because of the zero cover concrete. We can also find the compressive strains at which the maximum moments occur; this can be achieved by looking at moment-strain (M-S) diagrams.

According to Figure 4. 30, the maximum moments do not occur at the compressive strain of 0.004; rather these moments occur at different compressive strains, depending on the axial load level. So, this result contradicts the results obtained from Figure 4.19 and 4.26. This is because the cover concrete is considered to be zero in Figure 4. 30. Also, it is vivid that the bending moments that happen at compressive strain of $\epsilon_{cu} =$

0.0156 and $\epsilon_{cc}=0.00453$ are not the maximum moments; rather the maximum moments, under any axial load level, occur at a compressive strain between ϵ_{cc} and ϵ_{cu} .

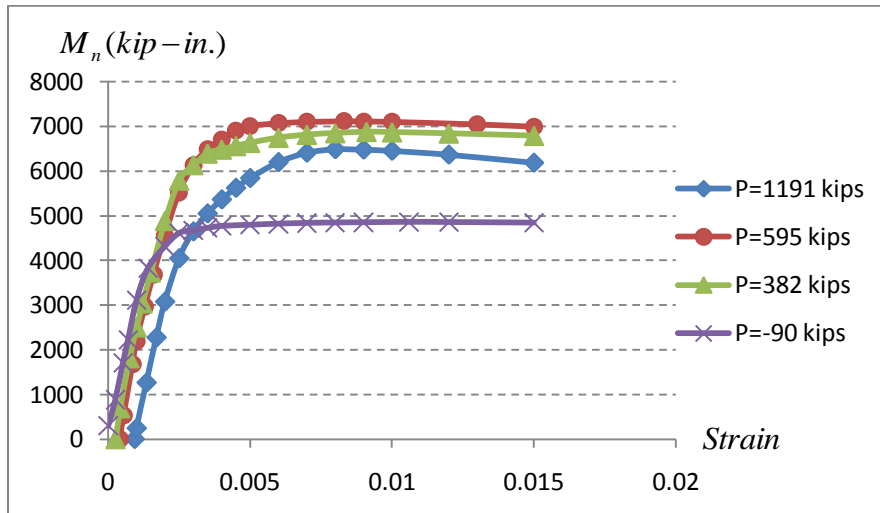


Figure 4. 30. M-S diagrams for circular cross section with zero cover.

As a conclusion for this section, it can be said that the concrete cover of the section has a considerable effects on the capacity of the confined cross sections. Also, the compressive strain has a major effect on strength of confined columns; there is a specific value of compressive strain for which that the strength of the confined column is the maximum. Also, for confined cross sections, the detailed-curvature-based method gives larger F-M diagrams than does the detailed method; this is because in the detailed-curvature-based method, the compressive strain at the most compressed fiber of the cross section is not taken as constant.

4.5- Validation of detailed and detailed-curvature-based methods against the experimental results:

In section 4.2 of this chapter the unconfined-simplified method was compared to the unconfined-detailed method; it was seen that the unconfined-detailed F-M diagrams

were larger than the unconfined-simplified ones. In section 4.4, the confined-detailed and confined detailed-curvature-based methods were compared with each other; it was concluded that the confined F-M diagrams that were derived using detailed-curvature-based method were larger than those that were obtained using the detailed method. Thus, for unconfined concrete cross sections, the detailed method provides large F-M diagrams while for confined cross sections, the detailed-curvature-based method gives larger F-M diagrams than any other method.

Now in this section, the intention is to validate these two methods against the existing experimental data^[11]. This will guide us to determine the method that offers the optimal result.

The existing experimental results for two RC columns, circular and square, are used. Below are the details for the column with a square cross section.

Square cross section (40x40 cm):

$$f_y = 367 \text{ MPa.} \quad f'_c = 20.6 \text{ MPa.}$$

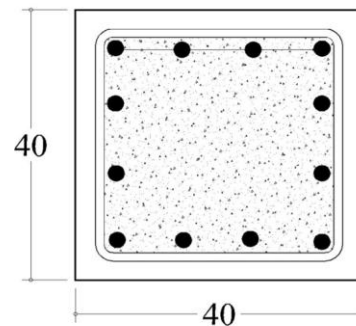
$$f_{ys} = 376 \text{ MPa.} \quad \text{Cover} = 3 \text{ cm}$$

Stirrups = D6 @5 cm.

Longitudinal bars = 12 D13

Given axial load = 170 kN.

$$\epsilon_{cc} = 0.0054, \quad \epsilon_{cu} = 0.028$$



For this column, for the given axial load the maximum bending moment is 156 kN.m. Analyzing this cross section with the direct-detailed method, the maximum bending moment for this axial load is found to be 115 kN.m; this moment is the same for both ϵ_{cc} and ϵ_{cu} . However, based on detailed-curvature-based method, the maximum bending moment for the given axial load is around 121 kN.m; this moment occurs at a compressive strain of about 0.0035. Therefore, 121 is less than 156 and more than 115; it means that both detailed and detailed-curvature-based methods are is safe side, but the detailed-curvature-based method is economically safe. As it is obvious, the difference between 121 and 115 is very less; this is because the level of axial load is very low. If a

higher value of axial load was used, the difference between the detailed and detailed-curvature-based results would have been large.

Following, the circular concrete column is detailed.

Circular cross section:

Column diameter = 40 cm.

$f_y = 377$ MPa. $f'_c = 23.3$ MPa.

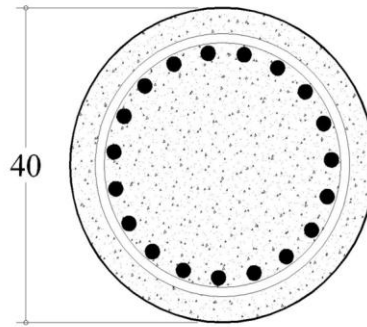
$f_{ys} = 374$ MPa. Cover = 2.7 cm

Stirrups = D6 @ 7 cm.

Longitudinal bars = 20 D13

Given axial load = 185 kN.

$\epsilon_{cc} = 0.0042$, $\epsilon_{cu} = 0.016$



For this column, the maximum moment achieved from experimental data is 160 kN.m.

The maximum moment that is obtained from using the detailed method is as follows:

For $\epsilon_{cc} = 0.0042$: $M_n = 145$ kN.m

For $\epsilon_{cu} = 0.016$: $M_n = 155$ kN.m

Also, based on the detailed-curvature-based method, the maximum bending moment, for this axial load, is 155 kN.m; this bending moment happens at the compressive strain of 0.0039. Therefore, for this cross section, the results from detailed and curvature-based methods are exactly the same (155 = 155); however, the compressive strain at which these maximum bending moments occur is different for each method. The compressive strain in the detailed method is 0.016 while this strain is equal to 0.0039 for the curvature-based method. Again, since the level of axial load is very low, there is no difference between these two methods; if the axial load level was higher, there would have been an increase in the moment based on the curvature-based method.

From analysis of these two concrete columns, we can conclude that for a given axial load, the maximum bending moment need not necessarily happen at the ultimate compressive strain, ϵ_{cu} or at ϵ_{cc} . For these two cross sections, the maximum bending

moments, for given axial loads, occur at a compressive strain lower than the crushing strain; this is because the cover concrete for these two cross sections is large.

Thus, based on this comparison, the detailed-curvature-based method gives the optimal F-M diagrams for confined RC columns.

Chapter five- Summary and Conclusion

The performance-based design method is the emerging design procedure especially for reinforced concrete structures. Some of the important structures, especially those located in areas of high seismic activity are currently designed considering various performance levels in the design process. It goes without saying that a realistic assessment of the performance of reinforced concrete structures is a basic need in this design method and procedure. The existing codes such as ACI and AASHTO ^[38], currently practiced by design firms, are strength-based, addressing just one stage of the performance at the ultimate state. Factor of safety in the old Allowable Stress Design (ASD) method is replaced by the Load Factors and Resistance Factors to address the probabilistic nature of the demanded forces, the available strength at the ultimate stage. However, in a performance based design process, every stage of the performance, such as spalling of the cover concrete, relative deflections and cracking, even failure of a structural member, can be a performance limit state that demands a reasonably accurate realistic prediction of the performance in the design stage.

The realistic performance and strength assessment of structures and structural members is also a need for existing structures, namely a deficient bridge column, when deciding whether retrofit or replace it.

However, accuracy of the performance assessment involves many factors. Some major factors for a reinforced concrete column, for instance, are the rules for monotonic and cyclic stress-strain response of the constituent material including the confined core of the column, the assumption used for the curvature distribution on the column when the column deforms beyond its peak strength, the effect of loading history and pattern, and finally the analytical procedure used in the performance assessment.

In this study, various commonly used analytical procedures to extract the Axial Force-Bending Moment Interaction response curve, as a strength indicator for reinforced concrete column sections, called F-M throughout this report, are examined, while other factors such as material models and load pattern are kept constant.

Furthermore, the loading pattern has been considered to be monotonic, and the material models and cyclic rules are the same for all of the procedures explored.

Throughout the text, four different analytical methods, namely simplified method, simplified-curvature-based method, detailed method, and detailed-curvature-based method, were used to construct the unconfined and confined Axial Force-Bending Moment (F-M) interaction diagrams for RC columns with both circular and square cross sections. The columns were under combined axial load and uniaxial bending moment. The KSU_RC software was used to implement the calculations for the detailed methods. The F-M diagrams derived using the simplified method were exactly the same as those that were obtained using the simplified-curvature-based method. This is because both methods are using a pre-assumed compressive strain at extreme fiber of the cross sections to compute the maximum (ultimate) bending moment. The pre-assumed compressive strain, which is used for both confined and unconfined cross , is equal to the ultimate compressive strain of the cross sections. Since both of the methods use the concept of equivalent rectangular stress block and the same compressive strain, the output of these methods, simplified and simplified-curvature-based, are the same.

The detailed method was compared then with the simplified method. The F-M diagrams which were derived using the detailed method showed greater strength, mostly in the compression controlled zone, than did the simplified F-M diagrams. This can be attributed to the fact that the detailed method uses the exact stress distribution over the cross section while the simplified method uses the equivalent rectangular stress block concept. Consequently, the simplified method underestimates the concrete compressive force and also overestimates the line of action (from the top fiber) of this compressive force leading to a smaller internal moment arm, which results in a lower strength based on the simplified method.

The detailed method was used to obtain the F-M diagrams for a compressive strain of 0.003 at the most compressed fiber of the cross section. Both confined and unconfined F-M diagrams were derived for circular and square cross sections. At this compressive strain and for values of depth of the neutral axis less than the height of the cross section, the confined F-M diagrams showed a higher strength than did the unconfined ones; however, for values of depth of the neutral axis less than the height of the cross section,

the unconfined and confined F-M diagrams are approximately the same. Obviously, at compressive strains close to 0.003, the compressive force of the confined cross section is greater than the compressive force of the unconfined concrete, when the same area of the cross section is in the compression zone.

Considering confinement, the results of the detailed method and the detailed-curvature-based method were compared. The F-M diagrams derived based on detailed-curvature-based method showed greater strength than those constructed using the detailed method. The reason for this is that the computations of F-M diagrams based on the detailed method are done using a pre-assumed compressive strain; however, there is no pre-assumed compressive strain used in detailed-curvature-based method. Using the detailed-curvature-based method and the computed strains at different stages by the program, the Moment-Strain (M-S) diagrams were constructed. These diagrams show the relationship between the bending moment and compressive strain for a given axial load. It is evident from the M-S diagrams that the maximum bending moment for a confined cross section does not necessarily occur at either ϵ_{cc} , the strain corresponding to the peak confined stress or ϵ_{cu} , the ultimate confined strain capacity. It was also shown that the maximum bending moment, for a given axial load, does not occur at a specific compressive strain and the compressive strain at which the maximum moment occurs depends on the concrete cover of the cross section.

Finally, the detailed and detailed-curvature-based methods were validated against the existing experimental data, which included two RC columns with circular and square cross sections. Based on this validation, both detailed and detailed-curvature-based methods were in safe side or conservative; however, the detailed-curvature-based method was economically conservative. In other words, while the experimental point was outside of the region enclosed by the interaction curve, the curvature-based curve was closer to the test points.

In general, the detailed-curvature-based method had better performance in providing a realistic assessment of the axial force-bending moment interaction for RC column sections. This method has also the capacity to capture the effects of the load pattern on the performance and capacity of a reinforced concrete cross section.

References:

1. Esmaily, A., and Xiao, Y. "Behavior of Reinforced Concrete Columns Under Variable Axial Loads." *ACI Structural Journal*, V. 101, No. 1, Jan.-Feb. 2004, pp. 124-132, January-February 2004.
2. Esmaily, A., and Xiao, Y. "Behavior of Reinforced Concrete Columns under Variable Axial Loads: Analysis." *ACI Structural Journal*, Vol. 102, No. 5, pp. 736-744, September-October 2005.
3. Esmaily, A., Xiao, Y. "Seismic Behavior of Bridge Columns Subjected to Various Loading Patterns." Pacific Earthquake Engineering Research Center, PEER 2002/15, pp. 321, December 2002.
4. Esmaily, A., Lucio, K. "Analytical Performance of Reinforced Concrete Columns using Various Confinement Models." *ACI SP-238-6*, pp-95-110, 2006
5. "Building Code Requirements for Structural Concrete (ACI 318-08) and Commentary", American Concrete Institute, 2008.
6. Esmaily, Asad. "Advanced theory of reinforced concrete." Class Notes, Civil Engg. Dept. KSU, 2009.
7. MacGregor, James G., and James K. Wight. *Reinforced Concrete-Mechanics and design*. New Jersey: Pearson, 2009.
8. Beer, Ferdinand P., et al. *Mechanics of Materials*. New York: McGraw Hill, 2002.
9. Harries, Kent A., and Gayatri Kharel. "Behavior and Modeling of Concrete Subjected to Variable Confining Pressure." *ACI Material Journal*, Vol. 99, No. 2, pp. 180-189, March-April 2002.
10. Richart, Frank A." A study of the failure of concrete under combined compressive stresses." *University of Illinois Bulletin*, Vol. XXVI, No.12, November-1928.
11. "Cyclic Loading Test Data of Reinforced Concrete Bridge Piers." Dep. Of Civil Engineering, Tokyo Institute of Technology, Tokyo, Japan.
12. Mander J.B, Priestly, M.J.N., and Park R. "Seismic design of bridge piers." Research Rep. No. 84-2, Dep. of Civil Engineering, Univ. of Canterbury, New Zealand, 1984.
13. Dhakal R. P., and Koichi, Maekawa. "Reinforcement Stability and Fracture of Cover Concrete in Reinforced Concrete Members." *J. Struct. Eng.*, pp 1253-1262, October 2002.
14. Raynor, Dan J., Dawn E., Lehmana, and John F. Stanton. "Bond-slip response of reinforcing bars grouted in ducts." *ACI structural journal*. pp 568-576, Oct.2002
15. Chang, G., and Mander, J. "Seismic energy based fatigue damage analysis of bridge columns: Part I- Evaluation of seismic capacity." NCEER Technical Rep. No. 94-0006, Buffalo, N.Y. 1994.

16. Hoehler, M. S., and Stanton, J. F. "Simple phenomenological model for reinforcing steel under arbitrary load." *J. Struct. Eng.*, pp 1061-1069, 2006.
17. Mirmiran, A., Zagers, K., and Wenqing, Y. "Nonlinear Finite Element Modeling of Concrete Confined by Fiber Composites." *Finite Elements Analysis and Design*, Elsevier, 35(1), pp. 79-96, 2002.
18. Samaan, Michel, Amir Mirmiran, and Mohsen Shahawy. "Model of Concrete Confined by Fiber Composites." *J. Struct. Eng.*, pp. 1025-1031, 1998.
19. Lam, L., and J., G., Teng. "Design-oriented stress-strain model for FRP-confined concrete." *Construction and Building Materials*, Elsevier. 17. pp. 471-489, 2003.
20. Teng, J., G., and Lam, L. "Behavior and Modeling of Fiber Reinforced Polymer-Confined concrete." *J. Struct. Eng.*, Vol. 130, No. 11, pp. 1713-1723, November, 2004.
21. Teng, J. G., Y. L. Huang, L. Lam, and L. P. Ye. "Theoretical Model for Fiber-Reinforced Polymer-Confined concrete." *J. Struct. Eng.*, Vol. 11, No. 2, pp. 201-210, April, 2007.
22. Wu, Y. F., and Wang, W. L. "Unified strength model for square and circular concrete columns confined by external jackets." *J. Struct. Eng.*, Vol. 135, No. 3, pp. 253-261, March 2009.
23. Shao, Yutian, Seyed Aval, and Amir Mirmiran. "Fiber-Element Model for Cyclic Analysis of Concrete-Filled Fiber Reinforced Polymer Tubes." *J. Struct. Eng.*, Vol. 131, No. 2, pp. 292-303, Feb. 2005.
24. Teng, J. G., T. Jiang, L. Lam, and Y. Z. Luo. "Refinement of a Design-Oriented Stress-Strain Model for FRP-Confined Concrete." *J. Struct. Eng.*, Vol. 13, No. 4, pp. 269-278, August 2009.
25. Sheikh, S. A., and Uzumeri, S. M. "Analytical model for concrete confinement in tied columns." *J. Struct. Div.*, Vol. 108, No. ST12, pp.2703-2722, December 1982.
26. Mander, J. B., M. J. N. Priestley, and R. Park. "Theoretical stress-strain model for confined concrete." *J. Struct. Eng.*, Vol. 114, No. 8, pp. 1804-1826, August 1988.
27. Legeron, Frederic, and Paultre, Patrick. "Uniaxial confinement model for normal-and high-strength concrete column." *J. Struct. Eng.*, Vol. 129, No. 2, pp. 241-252, Feb. 2003.
28. Martinez, J. E., and Elnashai, A. S. "Confined concrete model under cyclic load." *Materials and Structures*, Vol. 30, pp. 139-147, April 1997.
29. Sakai, J., and Kawashima, K. "Unloading and Reloading Stress-Strain Model for Confined Concrete." *J. Struct. Eng.*, Vol. 132, No. 1, pp. 112-122, January 2006.

30. Richart, F. E., Anton Brandtzaeg, and Rex L. Brown. "The failure of plain and spirally confined concrete in compression." University of Illinois Bulletin, Vol. XXVI, No. 31, April 1992.
31. Kent, D. C., and Park, R. "Flexural members with confined concrete." J. Struct. Div., ASCE, Vol. 97, No. 7, 1971.
32. Sheikh, S. A., and Yeh, C. C. "Flexural behavior of confined concrete columns." ACI Journal, Title no. 89-39, pp. 389-404, May 1986.
33. "Structural Engineering Design Provisions." Uniform Building Code (UBC-97), 1997.
34. Nelson, A. H.; David Darwin; and Charles W. Dolan. "Design of concrete structures." New York, McGraw Hill, 2004.
35. Esmaily, A. "Advance theory of reinforced concrete- Analytical methods." Civil Eng. Dep., KSU, 2007.
36. Binici, B. and Khalid M. Mosalam. "Analysis of reinforced concrete columns retrofitted with fiber reinforced polymer lamina." Composites: Part B 38, Elsevier, pp. 265-276, 2007.
37. Esmaily, A. "KSU_RC, Moment-Curvature, Axial Force-Bending Moment Interaction, and force deflection analysis of RC cross section." http://www.ce.ksu.edu/faculty/esmaaily/KSU_RC.htm, 2010.
38. "LRFD Bridge Design Specifications." American Association of State Highway and officials (AASHTO), 2007.
39. Bea, Sungjin and Oguzhan Byrak. "Early Cover Spalling in High-Strength Concrete Columns." J. Struct. Div. ASCE, Vol. 129, No. 3, pp. 314-323, 2002.

Appendix – Notations

P = Axial force

A = The cross section area

M = Bending moment

y = Distance from top fiber to the centroid of the cross section

I = Moment of inertia of the cross section

f_{\max} = Maximum compressive stress

P_{\max} = Maximum axial load

M_{\max} = Maximum bending moment

E = Modulus of elasticity

ϕ = Curvature

ε_x = Strain in x axis direction

ε_y = Strain in y axis direction

ε_z = Strain in z axis direction

ν = Poisson ratio

σ_x = Stress in x axis direction

σ_y = Stress in y direction

σ_z = Stress in z direction

ε_t = Transverse strain

ε_c = Axial compressive strain

η = Dilatation ratio for concrete

σ_1 = Compressive stress in axial direction

f'_c = Axial compressive strength of plain concrete

f_c = Compressive strength of confined concrete

f'_{cc} = Maximum compressive strength of confined concrete

ε_{cc} = Ultimate compressive strain of plain concrete

ε_{co} = Compressive strain corresponding to maximum compressive strength of plain concrete

f'_{co} = Maximum compressive strength of plain concrete

E_c = Modulus elasticity of concrete

E_s = Modulus elasticity for steel reinforcement

E_{sec} = Secant modulus of elasticity of concrete

f_l = Lateral pressure provided by lateral reinforcement.

f'_l = Effective lateral confining pressure
 k_e = Effectiveness ratio
 A_c = Area of concrete enclosed by stirrups
 A_e = Effective area of confined core concrete
 ρ_{cc} = The area of lateral reinforcement to the area of core concrete
 f_{yt} = Yielding strength of transverse reinforcement
 A_{st} = Area of the transverse reinforcement
 s = Center to center distance between stirrups
 d_s = Diameter of stirrups (hoops)
 ρ_s = The ratio of volume of transverse reinforcement to the volume of confined core concrete
 ϵ_{cu} = Ultimate strain for confined concrete
 ϵ_{st} = Tension strain in bottom layer of longitudinal reinforcement
 f_y = Yielding strength of longitudinal reinforcement
 V_b = Seismic base shear force
 P_n = Nominal axial force capacity
 A_g = Gross area of cross section
 A'_s = Area of compressed longitudinal reinforcement
 C_c = Compressive force of concrete compressive block
 M_n = Nominal bending moment capacity
 a = Depth of ACI compressive block
 c = Depth of the neutral axis
 d = Effective depth of cross section
 h = Height of the cross section
 I_g = Moment of inertia of gross section
 f_r = Modulus of rupture of concrete